AD-A137 208 EFFECTS OF FUEL SPECIFICATION AND ADDITIVES ON SOOT FORMATION(U) CALIFORNIA UNIV IRVINE COMBUSTION LAB G S SAMUELSEN ET AL. DEC 83 AFESC/ESL-TR-83-17 1/2

UNCLASSIFIED F08635-79-C-0158 F/G 21/5 NL

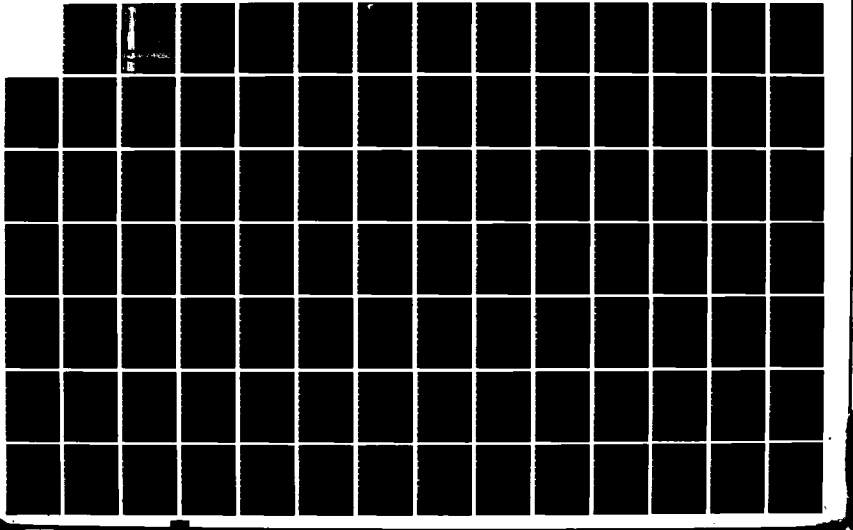

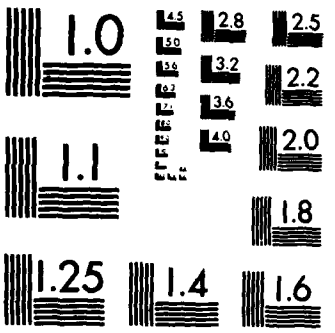

(12)

ESL-TR-83-17

EFFECTS OF FUEL SPECIFICATION AND ADDITIVES ON SOOT FORMATION

G.S. SAMUELSEN, R.L. HACK
R.M. HIMES and M. AZZAZY

UCI COMBUSTION LABORATORY
MECHANICAL ENGINEERING
UNIVERSITY OF CALIFORNIA, IRVINE, CA 92717

DECEMBER 1983

FINAL REPORT
MAY 1979 - JANUARY 1983

AFESC

ENGINEERING & SERVICES LABORATORY
AIR FORCE ENGINEERING & SERVICES CENTER
TYNDALL AIR FORCE BASE, FLORIDA 32403

NOTICE

PLEASE DO NOT REQUEST COPIES OF THIS REPORT FROM HQ AFESC/RD (ENGINEERING AND SERVICES LABORATORY). ADDITONAL COPIES MAY BE PURCHASED FROM:

NATIONAL TECHNICAL INFORMATION SERVICE
5285 PORT ROYAL ROAD
SPRINGFIELD, VIRGINIA 22161

FEDERAL GOVERNMENT AGENCIES AND THEIR CONTRACTORS REGISTERED WITH DEFENSE TECHNICAL INFORMATION CENTER SHOULD DIRECT REQUESTS FOR COPIES OF THIS REPORT TO:

DEFENSE TECHNICAL INFORMATION CENTER
CAMERON STATION
ALEXANDRIA, VIRGINIA 22314

Unclassified

SECURITY CLASSIFICATION OF THIS PAGE (When Data Entered)

REPORT DOCUMENTATION PAGE		READ INSTRUCTIONS BEFORE COMPLETING FORM
1. REPORT NUMBER ESL TR-83-17	2. GOVT ACCESSION NO. AD-A137208	3. RECIPIENT'S CATALOG NUMBER
4. TITLE (and Subtitle) EFFECTS OF FUEL SPECIFICATION AND ADDITIVES ON SOOT FORMATION		5. TYPE OF REPORT & PERIOD COVERED Final Report May 1979 - January 1983 6. PERFORMING ORG. REPORT NUMBER
7. AUTHOR(s) G.S. Samuelsen, R.L. Hack, R.M. Himes and M. Azzazy		8. CONTRACT OR GRANT NUMBER(s) F08635-79-C-0158
9. PERFORMING ORGANIZATION NAME AND ADDRESS UCI Combustion Laboratory Mechanical Engineering University of California, Irvine, CA 92717		10. PROGRAM ELEMENT, PROJECT, TASK AREA & WORK UNIT NUMBERS JON: 19002038 PE: 62601F
11. CONTROLLING OFFICE NAME AND ADDRESS Department of the Air Force Hq AF Engineering and Services Center/RDVC Tyndall Air Force Base, Florida 32403		12. REPORT DATE December 1983 13. NUMBER OF PAGES 113
14. MONITORING AGENCY NAME & ADDRESS(if different from Controlling Office)		15. SECURITY CLASS. (of this report) Unclassified 15a. DECLASSIFICATION/DOWNGRADING SCHEDULE

16. DISTRIBUTION STATEMENT (of this Report)

Distribution Unlimited, Approved for Public Release

17. DISTRIBUTION STATEMENT (of the abstract entered in Block 20, if different from Report)

18. SUPPLEMENTARY NOTES

Availability of this report is specified on reverse of front cover.

19 KEY WORDS (Continue on reverse side if necessary and identify by block number)

Jet Fuel	Soot	Extractive Probe	Soot Composition
JP-4	Combustion	Probe Perturbation	
JP-8	Optical Probe	Fuel Composition	
Hydrocarbons		Additives	

20. ABSTRACT (Continue on reverse side if necessary and identify by block number)

The objective of this program was to develop and employ the methods necessary to identify the causal effects of fuel properties, additive properties, and combustor operating conditions on soot formation and to provide information needed to evaluate and develop models destined for gas turbine design. Present knowledge of these effects is limited to systems which are either too simple to adequately represent gas turbine combustion or too complex to permit access to detailed optical diagnostics. The projected use by Air Force aircraft of relax-

DD FORM 1 JAN 73 1473 EDITION OF 1 NOV 65 IS OBSOLETE

Unclassified

SECURITY CLASSIFICATION OF THIS PAGE (When Data Entered)

ed specification fuels having an increased tendency to produce soot portends greater difficulty meeting the future USAF aircraft smoke emission goals and makes this information essential.

To answer these technical questions, a multifaceted study was undertaken to (1) test candidate model laboratory combustors in the conduct of fuel effects studies, (2) develop and test nonintrusive laser optical techniques for the measurement of local soot size and number density, (3) develop and assess the effect of extractive probe perturbation to local values of soot size and number density, (4) employ an extractive probe and sampling system to assess the effect of fuel molecular structure and additives on the physical and chemical properties of soot, and (5) determine the effectiveness of the ASTM smoke point in predicting sooting behavior in complex flows.

Two candidate model laboratory combustors were used -- a swirl-stabilized centerbody and a Dilute Swirl Combustor (DSC). The DSC proved more satisfactory with respect to overall performance and accommodation to optical diagnostics.

Two optical probes were developed, a prototype Large-Particle Optical System ($2.4\ \mu m \geq d_p \geq 0.4\ \mu m$) and an Expanded-Particle Optical System ($2.4\ \mu m \geq d_p \geq 0.05\ \mu m$). The expanded system was evaluated for both gaseous and liquid fuels, and validated in nonreacting flows with calibrated polystyrene latex particles. The prototype system was also tested with polystyrene seeds and used to evaluate the perturbation of an extractive probe. In-flame measurements of soot particulate using an extractive and large-particle optical probe were compared for the swirl-stabilized centerbody combustor. Except for large ($\sim 5\mu m$) particulate present in the extracted samples, the soot particle size compared favorably with optically measured values, and the soot particle morphology reflected that formed in gas turbine combustors. Two nonflame sources for the large particulate were suggested by the optical data: particles formed or elongated during transport subsequent to extraction, and particles attrited from upstream carbon deposits on a solid surface. The extractive probe produced a change in the local particle number density which varied from little change to a 70-fold suppression in reacting flow and a 200-fold increase in cold-seeded flow depending on the location within the combustor of the optical sampling volume, the location of the extractive probe relative to the optical sampling volume, and the combustor operating conditions.

Finally, soot samples were extracted from a swirl-stabilized, liquid fuel-fired centerbody combustor to (i) assess the validity of the ASTM smoke point test in predicting the sooting characteristics of fuels in complex combustion systems and (ii) assess the effect of fuel molecular structure and smoke suppressant additives on the physical and chemical properties of soot. Fuels utilized were shale JP-8, isooctane, and blends of isooctane with either decalin, toluene, tetralin, or 1-methylnapthalene such that smoke points similar to JP-8 were achieved. Each fuel was separately blended with 0.05-percent (by weight) ferrocene smoke suppressant. The results indicated that the ASTM test can be misleading, increased fuel molecular complexity increases soot content of higher molecular weight polycyclic aromatics, and ferrocene additive reduces small particle number density but not necessarily the soot mass loading.

PREFACE

This program was conducted by the UCI Combustion Laboratory, Mechanical Engineering, University of California, Irvine, 92717, under Contract No. F08635-79-C-0158 with the Air Force Engineering and Services Center, Engineering and Services Laboratory (AFESC/RD), Tyndall AFB, Florida. Spectron Development Laboratories, Inc., 3303 Harbor Blvd., Suite G-3, Costa Mesa, CA, 92626 served as a major subcontractor to the program.

Work on this program was performed between 8 May 1979 and 31 January 1983. Major Harvey Clewell and 1stLT Jeffery Jenkins were AFESC/RDV project officers.

The individuals who participated in and provided major contributions to the program include graduate students Richard L. Hack, Richard M. Himes, and Randall A. Smith; Laboratory Staff John T. Taylor and Craig P. Wood; Mechanical Engineering Staff Jeanne M. Bettencourt and Verna M. Bruce; Spectron Development Laboratories Staff William D. Bachalo, Chie C. Poon, Joseph E. Wuerer, Charles Ragsdale, and Medhat Azzazy.

This report has been reviewed by the Public Affairs Office (PA) and is releasable to the National Technical Information Service (NTIS). At NTIS it will be available to the general public, including foreign nationals.

This report has been reviewed and is approved for publication.

Paul E. Kerch

PAUL E. KERCH, Capt, USAF, BSC
Project Officer

Jimmy W. Fulford

JIMMY W. FULFORD, Lt Col, USAF
Chief, Environics Division

John T Slankas

JOHN T. SLANKAS, Maj, USAF
Chief, Environmental Sciences Branch

Robert E. Brandon

ROBERT E. BRANDON
Deputy Director
Engineering and Services Laboratory

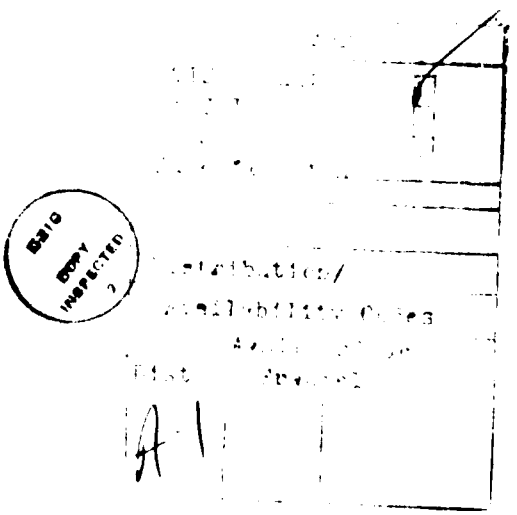

(The reverse of this page is blank)

TABLE OF CONTENTS

TABLE OF CONTENTS (CONCLUDED)

LIST OF FIGURES

LIST OF FIGURES (CONCLUDED)

LIST OF TABLES

LIST OF TABLES (CONCLUDED)

SECTION I

INTRODUCTION

During the last decade, world consumption of petroleum resources outpaced discovery for the first time. Conservation efforts resulting from the economic pressure of high foreign oil prices have helped stem the growing appetite for energy, but dwindling domestic reserves will necessitate the development of alternative energy sources to meet future energy needs. Shortages of liquid fuels relative to the basic demand have already occurred due to competition within the transportation sector for specific fractions of the refined petroleum crude.

Two approaches are being pursued to assure adequate aviation fuel availability. The first is to extend the conventional crude oil fuel supply by relaxing specifications, thereby reducing the level of processing required and expanding the usable fraction of the crude. The second is to investigate the acceptability of fuels produced from alternative sources such as coal, oil shale, and tar sands to meet the same relaxed specifications as those for petroleum-derived fuels. Fuels derived by the first approach are labelled "relaxed-specification" or "broad-specification" fuels, whereas those derived by the second approach are labelled "alternative," "syn," or "synthetic" fuels.

These potential changes in fuel processing and fuel source make future fuel composition effects on gas turbines a primary consideration and concern. Currently, a 20-percent aromatics specification exists to avoid a series of combustion-related problems which were encountered with fuels containing higher than specification amounts. The problems are associated with an increased production of soot and include increased flame radiation, deposit of carbonaceous material, and emission of particulates, all of which have deleterious effects on the gas turbine engine. The aromatics specification is of interest because specification for petroleum-derived fuels may be relaxed to levels as high as 35 percent (Reference 1), and fuels derived from alternative sources are richer in aromatic content than their petroleum counterparts. Changes and advances in the technology of combustion are necessary, therefore, to overcome the problems which accompany the composition of future fuels.

Unfortunately, efforts to produce low-emission combustors are hampered by (1) the wide range of conditions over which gas turbine engines must operate, and (2) the lack of understanding of the processes that dictate combustor performance (Figure 1). With gas turbines, not only may combustion pressure vary over a wide range, especially in aircraft systems, but also the large differences in fuel and air flows between idle and full-power conditions can produce substantial variations in the primary zone fuel/air ratio. Soot, not an equilibrium product of combustion, is influenced not only by the reaction kinetics and paths of the gaseous species, but by the physical processes of atomization, evaporation, and fuel/air mixing (Reference 2).

The principal approaches being considered to reduce soot emissions from combustors operating on synthetic or relaxed-specification fuels are smoke-suppressant fuel additives and combustor modifications. Smoke-suppressant fuel additives avert the economic penalties associated with retrofit by providing an alternative for existing gas turbine engines. Combustion modification will be

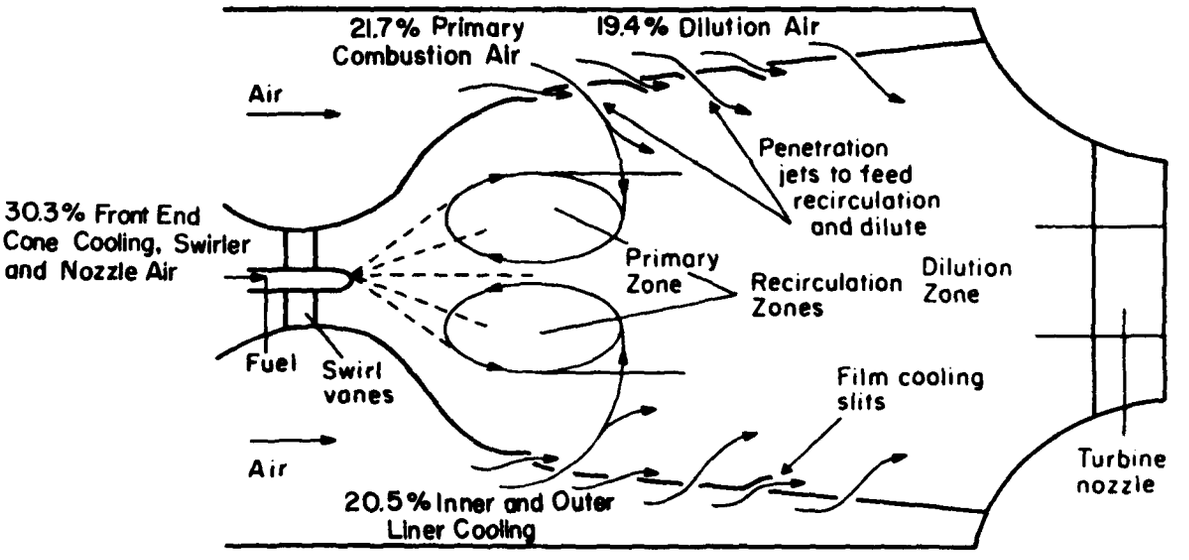

Figure 1. Schematic of Gas Turbine Combustor with Air Flows Characteristic of a JT9-D (References 3 and 4)

important for the next generation of gas turbine engines which will eventually replace the current inventory. In order to implement either of these approaches, it is necessary to gain an understanding of the mechanisms responsible for soot formation and burnout in complex (i.e., turbulent and recirculating) flows. Toward this end, experimental evidence is needed with respect to the effects which fuel properties, fuel-additive properties, and combustor operating conditions have on soot formation and burnout. Of interest are the mass emission, size distribution, and composition of the soot particulate. Extractive probe measurements can be utilized for this set of information but, in complex flows where backmixing can exacerbate and widely distribute perturbations introducted by the presence of a physical probe, caution must be exercised in the use of such methods including, for example, limiting the measurements to the combustor exit-plane, far downstream of the recirculation zone.

Also of interest is experimental evidence of the spatial distribution of the local soot size and soot number density, not only in the wake of the recirculation zone, but within the recirculation zone itself. Such measurements must be nonintrusive, employing, for example, laser-based optical diagnostics. Prior to the present program, optical probes had not been developed and demonstrated for pointwise measurement of soot size and number density in a complex flow.

In addition to obtaining experimental evidence of fuel effects and combustor operating conditions on soot formation and burnout, methods for specification of the burning quality of aviation fuels need to be reassessed. The ASTM D-1322 Smoke Point Method, used to measure the smoking propensity of aviation fuels in a laminar diffusion flame, may not represent the sooting behavior of aviation fuels in complex flows.

The present study was established to address these questions with the following set of objectives:

- To test the suitability and performance of candidate laboratory complex flow model combustors for the purpose of conducting fuel effects studies.
- To develop, test, evaluate and employ optical probes for the purpose of measuring the spatial distribution of soot size and number density in a complex flow.
- To develop, test, evaluate, and employ an extractive probe for the purpose of obtaining soot samples suitable for physical and chemical analysis.
- To conduct the following exploratory studies using the methods developed to obtain the first insights into the production of soot within a complex flow:
  - (1) Assess the performance of the optical probes in the measurement of the local soot number density and soot size.

(2) Assess the perturbation of an extractive probe on the local measurement of soot number density and soot size.

(3) Assess the effect of fuel molecular structure and of the smoke suppressant fuel additive, ferrocene, on the loading and chemical properties of soot.

(4) Assess the validity of the ASTM Smoke Point Method in predicting the sooting propensity of aviation turbine fuels in complex flows.

SECTION II

BACKGROUND

A. SOOT FORMATION

The problem of controlling the formation of soot is difficult because of the many factors that impact the process. Each aspect of the combustion process in a gas turbine influences the formation of soot,as well as variations in the chemical composition of the fuel. The factors involved are frequently interrelated, thus requiring an understanding of the mechanisms responsible in order to facilitate the development of a control strategy.

1. Combustor Effects

Soot may be generated where mixing is inadequate and regions of fuel are enveloped in oxygen-deficient gases at high temperature. The relatively high pressures encountered in gas turbines are a major contributing factor to the formation of these regions. Reduced spray penetration, increased fuel evaporation rates, and accelerated chemical reaction rates result from the high-pressure environment and concentrate the fuel combustion in a fuel-rich soot-forming region just downstream of the nozzle. Broadened burning limits also result from elevated pressures and serve to form sooting regions which normally would be too rich to burn (Reference 5). In general, soot production rates have been found to be directly proportional to pressure (Reference 6), although a plateau at a critical Reynold's number has been asserted (Reference 7). Elevated pressures are a necessary concomitance of gas turbine combustion, however, and thus represent a relatively inflexible parameter.

Fuel injection methods are a means of partially overcoming the adverse effects of high pressure on soot formation. Dual-orifice pressure atomizers have traditionally been the injection method of choice as they provide the wide range of stable operating conditions required in gas turbine operation. A central pilot orifice supplies all the fuel required at low fuel flow, and a surrounding annular main orifice supplies most of the fuel at normal operating conditions. The atomizer promotes the formation of soot by centralizing the fuel in the oxygen-deficient core of the primary zone. As a result, the dilution zone must be relied upon to oxidize the soot generated. The relatively low sooting propensity of current specification fuels has resulted in acceptable emission levels under most conditions. The increased soot loading found with future fuels, however, would portend unacceptable soot emissions with this injection method.

Improvements can be gained by increasing the air flow into the primary zone, but only at the expense of stability and ignition performance, hence, the major drawback to airblast atomizers. A piloted airblast atomizer circumvents this problem by combining both fuel-injection techniques (Reference 8). Fuel is supplied to a pilot nozzle at low-fuel flows with increased fuel flows supplied to an airblast atomizer. The airblast atomization process insures good mixing of fuel and air prior to combustion which significantly reduces the soot formation. For example, comparative measurements of the atomization characteristics of airblast and pressure-atomizing injectors have shown that airblast injectors are capable of providing a finer spray with droplets having a

30-percent lower Sauter mean diameter than the spray produced by a pressure-atomizing injector (Reference 9). Combustor liner temperature data from the CF6-50 engine with airblast fuel injection and leaner combustion (Reference 10) demonstrated far less sensitivity to fuel hydrogen content than conventional systems equipped with pressure-atomizing fuel nozzles (Reference 11). Atomization has even been found to improve with increasing chamber pressure, thereby promoting more rapid fuel vaporization, mixing and combustion (Reference 12). These merits have prompted the installation of airblast atomizers in a wide range of industrial and aircraft engines in recent years.

These approaches, airblast atomization and leaner combustion with higher pressure ratios, are relatively straightforward compared to the major design modifications being considered for advanced combustors. Variable geometry, staged fuel injection, and prevaporized/premixed burners are all methods being evaluated for reduced pollutant emissions over the entire range of operating conditions. Applications of these major modifications, however, have had mixed results and are hampered primarily because of the incomplete understanding of the gas turbine combustion process (Reference 13).

2. Fuel Effects

The use of broad-specification and alternative fuels will impact soot formation in current gas turbine engines in two main respects. First, physical properties such as volatility and viscosity can affect the atomization and evaporation of the fuel which impedes the fuel/air mixing process, thereby promoting the formation of soot. Second, future fuel composition will vary significantly from current petroleum fuels due to the relaxed aromatic content specifications projected for petroleum fuels, and higher aromatic content of shale oils and coal liquids.

Tentative specifications for an Experimental Referee Broad Specification (ERBS) fuel are presented in Table 1 and compared to those for Jet-A. One important difference is that Jet-A specifications stipulate specific limits on the concentrations of aromatics and naphthalenes while specifications for ERBS are based on the hydrogen content of the fuel. The lower hydrogen content of the tentative ERBS specification permits the aromatic content to increase into the range of 35 percent to 40 percent by volume. The higher aromatic content is reflected in changes in the distillation temperature range and physical properties.

The higher surface tension and kinematic viscosity of ERBS is anticipated to lead to an increase in SMD (References 4 and 15) which implies a deterioration in atomization. The larger droplet size will be compounded further by the reduced fuel volatility, all of which will increase the time for droplet evaporation. Actual tests in an Allison T-63 engine (Reference 16), however, have found the viscosity and distillation curve (end point) to have little effect on the measured smoke and radiation. Thus, changes in the physical properties of fuels appear to have only minor effects on the formation of soot.

Fuel molecular structure, on the other hand, has been shown to have a far more important role in soot formation. Extensive studies in a well-stirred reactor (References 17 and 18), which allows the study of the chemical process

TABLE 1. JET A AND ERBS FUEL SPECIFICATIONS (Reference 4)

Property	Jet-A	ERBS
Aromatic Content (% vol.), max.	20	--
Hydrogen Content (% wt.), max.		12.8+2
Sulphur Mercaptan (% wt.), max.	0.003	0.003
Naphthalene Content (% vol.), max.	3.0	--
Distillation:		
10 Percent (°K), max.	477	477
90 Percent (°K), min.	--	534
Final Boiling Point (°K), max.	573	--
Residue (% vol.), max.	1.5	--
Loss (% vol.), max.	1.5	--
Flashpoint (°K), min.	311	311/321
Freezing Point (°K), max.	233	244
Maximum Viscosity (CS)	8 @ 253°K	12 @ 249°K
Heat of Combustion (J/kg), min.	42.8×10^6	--
Thermal Stability:		
JFTOT Breakpoint Temperature (°K), min.	533	511
Method	Visual	TDR = 13.

without heat and mass transfer limitations, have shown that nonaromatic hydrocarbons introduced prevaporized were capable of being burned at substantially higher equivalence ratios than aromatics without forming soot. Blazowski (Reference 18) was able to group the hydrocarbons tested into three categories (Table 2). The first group, composed of aliphatic hydrocarbons, produced large amounts of exhaust hydrocarbons without sooting. The second group, consisting primarily of single-ring aromatics, produced similar amounts of soot as the fuel/air mixture was increased. Finally, the third group, made up entirely by 1-methylnaphthalene, produced even higher quantities of soot than those in the second group. For a given fuel, the leanest mixture ratio at which soot was observed was also found to correspond to the conditions at which significant concentrations of exhaust hydrocarbons were first detected. Mixtures of toluene and isooctane representing a broad range of hydrogen content resulted in increasing amounts of soot with increasing aromatic content. The linear hydrogen content correlation which resulted, however, was suggested to be representative of Group 2 hydrocarbons with the possibility that blends of 1 methylnaphthalene and isooctane might produce an even steeper soot production versus hydrogen content trend. Tests run on a JT9D combustor (Reference 4) appear to support this assertion. A linear trend of increasing Smoke Number was found with increasing aromatic content except for a 16.2 volume percent naphthalene blend which produced more than twice the Smoke Number expected from the correlation found with the other fuels. The critical difference appears to be the amount of dicyclic aromatics in the fuels.

TABLE 2. CATEGORIZATION OF HYDROCARBONS WITH SIMILAR SOOTING CHARACTERISTICS IN A WELL-STIRRED REACTOR (Reference 18)

Group 1	Group 2	Group 3
Ethylene	Toluene	1-Methylnaphthalene
Hexane	O-Xylene	
Cyclohexane	M-Xylene	
N-Octane	P-Xylene	
Isooctane	Cumene	
1-Octene	Tetralin	
Cyclo-Octane	Dicyclopentadiene	
Decalin		

Thus, the indications are that fuel molecular structure plays a dominant role in soot formation which may necessitate the control of both hydrogen and dicyclic aromatic content in future fuel specifications.

B. SMOKE-SUPPRESSANT FUEL ADDITIVES

Even though design modifications are the most economical long-term approach to the control of soot emissions, fuel additives may prove useful for short-term use in current generation gas turbine engines. Reduction in overall particulate emissions is not the only important consideration, however, as metal oxide deposits on combustor surfaces and health effects attributed to the fuel additives also need to be considered. The number of flame parameters which influence the effectiveness of the various additives is indicative of a complex mechanism governing the process which will need to be understood to use the additives effectively.

One of the first uses of additives for smoke reduction in gas turbines was in a Rolls Royce Dart engine using ferrocene and Lubrizol 565®, an organic derivative of barium (Reference 19). Smoke numbers obtained from a lamp indicated that a 0.05 percent concentration by weight of ferrocene should reduce smoke, whereas a 0.25 percent concentration of Lubrizol 565® demonstrated a greater tendency to smoke. Engine results, however, were exactly opposite with significant smoke reductions from the Lubrizol 565® additive and no appreciable carbon reduction with the ferrocene additive.

Ground-test results using a J79-8 engine (Reference 20) found additives containing alkylnitrates, boron, lead alkyls, and organic peroxides to be ineffective, whereas ferrocene and unidentified manganese and barium compounds substantially reduced smoke emissions. Combustor deposits, however, were prevalent with these latter additives and in the case of a 0.1-percent by volume barium concentration, the engine stalled after 2.5 hours at military power because of thick white deposits of barium carbonate in the combustor and turbine. Adverse affects of the other additives were not as pronounced, but thin deposits of black cubic Mn_2O_3 and orange tetragonal Mn_3O_4 were found

with the manganese additive and dusty brown iron oxide with the ferrocene additive after 5 hours of operation.

From work with a Phillips 2-inch combustor (Reference 6) using different organometallic additives at different concentrations, it was concluded that the additives were most beneficial at intermediate turbine-inlet conditions (10-15 atm; 1500-1700°F) and that additive type and concentration are both important. The concept of an optimum additive concentration is supported by results found with ferrocene in J52, J57, and TF-30 gas turbine engines (Reference 21). A reduction in mass emissions peaked around 0.05-0.06 percent ferrocene by weight with concentrations outside of this range increasing the overall mass emissions. The further complexities introduced by combustor design and operating conditions were evidenced from the conflicting results obtained with the J79 and TF-41 engines. Ferrocene reduced emissions from both engines at 85-percent normal rated conditions, but increased emissions at military power.

Three mechanisms by which additives seem to function in flames have been identified (Reference 22). These mechanisms are not independent, with several of the additives exhibiting behavior attributable to a combination of the mechanisms. The first mechanism is ionic in nature and occurs with additives (Na,K,Cs,Ba) which are easily ionized in the flame. The additive ions act on the natural flame ions and are thought to either reduce the coagulation rate by increasing the electrostatic repulsion between soot particles (Reference 23) or to reduce the number of effective nuclei for soot formation by decreasing the number of natural flame hydrocarbon ions (Reference 24). The result is a decrease in the amount of soot formed, or a shift in particle size to smaller particles which burn out more quickly. The second mechanism involves additives (Ba,Ca,Sr) which produce hydroxyl radicals through reactions with flame gases. By maintaining the hydroxyl concentration throughout the flame, an accelerated rate of carbon oxidation is achieved (Reference 25). Finally, the third mechanism occurs late in the flame where soot oxidation occurs. The occlusion of the metal (Mn,Fe,Co,Ni) in the soot particle is thought to accelerate the rate of oxidation by a reaction such as (Reference 25):

$$M_xO_y + C_{(s)} \rightarrow CO + M_xO_{x-1}.$$

Primary zone radiation is typically unaffected due to the additive functioning in the later flame zones.

The three most common metals appearing in additives are manganese, iron, and barium. Of these, iron appears to be the safest with exposure to iron oxide combustion products in high concentrations being only irritating (Reference 22). Manganese oxides and water soluble barium compounds, such as barium carbonate, are very toxic and can be fatal with chronic exposure to high concentrations. Due to the toxicity effects of barium and manganese additives, ferrocene has become the most popular additive.

C. JET FUEL SPECIFICATION TESTS

Since gas turbine engine performance is directly related to fuel quality, several laboratory tests have been developed (Table 3) over the years to assess fuel performance, including fuel-burning and compositional tests. Broad-specification and alternative fuels and their attendant propensity to form

soot, however, have renewed interest in the relevancy of the smoke point tests as measures of fuel performance in gas turbines. Smoke point tests have been open to question for some time, primarily because of the appreciable differences between the laminar diffusion flame in the performance test and the complex flow found in a gas turbine.

1. Smoke Point Tests

The smoke lamp was developed in Britain over 50 years ago to define the quality of illuminating oil used in wick-fed lamps (Reference 26). The height of a diffusion flame burning in air was observed to be related to the fuel molecular structure, paraffins giving high flames without smoking and aromatics much lower flames. A series of standardized tests (IP-57, Federal Test Method 2107, Indiana Smoke Lamp Test Method, and ASTM D-1322) based on these observations was subsequently developed. Problems identified with these test methods were flame instability, difficulty in reading and defining the exact flame height, and variability due to barometric pressure and humidity. To compensate for humidity effects, the ASTM D-1322 method introduced the use of toluene/isooctane blends to calibrate the lamp.

TABLE 3. JET FUEL LABORATORY TESTS

			Reference
A.	Burning Tests		
	IP57[a]	Smoke Point of Kerosene	26
	IP10	Burning Quality of Kerosene	26
	---	Indiana Smoke Point Lamp	26
	D1322[a]	Smoke Point of Jet Fuel	27
	SVI[a]	Smoke Point Volatility Index	26
	D1740[a]	Luminometer Number	28
B.	Composition Test		
	NACA	K Factor	26
	D1319[a]	Hydrocarbon Types (e.g. Aromatics) by FIA	29
	D1840[a]	Naphthalene Hydrocarbons	30
	D3701 or D1018[a]	Hydrogen Content	31
	D1218	Reactive Index	32
	D611[a]	Aniline Point	33
C.	Correlation Tests		
	Proposed	Estimating Smoke Point	26
	D3342[a]	Estimating Hydrogen Content	34

[a] Currently used in jet fuel specifications

Early combustor tests demonstrated that high-boiling aromatics were much worse than other fuel components in terms of carbon deposits and liner temperatures (Reference 26). As the 400°F-cut point essentially separates the multiring aromatics from single-ring types, the Smoke Volatility Index (SVI) was developed for wide-cut fuels (e.g., JP-4) to provide a better definition of burning quality:

$$SVI = SMOKE\ POINT + 0.42\ (VOL\%\ UNDER\ 400°F)$$

Unfortunately, kerosenes of the JP-5 and Jet-A type, along with the less volatile synthetic fuels boil mostly above 400°F, leaving only the smoke point to define combustion quality.

In combustor tests relating changes in liner temperature to smoke point of a wide range of fuels (Reference 26), a decrease in smoke point from 25 to 20 mm (corresponding to an increased propensity to form soot) resulted in no significant change in liner temperature. Analysis of the fuels for aromatic content showed a pronounced distinction between single and multiring aromatics in this region of smoke point. Pratt & Whitney discovered soon after that dicyclic aromatic content proved to be an effective indication of combustion quality in this region of smoke point.

The effect of polycyclic aromatics on soot formation was also demonstrated in a J57 combustor with JP-5 fuel blended such that equal smoke points were obtained with tri-ethyl benzene (monocyclic) as one additive and methyl naphthalene (dicyclic) as the other. At constant smoke point, fuels containing polycyclic aromatics produced more radiant heating in the J57 combustor than those containing monocyclic aromatics (Reference 35). Tests similar to those for the J57 were performed for the J79 combustor using the same fuel blending specifications (Reference 36). Once again, for fuels blended to the same smoke point, those with polycyclic aromatics produced higher liner temperatures.

2. Alternative Fuel Specifications

Weaknesses in the smoke point test have resulted in a search for a specification based upon a fundamental fuel property which will more accurately reflect the combustion performance of a fuel in a gas turbine engine. Fuel hydrogen content has been promoted as a viable test of fuel quality for over thirty years. In recent years, soot formation measurements in actual combustors, using either liner temperature or flame radiation, have resulted in good correlations being found with fuel hydrogen content (References 11, 16, 37, and 38). Fuel molecular structure, however, may also be important under certain operating conditions (Reference 39). Fuels blended to achieve an equivalent hydrogen content with varying molecular structure resulted in a range of measured flame radiation with the naphthalene containing fuels deviating significantly from any hydrogen correlation. It should be noted, however, that the naphthalene hydrocarbons present in these fuels greatly exceeded any current or proposed jet fuel specifications.

The influence of flame temperature on soot formation in laminar diffusion flames has also been demonstrated (Reference 40). A greater tendency to soot was found at higher temperatures because the rate of pyrolysis increases with flame temperature, thereby generating a greater concentration of soot precursors. Since the adiabatic flame temperature increases as the fuel hydrogen content is reduced, the hydrogen correlations noted above may be due to the variations in flame temperature with fuel composition. Recent experiments (Reference 41) in a complex flow combustor, however, indicated relatively small changes in flame temperature with variations in fuel composition compared to the corresponding changes in soot concentration. Before any definitive conclusions can be made, more work will be required to ascertain to what degree each of these parameters affects soot formation.

D. OPTICAL PROBES

Almost all optical sizing techniques are based on the scattering phenomenon which takes place when particles are illuminated by incident radiation (a laser light source, for example). When a particle is immersed in a parallel laser beam, scattering causes the incident intensity to be redistributed in all directions. The actal distribution is a function of wavelength, λ , refractive index m, particle size d, scattering angle Θ, and for polarized light, the polarization angle ϕ (the angle between the polarization vector and the scattering plane). By measuring the scattered intensity, particle size can be determined from Mie theory if the incident intensity, wavelength, refractive index, and the angles Θ and ϕ are known. Furthermore, based on variations of this scattered intensity technique, it is possible to simplify the methodology by eliminating the intensity dependence from two or more measurements obtained at different wavelengths, angles, or combinations of these quantities. Such variations are applicable for either single-particle or multiple-particle sizing. A summary of the techniques is tabulated in Table 4. The table also contains the basis of the technique, the parameters for the determination of size, and the approximate lower limit of the technique.

Techniques (1) to (4) and (10) to (12) are based solely on scattering. For absorbing particles, a second technique is available -- extinction. Extinction represents the effects due to scattering and absorption. While scattering merely affects the angular distribution of intensity, absorption represents an attenuation of the incident radiation in the forward direction. Thus, extinction (because of absorption) is mainly a column measurement, i.e., the integrated absorption and scattering along the trajectory of the incident beam. To obtain local size averages, extinction measurements must undergo numerical inversion techniques to unravel the column effects, unless the incident beam is highly focused. Therefore, scattering measurements other than in the forward direction would often offer better spatial resolution than extinction although the measured scattered intensity may be much less than that from extinction measurements. As in scattering, extinction is a function of incident intensity, wavelength, refractive index and particle size so that if the refractive index is known, the intensity dependence can be removed by multiple-wavelength measurements (Technique 5, Table 4). The extinction technique is also applicable for either multiple-particle sizing and single-particle sizing. A further variation based on scattering and extinction phenomena is the determination of scattering and extinction produced by the particle field (Technique 6, Table 4). This technique has a very small lower limit. However,

TABLE 4. CURRENT PARTICLE SIZING TECHNIQUES

Technique	Basis	Parameters	Lower Limit (μm)	Reference
MULTIPLE-PARTICLE SIZING				
(1) Scattered intensity/angle dependence	scattering	Θ,m	0.02	42
(2) Scattered intensity/wavelength dependence	scattering	λ,m	0.05	43
(3) Polarization ratio/angle dependence	scattering	Θ,ϕ,m	0.1	44
(4) Polarization ratio/wavelength dependence	scattering	ϕ,λ,m	1	45
(5) Extinction/wavelength dependence	extinction	λ,m	0.02	44
(6) Scattering/extinction ratio	scattering and extinction	λ,m	0.005	44
(7) Power Spectrum of scattered radiation	scattering	λ,T	0.02	46 47
SINGLE-PARTICLE SIZING				
(8) Particle-sizing interferometry	scattering	λ,m	3	48
(9) Optical variable frequency grid	scattering	λ,m	10	49
(10) Scattered intensity/angle dependence	scattering	Θ,λ,m	0.3	50 51
(11) Scattered intensity (off axis)	scattering	I,Θ,λ,m	1	52
(12) Scattered intensity (on axis)	scattering	I,λ,m	0.1	53
(13) Cross-beam extinction	scattering	I,λ,m	0.004	54

inherent difficulties, because of its dependence on the scattered intensity, cast uncertai ies in its application.

One multiple-particle technique which is gaining attention is based on the power spectrum of scattered radiation (Technique 7, Table 4). When monochromatic light is scattered from a fine aggregate of particles, the random motion of the particles causes a Doppler shift in the incident light. If the scattered light is spectrally analyzed, a power spectrum can be recovered such that the average particle size is related to the wavelength, diffusion coefficient and temperature of the aggregate. This technique has been applied to size soot particles in an acetylene-oxygen flame (Reference 47).

A well-used technique, also based on the scattering phenomenon, is particle-sizing interferometry. The technique is based on the observation of the scattered modulation as a particle traverses a region containing stationary interference fringes formed by two crossed coherent beams. Velocity of the particle can be recovered in the same measurement, a fact which has made this technique powerful and popular. The technique is valid only for particles > 3 μm. A variation of this technique was recently described (Technique 9, Table 4). It is based on projecting the image of a particle as it traverses a single beam onto a transparent screen with a grid with graduated spacing. A detector behind the screen will, therefore, produce a modulation of variable frequency and visibility. The grid separation where null visibility occurs signifies the particle size. The frequency will provide velocity information, much like particle-sizing interferometry. This technique has been used to size incandescent seed particles in a methane-air flame. A unique feature of this technique is that incandescent particles can be sized in situ without illumination and, therefore, offers obvious simplification in experimentation. The practical low limit is only 10 μm.

An extinction technique for single-particle sizing of very fine particles was attempted (Technique 13, Table 4). The technique was based on the extinction measurement of a tightly focused laser beam. It was projected that particles as small as 0.04 μm would be measurable from the consideration of signal-to-noise ratio (SNR) of extinction cross-section and shot noise of the electronic data acquisition system. A careful analysis of this technique shows that a tightly focused beam (f/2 or better) is required to reduce the integrated effect in extinction measurement. Also, at elevated particle speed (e.g., 10 m/s in the present program compared to < 1 m/s in Reference 56) and particle density (hence, data rate), the prominent but adverse effect due to the oscillation of the datum of the electronic high-pass filter, an instrument essential in this technique, will mask the observation of small particles with small attenuation. The net effect is that the actual usable range may be narrower than the projection based on SNR consideration only. The technique, however, can be very useful for sizing fine particles at low speed (< 1 m/s) and low density.

For meeting the objectives of the present program which requires the local measurements of soot size and number density in a complex flow, a single-particle sizing technique is required. Multiple-particle sizing techniques can only provide the average particle size if a certain particle size distribution is assumed or known a priori. The techniques based on scattering at various angles are preferred because the probe volume is conveniently reduced, thus

providing a better spatial resolution. The power spectrum technique enjoys the same merit in small probe volume but requires knowledge of local temperature, a quantity not easily obtainable. Among the six single-particle sizing techniques, only the cross-beam extinction offers the opportunity to approach the goal in particle size in the program. However, difficulties in instrumentation have virtually precluded its usefulness. A new technique is required to meet the present challenge.

E. EXTRACTIVE PROBES

Sample probes can be conveniently divided into two categories: point measurement and rake measurement. Point measurements are made at a single location in the flame or exhaust plane. Hence point measurement probes permit spatial differentiation of a flow field and present the possibility of flow field mapping. However, utilization of a point probe for measurement of overall flow field trends is time-intensive. Rake probes eliminate this problem by sampling at various points across the flow field, simultaneously. The drawbacks of rake probes is their inability to provide spatial differentiation and, unless very sophisticated, isokinetic sampling across the entire flow field.

For the present program, an extractive probe is required to validate the optical measurements, and to collect soot samples for composition analyses. Presented below are considerations in the design of soot extraction probes, followed by a summary of previous designs.

1. Design Considerations

a. Probe Size

With physical probe measurements in flow fields, the presence of the probe can perturb the aerodynamics and local heat transfer, and, ultimately, the data collected. As a result, probes with small physical dimensions are necessary to minimize probe-perturbation effects.

b. Probe and Sample Cooling

Cooling serves two purposes in sampling probes. First, and most important, probe cooling is necessary to maintain probe integrity in the harsh thermal environment of the flame. Secondly, to achieve a representative sample, the sample must be "frozen" in the state it enters the probe. Hence, reactions must be quenched upon entering the probe by designing for a rapid and uniform reduction of the sample temperature.

Convective quenching (Figure 2) incorporates a fluid passing adjacent to but separated from the sample stream. Although not the most rapid means of reducing the sample temperature, it is the easiest to incorporate into the probe design because of the concurrent need for cooling to maintain the probe integrity. The typical approach is to provide a concentric tube surrounding the sample line in which a fluid, usually water, is circulated to extract the thermal energy.

Aerodynamic quenching (Figure 2) relies on the expansion of the sample gas through a control flow area constriction as the means for reducing

the sample temperature. While providing the most rapid means of quenching, care must be exercised in the design and construction of the nozzle and expansion zone so that an internal shock wave is not created which would heat the sample to untolerable levels.

Dilution quenching (Figure 2) employs a relatively cool fluid injected directly into the sample stream. The diluent is usually a gas but water has been used successfully. Diluent quenching is quite effective but necessitates more complex probes and metering systems, and care must be taken to prevent any undesirable reactions or effects resulting from the mixing of the sample and diluent streams.

One undesirable side product with gaseous dilution is jetting of the dilution stream. The individual jets of dilution fluids, if strong enough, can disrupt the sample flow and force particulate toward the wall opposite the jet. The net result is an impaction of particulates in the probe. To minimize the effect, the diluent stream must be diffusely injected. The core of the jet stream should not extend beyond the centerline of the sample line. From jet theory and the known amount of gas needed to accomplish the quenching, an apropriate injection mechanism can be configured.

c. Isokinetic Sampling

When probing for particulates, the particle-laden gas sample should enter the probe with the same average velocity as the mainstream flow (i.e., isokinetic sampling) to prevent biasing of the sample mass concentration and size distribution. If the sampling velocity is too low, streamlines diverge away from the probe entrance as shown in Figure 3. Smaller particles are able to follow the changes in streamlines but not the larger particles; momentum carries the large particles along their original stream lines and into the probe. The result is a biasing of the size distribution towards larger particles as well as an increase in mass concentration (more large particles for a given sample volume). If the sampling velocity is too high, the streamlines will be drawn toward the probe, biasing towards smaller, streamline-following particles with a decrease in mass concentration (Figure 3).

Three methods are used to determine isokinetic sampling conditions. One approach utilizes a pitot-static probe to measure the dynamic pressure and, therefore, the velocity of the flow, assuming that the gas density can be established. Hot wire or laser anemometry can be utilized to map the velocity field. While these two methods reduce the number of knowns required, they are expensive and, in the case of hot-wire anemometers, not readily suitable for a reacting flow. The third approach, the pressure-null system, is the simplest in principle and can be readily incorporated into a probe design. Static pressure ports are located on the exterior surface of the probe and on the interior wall containing the sample stream. Since the static pressure is a function of the magnitude of the velocity, matching the pressures between ports (i.e., zero pressure differential) results in isokinetic sampling. The prime limitation with the pressure-null system is that only a matched-velocity magnitude is assured; there is no guarantee that the direction of the flow entering the probe is coincident with the direction of the free stream. The most extreme example is sampling within a recirculation zone where the direction of sampling could be 180° away from the direction of gas flow even though the magnitudes are equal.

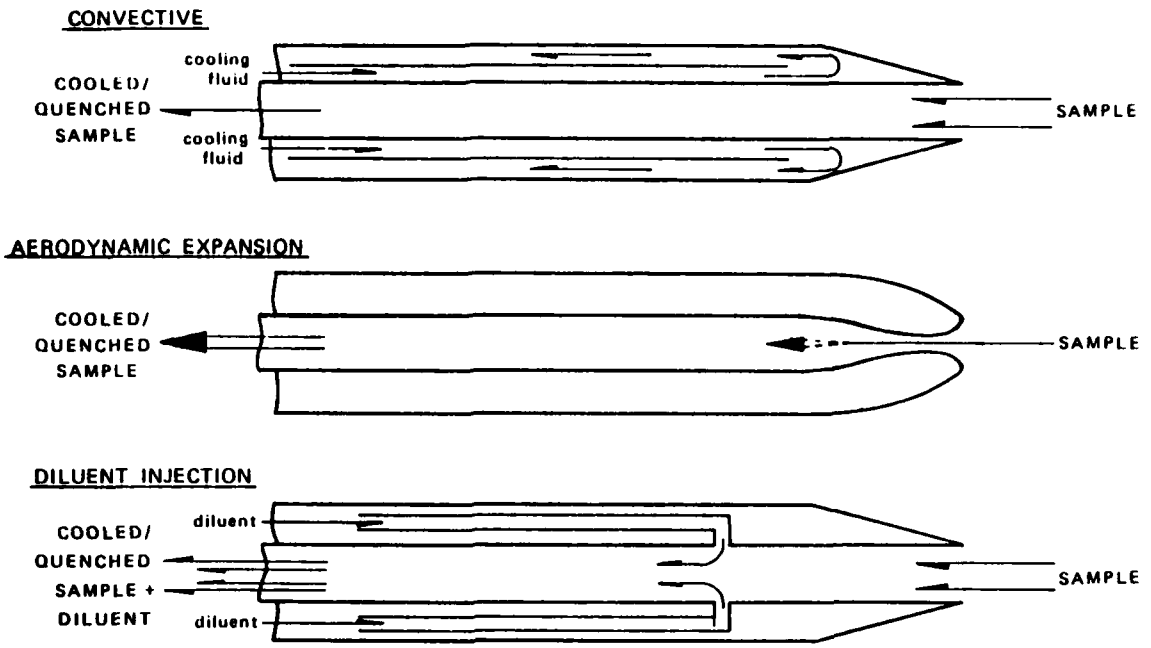

Figure 2. Sample Quenching

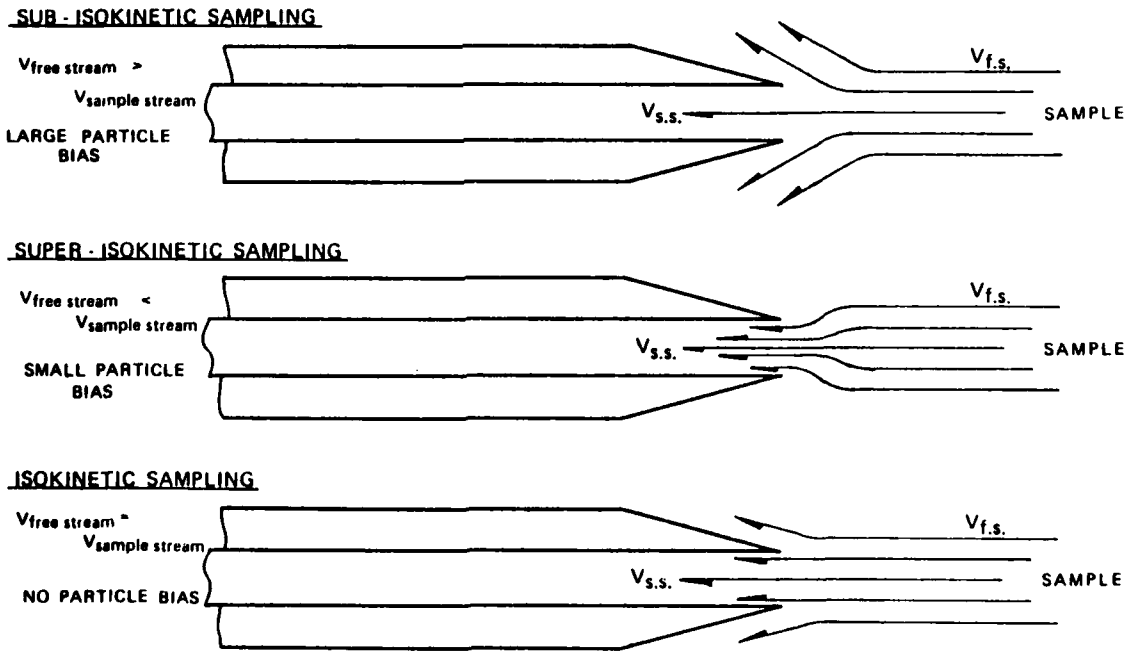

Figure 3. Isokinetic Sampling

Use of the pressure-null system for isokinetic sampling requires that the velocity, both magnitude and direction, of the free stream and sample stream be identical.

Anisokinetic sampling errors have been the subject of much inquiry. The magnitude of such errors increases with increasing size and density of sampled particulate, with decreasing gas viscosity, and with increasing deviation from isokinetic conditions (Reference 55). However, for soot particle sampling where the particulate size is typically less than 1 μm, inertial effects should be minimal (Reference 56) and hence, biasing from anisokinetic sampling should be negligible.

d. Prevention of Water Condensation

The exhaust sampling of any hydrocarbon fuel will contain water vapor, the amount depending upon the fuel composition and the fuel-to-air ratio of the combusting mixture. During quenching of the sample, water vapor condensation will occur if the dew point temperature of the sample is reached. Condensed water within the probe will adversely effect problems of particulate deposition and must be avoided by carefully controlling the temperature of the sample or by depressing the dew point of the sample. Typically, if the temperature of the sample throughout the sample train can be maintained above 50°C (125°F), condensation should not occur except in the most extreme (rich) conditions. Depressing the dew point (by diluting the sample) to below room temperature will insure that no water will drop out at any point in the sample line.

e. Prevention of Hydrocarbon Condensation.

As with water, lower sample temperatures increase the chance that heavier hydrocarbon species may condense during transit. The impact of such condensation is even more detrimental than with condensed water as condensed hydrocarbons can create sticky films within the sample line,as well as add to any gravimetric results. The prevention methods are the same as for water with one notable exception. The temperature of the sample should be maintained above 90°C (200°F).

f. Short Sample Probe Lengths

Particulate deposition upon sample tube walls represents a primary concern when samples of particle-laden flows are taken. These materials are lost to both weight concentration and size distribution analyses as well as creating another cleanup step. The simplest method to prevent wall deposition is to minimize the surface-to-volume ratio by enlarging the probe sampling tube diameter at the risk of perturbing the flow. If size constraints can accommodate a 1.27 cm (0.5 inch) O.D. probe, then the sample tube within the probe can be sintered metal with nitrogen perculation through the wall (Reference 57). This serves to prevent deposition as well as to provide sample dilution. Tight bends can promote deposition and must be avoided. Ideally the probe should be straight. However, a straight probe is often not suitable since it is necessary to transport the sample out of the exhaust stream. Bends placed in the probe should be gentle to minimize the ballistic deposition of particulate at the bend.

g. Thermophoresis

The final consideration for probe design is thermophoresis. Thermal gradients in the flow field can create non-negligible forces that act upon and transport the particulates from the hotter (sample stream) to the cooler (wall) regions. In particulate sampling probes, especially those requiring water cooling, this effect can be acute. Thermophoresis effects can be controlled or prevented by increasing the temperature of the sample tube wall, although this diminishes its quenching effect, and by diluting the sample stream.

2. Previous Probe Designs

A summary of various noteworthy probe designs is presented below.

a. SASS (Reference 58)

The primary function of the SASS probe is particulate sampling from boilers. As a result, the probe is not intended to be utilized in jet engine systems because of its size. However, it serves as an example of the considerations previously discussed.

The SASS probe is based on a point measurement design, and incorporates aerodynamic quenching of the sample. Probe cooling is not incorporated since it is not subjected to excessive temperature in the exhaust stack. In fact, the sample probe is electrically heated to prevent condensation. One aspect of the design is the presence of a tight bend close to probe entrance, which may create particle deposition problems. Isokinetic sampling is set using an S-type pitot tube to measure mainstream velocity and utilizing various entrance nozzles ranging from 3.2 mm (1/8 inch) to 12.7 mm (1/2 inch).

b. Westinghouse (Reference 59)

This probe was designed to assess the overall sooting characteristics at the exit plane of jet engines and, as a result, is based on a rake system with 24 separate inlets placed in a diamond configuration with individual nozzle diameters of 1.70 mm. No attempt to quench the sample within the probe is made, although the sample is diluted downstream of the probe in the sampling system. Probe cooling was not deemed to be necessary.

c. Purdue (Reference 60)

This probe was utilized by Purdue for point measurement of soot in a laboratory combustor. The probe is straight except close to the sampling end where a 3.4 cm (1.34-inch) offset in the probe is incorporated to accommodate radial traverses of the flame. The probe is 9.5 mm (0.375 inch) OD with 2.8 mm (0.125-inch) ID sampling tube. Water cooling of the probe serves the dual purpose of maintaining probe integrity and sample quenching. The flow rate of the water is adjusted to yield a probe exit temperature of approximately 80°C (175°F) to quench the sample and yet prevent water and

hydrocarbon condensation. Citing the difficulties with isokinetic sampling, no attempt is made to sample isokinetically. Estimates of the error induced by nonisokinetic sampling range from 6 to 12-percent. Finally, no attempt to dilute the sample was made.

d. Exxon (Reference 18)

This probe is similar to the Purdue design, and was constructed to measure soot production within a well-stirred laboratory. The sample line is 2 mm (0.079-inch) in diameter with constant cross section. The probe is water-cooled for integrity and sample quenching with the flow rate adjusted for 80°C (175°F) exit temperature, again to insure that no water or hydrocarbon condensation occurs. Isokinetic sampling provisions are not included.

e. MIT (Reference 61)

Another point measurement sample probe for laboratory use, this probe has also been used by others such as Reference 7. Physical dimensions of the probe are not cited, nor is mention made of whether isokinetic sampling was used. The probe incorporates a very novel sample quenching mechanism; approximately 1-percent of the total cooling water is directly injected into the sample stream. To quench the sample stream and prevent particle deposition, the direct injection of water literally "washes" the soot out of the probe and into a settling tank for subsequent filtration and analysis. The construction of such a probe is quite difficult because of the sealing and adjustable injection capabilities necessary.

3. Summary

For virtually all laboratory scale combustion systems, a small-diameter, single-point sample probe is the most appropriate configuration; a result of the need for spatial resolution combined with small perturbations. Water cooling of the probes is imperative if the flame zone is to be sampled. Beside retaining the probe integrity, water cooling is effective in quenching the sample through convective heat transfer. With caution, either aerodynamic or inert gas injection can be used to further promote quenching. The probe configuration is dependent upon the needs of the combustor; however, tight bends should be avoided.

F. SAMPLING SYSTEMS

Upon exiting the probe, the particle-laden sample must be conveyed to a filtering media for separation from the gas stream and subsequent analyses. Below, the considerations for a sampling train are delineated, followed by a summary of previous designs.

1. Sample Transport

The sampling system, or, more specifically, the pump, should at least have the capability of providing isokinetic sampling. A good rule of thumb is a maximum capacity of 150 to 200-percent of the isokinetic condition.

Restrictions and bends in the sample train should be avoided up to the filter train. Tight bends will cause particulate depositon due to ballistic impaction of the particles unable to follow the stream around the corner. Restrictions in the sample line are also responsible for particulate deposition for the same reason. After the sample is filtered, bends and restrictions are no longer of concern with respect to particulate deposition. Hence, all metering and flow switching devices should be downstream of the filters.

The condensation of water and heavy hydrocarbon species must be prevented, at least up to the filters and preferably throughout the entire system. As with the sample probe, condensation prevention can be accomplished through controlled sample temperature, dew point depression, or a combination of both. Heated sample transport lines leading from the probe to the filters and installation of filters within an oven are the two methods often employed for this purpose.

To achieve accurate soot mass concentrations, an accurate means of determining the volume of the extracted sample is necessary. While devices such as orifice plates and rotameters can be accurate, they only provide flow rate information and are therefore not amenable to volume determinations when transient or fluctuating flows are encountered. Ideally, an integrating flow meter device such as a wet test meter (WTM) or a dry test meter (DTM) should be used. These permit the actual volume sampled to a high degree of precision.

2. Sample Filtration

The filtration of the sample should occur as close to the probe entrance as possible. This reduces the amount of sample line surface area exposed to the sample and reduces the amount of particulate deposition.

The choice of a filtration substrate is dependent upon the types of analysis to be conducted. If morphological studies are to be conducted with scanning electron microscopy, membrane filters such as those offered by Gelman, Millipore, and Nuclepore should be considered because of the smooth surface upon which the particulate is deposited. However, fiberous filters are preferred for gravimetric analysis because of their retention. They are also less subject to electrostatic charge buildup than the membrane filters; charges which can disturb analytical weighing devices such as electromicron balances. If chemical analysis of the collected sample is to be performed, the filter material must be compatible with the chemicals being utilized so that the results are representative of the sample.

Filters have been the primary means of collecting particulate samples from gas streams. However, other means are available. Impact separation, for example, utilizes a circuitous path and particle momentum to collect particulate on glass slides and provide particulate size separation. Cyclone separators utilize centrifugal forces to selectively separate particulates. Both of these methods provide samples that are not imbedded in a filter and both are suitable for sampling high particle concentration flows where frequent filter changes due to clogging are impractical. The expense of these collectors is a drawback.

The filter holder must securely hold the filter and provide a means of diffusing the flow so that the soot is evenly distributed across the filter. This becomes important in analyses that require a representative sample such as morphology size distribution and some chemical work.

3. Previous Sampling Train Designs

a. SASS (Reference 58)

The EPA SASS train is utilized for more than just particulate sampling and, as such, is more complicated than most sample trains. However, it does incorporate many of the considerations previously discussed. Filtration is immediately downstream of the heated sample probe. Three cyclone separators with three ranges (1-3 μm, 3-10 μm, and < 10 μm), are arranged in series to provide sequential filtration. A filter is placed downstream of the cyclones to collect particles < 1 μm. The entire filtration bank is housed within an oven. This compact design minimizes the amount of sample transport line exposed to particulate matter. Downstream of the oven is a gas cooler and a set of impingers for measurement of other pollutants. Volume sampled is monitored with a DTM. The vacuum is created with a pair of high-capacity rotary vacuum pumps.

b. Westinghouse (Reference 59)

In this sample train, extracted sample is transported via a heated sample line to a dilution chamber where air is added to quench reactions and suppress the dew point. Two turntable devices hold five filters each to provide sequential sampling. Nuclepore membrane filters (17 mm Dia., 0.03 μm pore size) or Gelman AE fiber filters (142 mm Dia) are used. No monitoring of the sample volume is attempted.

c. Purdue (Reference 60)

This sample train is remotely located from the combustor. Transport between the probe and the remainder of the sample train uses a stainless steel sample line 10 meters (32 feet) long, and 4.6 mm (0.188 inch) ID heated to 150°C (300°F). To minimize deposition, all sample train bends are kept to a 20 cm (7.9 inch) minimum radius. The filter holder is a single-stage fixture constructed with recommendations given in SAE ARP 1179 to promote even sample distribution. Depending upon the ultimate analysis of the sample, either a 47 mm Millipore type HA 0.45 μm membrane filter (for gravimetric analysis) or 4.47 mm Nuclepore 0.08 μm membrane filter (for microscopic analysis) is fitted. Volume is monitored downstream of the filters with a Rockwell Model 175S DTM. The system also incorporates a sample bypass so that the system can remain operational while filters are changed and a nitrogen purge to back-flush the sample line and probe of any deposits that collected during the run.

d. Exxon (Reference 18)

As with the sampling probe, the Exxon sample train is similar to the Purdue sample train. A sample transport line-heated 150°C (300°F) is used between the probe and filters,which are housed in an oven maintained at 150°C (300°F). Two filters are placed in series for sizing of the particulate, the

first stage of a 5 m pore size millipore filter. The second stage uses a 0.3 m Gellman AE filter. Sampled volume is determined with a WTM. A metal bellows pump driven by a 1/4-horsepower motor is used for sample extraction.

4. Summary

The sample system should position the filtration system as close to the probe inlet as possible to minimize the chances of particulate deposition. The path from the probe to the filtration system should be as straight and unobstructed as possible. All flow switching and metering of the flow should be located downstream of the filter media, and the metering should incorporate either a dry test or wet test meter because of high accuracy and integrating quality. The pump should be capable of twice the capacity necessary for isokinetic sampling, even though the necessity of isokinetic sampling has not been demonstrated.

In both the probe and sample system, care must be exercised to prevent the condensation of water and hydrocarbons. Dilution injection, heated sample lines, and the housing of filters in ovens are all means to prevent the condensation.

G. SOOT COMPOSITION

The composition of soot particles is not only important in elucidating the mechanisms responsible for soot formation, but also in identifying the presence of polynuclear aromatic hydrocarbons (PAH) which are known to be carcinogenic. Compound identification, however, first requires the collection, extraction, and isolation of the PAH fraction before an accurate analysis can be carried forth. Each stage of the analysis needs to be carefully assessed for its affect on the sample composition, as PAH not only have relatively high vapor pressures that can result in significant losses of sample, but can also photodegrade which alters the chemical composition. Once the PAH have been isolated, a number of methods are available for their analysis.

1. Sample Collection

In general, PAH are adsorbed in the atmosphere on suspended particulate matter having an average diameter of less than 10 m (Reference 62). In fact, the size distribution of PAH containing particles from coke-oven emission sources has shown that the largest amounts of PAH are adsorbed on particles in the diameter range of 0.9 to 3 μm (Reference 63). The most common method of particle collection in this range is by filtering a metered volume of air through a porous filter possessing an appropriate size limit and efficiency. Electrostatic precipitators, however, have also found limited application in the collection of samples for environmental assessment studies related to chemical composition. Impactors and cyclones are also frequently used in particle sizing studies, but have relatively low collection efficiencies in the submicron size range.

Fiber filters are ideal because of their relatively large sample capacity, low pressure drop, and compatibility with organic solvents. Particle collection with fiber filters involves diffusion, direct interception and inertial impaction (Reference 64) with the overall collection efficiency being a

function of these three parameters. Lundgren and Gunderson (Reference 65) tested the effects of loading, velocity, particle size and temperature on the efficiency of microquartz fiber filters. Filter penetration of 0.01 μm particles was found to decline significantly from 0.15-percent to near zero with an aerosol loading of only several micrograms per square centimeter. The effects of particle size and velocity are interrelated with no effective penetration seen with velocities less than 5 cm/sec or aerosols with a mass median diameter greater than 0.8 μm. Higher velocities with smaller particles, however, exhibited proportional increases in filter penetration. Increased temperature had the predictable effect of increasing the particle collection efficiency since the submicron particles are collected mainly by diffusion,which becomes more effective with increasing temperatures. However, particles with vaporization points below the filtering temperature can vaporize, pass through the filter, and subsequently condense,if cooled below the vapor dew point. Some of the drawbacks associated with filtration media are the catalytic effects on the degradation of some PAH (Reference 66) as well as the inherent variability of the elemental background levels in different filters or filter aliquots which can interfere with the sample analysis.

A study of the collection efficiency of quartz-fiber filters for PAH at 37°C and 20-percent relative humidity has indicated that over 90-percent of the PAH less volatile than pyrene are recovered on the filter whereas only 25 to 50-percent of the PAH more volatile than pyrene are collected (Reference 67). These findings are consistent with theoretical considerations (Reference 67), which indicate that quantitative absorption of PAH can only be expected below 30°C with an increasing fraction of PAH existing in the vapor state at higher temperatures. The rate and extent of absorption at a given temperature is also enhanced with increased mass emissions and decreased particle size due to the increase in the frequency of collision of vapor phase molecules with particle surfaces. Thus, the collection of soot from combustion systems requires an adsorbent sampler downstream of the filter at a temperature low enough to efficiently retain the PAH not held on the filterable particulates, but high enough to preclude the condensation of water.

Macroreticular resins are frequently used for the adsorption of these vapor-phase PAH with Amberlite XAD-2® and Tenax-GC® (Figure 4) being the most popular. Tenax-GC® has been found to have several disadvantages including incompatibility (soluble) with most nonhydrocarbon solvents (Reference 68), less capacity for lower boiling compounds than Amberlite XAD-2® (Reference 69), and persistent decomposition into diphenyl quinones (Reference 68). Amberlite XAD-2® resin has been recently found to produce mutagenic decomposition products when exposed to NO and NO_2, which can interfere with the gas chromatographic analysis of the vapor phase organics from combustion samples (Reference 70). These resins, in spite of their disadvantages, have been found to provide better than 90-percent recoveries for a variety of PAH (References 66 and 70).

2. Extraction and Fractionation

PAH of molecular weights less than approximately 300 are soluble in numerous organic solvents with benzene being one of the most efficient (Reference 66). Benzene, cyclohexane and dichloromethane have achieved widespread use, although other solvents have also been used, including acetone, chloroform, ether, hexane, isooctane, pentane and tetrahydrofuran.

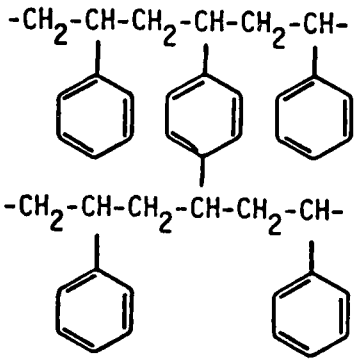

XAD-2

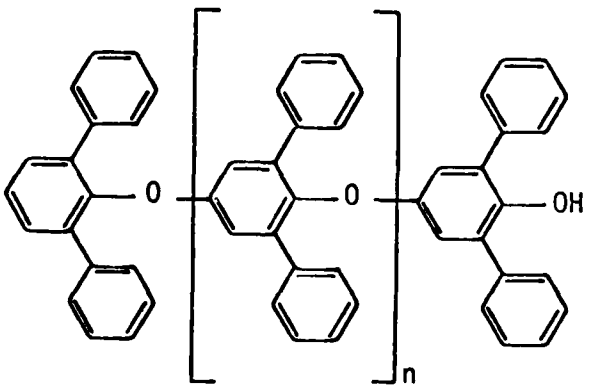

TENAX-GC

Figure 4. Chemical Structure of Amberlite XAD-2® and TENAX-GC® Polymer Sorbent Resins (Reference 70)

Dichloromethane, however, has been selected by the Environmental Protection Agency (Reference 71) for Level 1 organic analysis of SASS train samples based on its good solvent properties and high volatility. Solvent recoveries of PAH in general, however, have indicated that four-ring and larger PAH may be incompletely extracted (Reference 72). The attainment of accurate results thus becomes dependent on the determination of the extraction efficiencies for the removal of each organic compound from the sample. The task becomes quite formidable in the case of environmental analyses where hundreds of organic compounds are analyzed simultaneously.

The most common method has been Soxhlet extraction in which a sample is placed in a Soxhlet apparatus containing organic solvent and refluxed for several hours. The extraction times for particulate matter on which PAH are strongly adsorbed, such as carbon black (Reference 73), frequently run between 20-30 hours (Reference 74). An alternative to Soxhlet extraction is ultrasonic vibration at room temperature for which 95 to 98-percent recoveries of PAH from air particulate carbon have been reported (Reference 75). Ultrasonic vibration allows for faster extraction than with the Soxhlet apparatus, although there is controversy over which is the more effective.

Extraneous materials are frequently extracted along with the PAH as the extraction procedures are not selective, necessitating a fractionation procedure. Solvent partitioning is frequently used to remove compounds interfering with the analysis of PAH by partitioning the original solution with a second, immiscible solvent. If the partition coefficients for PAH differ from those of the other materials present, they will be preferentially concentrated in one or the other layer. Several solvent pairs have been used with dimethyl sulfoxide (DMSO) showing the most favorable partition coefficients for the extraction of PAH from alkane solvents (Reference 76). Three successive extractions from the original alkane solution into DMSO, followed by three successive back extractions from DMSO/water into n-pentane, yield: the aliphatic hydrocarbons in the original alkane; the alcohols, acids and phenols in the DMSO/water; the PAH, phthalates and bases in the final pentane solution (Reference 77). As the partition coefficients are governed by the extent of the interaction between the sulfur atom and the aromatic system, substituted aromatic compounds can yield unfavorable partition coefficients, possibly due to the groups blocking a region of high-electron density (Reference 77). Once again, accurate quantitative results entail the determination of extraction efficiencies for each organic compound.

3. Analytical Techniques

A variety of methods exist which can resolve complex groups of PAH compounds. The classical techniques of column adsorption, paper and thin-layer chromatography have been used to separate these complex PAH mixtures into simpler fractions prior to further separation by higher resolution techniques. The superior performance recently attained with high-performance liquid chromatography (HPLC), however, has almost completely replaced the use of these classical techniques except for the isolation of the PAH fraction from other interfering compounds. Advances in technology of chromatographic columns have made gas chromatography (GC) the most effective method for resolving PAH content (Reference 76), although HPLC is necessary to resolve high molecular weight PAH compounds posessing volatilities too low for GC applications (Reference 78).

The number of possible isomers within a series of PAH compounds increases significantly, creating resolution requirements handled best by capillary GC. The powerful, yet sensitive, methods of detection (flame-ionization and mass-spectroscopy) used in combination with capillary GC make this approach capable of trace analyses. A review of column and instrument parameters on the analyses of PAH (Reference 79) allows further optimization of the resolution obtainable with capillary columns as well as the limits of detection. Complementary information for the positive identification of resolved components is also provided by the retention data from the chromatographic system. Retention indices based on the standard series of n-alkanes, however, proved unreliable, necessitating the development of a new chemically similar homologous series of PAH. A system based on naphthalene, phenanthaene, chrysene, and picene has been developed which is capable of identifying over 200 PAH (Reference 80).

H. COMPLEX FLOW MODEL COMBUSTOR

Gas turbine combustors are used extensively in test stands to evaluate combustor performance and fuel performance. Diagnostic access, however, is restricted due to the (1) elevated pressures at which the combustor is operated and attendent heavy casings required for containment as well as remote operation, and (2) limited availability of side-wall optical paths. As a result, measurements are confined to the input (e.g., fuel flow, air flow, air temperature) and exit plane (e.g., exhaust temperature, exhaust composition, exhaust velocity).

The demand for an increased understanding of gas turbine combustor performance requires that measurements be made within the combustor. Hence, the UCI Combustion Laboratory (e.g., References 81 and 82) and others (e.g., Reference 83) have been engaged in the development of model complex flow combustors that encompass the basic flow field characteristics of practical devices yet satisfies the following criteria:

- Good optical access for advanced laser diagnostics.
- Stabilized by zone of strong backmixing.
- Capable of swirl inlet.
- Axisymmetric and clean, well-defined boundary conditions to accommodate modeling.

Examples of candidate geometries are presented in Figure 5. The centerbody combustor (CBC) configuration was introduced by the Fuels Branch at the Air Force Wright Aeronautical Laboratories (Reference 83) in a 25.4 cm (10-inch) duct design. For the present program, the UCI Combustion Laboratory adopted the CBC geometry and made two notable changes. First, a 1/5-scaled version was designed and built to accommodate the capacity of the laboratory air supply system. Second, swirl was added and evaluated to provide a zone of backmixing representative of gas turbine combustors.

a. Centerbody

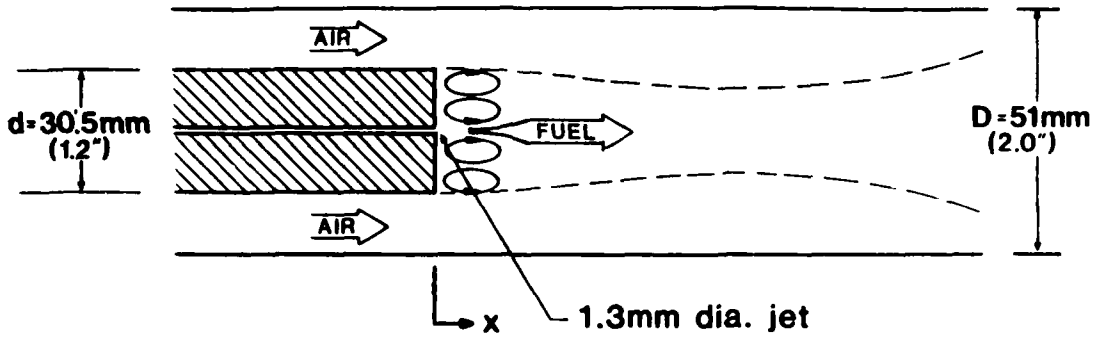

b. Swirl-Stabilized Centerbody

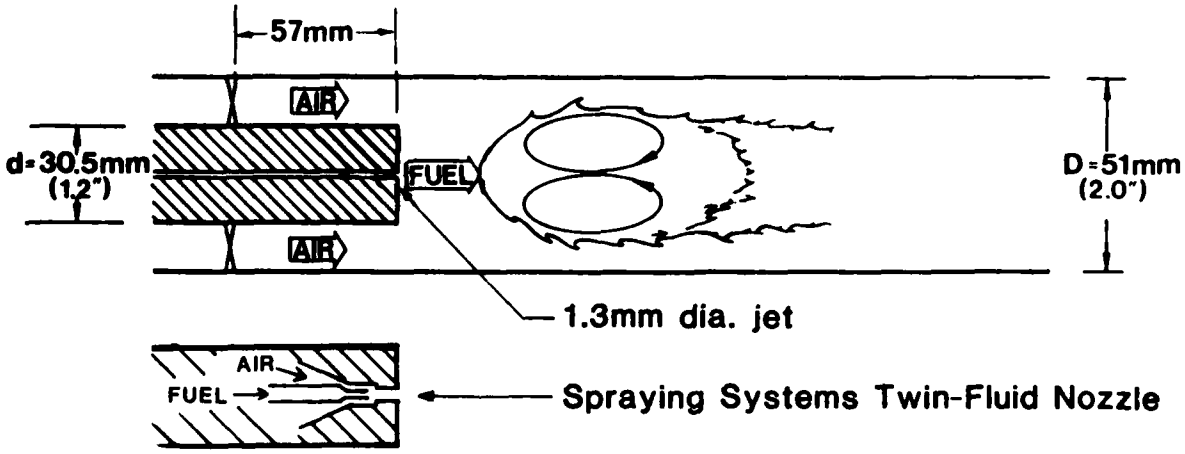

c. Dilute Swirl

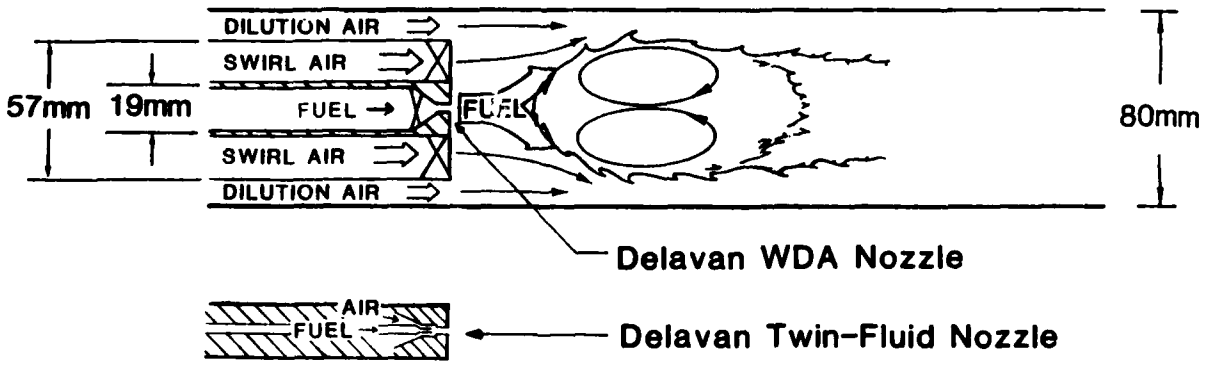

Figure 5. Candidate Complex Flow Model Combustor (References 81 and 82)

In parallel with the present program, the UCI Combustion Laboratory evaluated, under Air Force Office of Scientific Research (AFOSR) funding, the suitability of the CBC as a model combustor. Various limitations were identified (Reference 81), the most notable of which was exhaust plane suction for a variety of run conditions, and a novel geometry, dubbed the Dilute-Swirl Combustor (DSC), evolved (Reference 82). The DSC geometry (Figure 5c) features dilution air to simulate the role of radial air jets in diluting and containing the zone of recirculation within a practical combustor (Figure 1). As a result of the attractive features and performance of the configuration, the DSC was adopted as the model test bed for the last year of the present program.

SECTION III

APPROACH

A. OVERVIEW

To meet the objectives of the present study, an approach was adopted that tested and applied the methods developed at select stages of their evolution. The sequence is outlined in Table 5. The optical system was first designed for large-particle measurements ("Large-Particle Optical System") and tested in the swirl-stabilized centerbody combustor (CBC) in a study of extractive probe perturbation. During this study, the "Prototype" extractive probe was also tested and evaluated. Second, while the optical system was expanded to include small-particle resolution, a "Refined" version of the extractive probe was evaluated, along with the newly evolved method of soot physical and chemical analyses to address the effect of fuel molecular structure and additives on soot production and chemical composition in the swirl-stablized CBC. Third, the development of the Dilute-Swirl Combustor (DSC) and expanded optical probe ("Expanded-Particle Optical System") culminated in a concluding study in which in-flame optical measurements were made for a variety of operating conditions in the DSC configuration.

B. FUELS

Both gaseous and liquid fuels were selected for the program. The liquid fuels were introduced as prevaporized vapor, as well as liquid sprays. Prevaporization was employed to address soot formation in the absence of the thermal and transient effects associated with liquid droplet evaporation and droplet burning.

The gaseous fuels selected were propane and ethylene. Propane is common for fundamental combustion studies due to availability and kinetic behavior similar to high hydrocarbon fuels. Ethylene was elected in anticipation of a higher propensity to form soot. Isooctane was selected as the baseline liquid fuel as it represents a major component of JP-8 and serves as the reference fuel in the ASTM Smoke Point Test. To assess the validity of the ASTM Smoke Point Test and the effect of fuel molecular structure on soot composition, blends of isooctane with either decalin (decahydronaphthalene), toluene, tetralin (1,2,3,4-tetra-hydronaphthalene) or 1-methylnapthalene were prepared. These particular liquid hydrocarbons were chosen as they represent both a broad variation in fuel molecular structure (Table 6) and classes of compounds found in petroleum and synthetic fuels. Shale JP-8 was also chosen to provide a comparison with a chemically complex aviation fuel having specifications projected to be similar to interim fuel specifications for future fuels (Reference 1). Mixtures of pure hydrocarbon liquids were chosen to control and ensure the identification of the fuel composition.

TABLE 5. APPROACH

Step Methods Development (Section IV)	Experiments (Section V)		
	Topic	Methods Employed	Literature Citation
1. Optical Probe: Large-Particle Extractive Probe: Prototype Analyses: SEM Gravimetric Combustor: Swirl-Stabilized CBC			
2.	A. Large-Particle Optical System • Verification and Validation • Extractive Probe Perturbation Assessment	Optical Probe: Large Particle - Extractive Probe: Prototype Analyses: SEM Combustor: 51mm (2-inch) Swirl-Stabilized CBC	Reference 84 Reference 85 Reference 86 Reference 87
3. Extractive Probe: Refined Analyses: CHN, AA, PAH			
4.	B. Fuel Molecular Structure and Additive Effects Study • Polycyclic Aromatic Hydrocarbons • Ferrocene • ASTM Smoke Point	Extractive Probe: Refined Analyses: Gravimetric, SEM CHN, AA, PAH Combustor: 80 mm (3-inch) Swirl-Stabilized CBC	Reference 88
5. Optical Probe: Expanded-Particle Combustor: Dilute-Swirl DSC			
6.	C. Expanded-Particle Optical System • Verification and Validation • Optical Probe and Combustor Performance	Optical Probe: Expanded-Particle Extractive Probe: Refined Analyses: Gravimetric, SEM Combustor: 80 mm (3-inch) DSC	

Nomenclature: AA (Atomic Absorption Spectrophotometry); CBC (Centerbody Combustor);
CHN (Carbon/Hydrogen/Nitrogen Analysis); DSC (Dilute Swirl Combustor);
PAN (Polycyclic Aromatic Hydrocarbon Analysis); SEM (Scanning Electron Microscopy)

TABLE 6. FUEL MOLECULAR STRUCTURES AND PROPERTIES

Fuel	Structure	Molecular Weight	Boiling Point °C
Isooctane (2,2,4 Trimethylpentane)	$(CH_3)_2CHCH_2C(CH_3)_3$	114.23	114.8
Decalin (Cis) (Decahydronaphthalene)	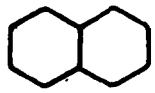	138.25	195.6
(Trans)		138.25	187.2
Toluene	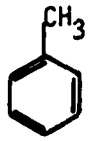	92.15	110.6
Tetralin (1,2,3,4 Tetrahydronaphthalene)	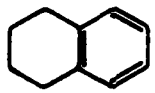	132.21	207.6
1-Methylnaphthalene	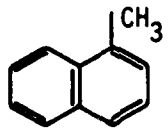	142.20	244.6

SECTION IV

METHODS DEVELOPMENT

A. OPTICAL PROBE

Based on an evaluation of the background provided in Section IID, the following four optical techniques were selected for optically sizing soot particles:

(1) Particle-size interferometry: To measure particles larger than 2.4 μm in diameter.

(2) Small-angle intensity ratio: To monitor particle sizes in the range $0.4 \leq d \leq 2.4$ μm.

(3) Large-angle intensity ratio: To resolve particle sizes in the range $0.08 \leq d \leq 0.6$ μm.

(4) Polarization intensity ratio: To resolve particle sizes greater than 0.05 μm in diameter.

Large-Particle Optical System

Expanded Particle Optical System

The optical probe was first developed and applied as a "Large-Particle Optical System" (see Table 5, APPROACH) and later developed into an "Expanded-Particle Optical System". The choice of the techiques was based on two criteria: (1) to allow for a wide dynamic range, and (2) to minimize the overlap region between any of the techniques. The optical configuration and limitations of each technique are presented in Table 7. The theoretical analysis of each diagnostic method is addressed below, including a detailed description of employing the theoretical analysis in interpreting the experimental data. Second, the experimental apparatus is detailed.

1. Theoretical Aspects

a. Particle-Sizing Interferometry

For large values of the nondimensional size parameter α defined as

$$\alpha = \frac{\pi d}{\lambda} \quad , \tag{1}$$

the scattering of electromagnetic radiation is separable into the simplified theories of diffraction, refraction and reflection. For particles larger than $\alpha > 15$, diffraction becomes insignificant at angles greater than 10°. In such cases, signal visibility can be used to size the particles. The complex fields scattered from each of the two crossed beams, Figure 6a, are taken separately and designated E_{s1} and E_{s2}. Therefore, the total scattered field is

TABLE 7. PARTICLE SIZING TECHNIQUES

Technique	Basis	Capabilities	Comments
Particle-Sizing Interferometry	Forward Scatter 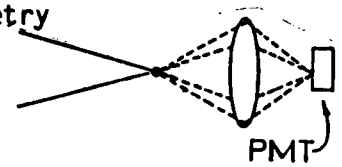	• Particle Sizing 3 μm to 200 μm • Particle Velocity • Gas Velocity • Individual Particles • Particle Mass Flux	• Limited to Lower Number Density • Relatively Independent to Index of Refraction • Equivalent Sphere for Randomly Oriented Irregular Shape
Scattering-Intensity Ratioing	Near Forward Scatter 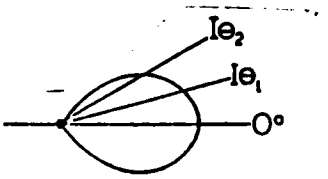	Large Angle: 0.08 <d<0.6 μm Small Angle: 0.4 < d < 2.4 μm	• Applicable to High Number Density Environment • Minimizes Refractive Index Effects • Equivalent Sphere for Large Number of Randomly Shaped Particles
Polarization Ratioing	Scattering at Large Angles 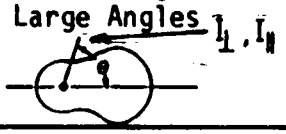	• Particle Sizing 0.05 m or Larger • Multiple Particles	• For Very High Number Densities, $10^6/cm^3$ or Greater

$$E_s = E_{s1} + E_{s2} , \qquad (2)$$

and the intensity is

$$I = E_s^* E_s , \qquad (3)$$

Therefore, the intensity of the two beams will be

$$I = \frac{1}{n} \left(|E_{s1}|^2 + |E_{s2}|^2 + 2 |E_{s1}| \, |E_{s2}| \cos \beta \right) \qquad (4)$$

where β is the phase angle between the scattered fields.

The Doppler signal may be regarded as a pedestal dc component. Superimposed on it are the Doppler bursts as shown in Figure 6b. The pedestal or dc component of the signal is

$$2 \int_A \iint |E_{s1}| \; |E_{s2}| \cos \beta \, dA \quad , \tag{5}$$

where the integration is being done over the collection lens area. The Doppler bursts are viewed as

$$\int_A \iint (|E_{s1}|^2 + |E_{s2}|^2) \, dA \quad . \tag{6}$$

Signal visibility is defined as the magnitude ratio of the two signals. Thus

$$V = 2 \frac{\int_A \iint |E_{s1}| \; |E_{s2}| \cos \beta \, dA}{\int_A \iint (|E_{s1}|^2 + |E_{s2}|^2) \, dA} \tag{7}$$

or simply

$$V = \frac{I_{max} - I_{min}}{I_{max} + I_{min}} \tag{8}$$

where I_{max} and I_{min} are illustrated in Figure 6b.

The field intensity is related to the scatterer diameter through a complicated function which can be derived from the general Lorentz-Mie theory. Typical theoretical visibility curves are shown in Figure 6c.

b. Intensity Ratioing

When a beam of light passes through a mixture of gases containing aggregates of particles (e.g., soot or droplets), it interacts with both the gas molecules and the particles, and is reemitted or diffracted out of the direction of the beam (Figure 7). The part of light which is diffracted is referred to as scattered light. The incident and scattered light may be fully characterized by their intensity, polarization states and phase functions. For randomly distributed scatterers, as is the case in most combustion systems, the total scattered light is regarded as the incoherent superposition of individual contributions. In general, the intensity of the scattered light I_s at a certain scattering direction Θ (defined as the azimuthal angle between the incident and scattered light), state of polarization and spectral region, are proportional to the incident light intensity $I_L(\lambda)$, total number of scatterers per unit volume N, and the spectral differential scattering cross section $\frac{d\sigma}{d\Omega}$. Thus

$$I_s(\Theta, \lambda, d) = I_L(\lambda) \, N\ell \int_{\Delta\Omega} \frac{d\sigma_\lambda(\Theta, d)}{d\Omega} d\Omega \quad , \tag{9}$$

a. Beam Crossing

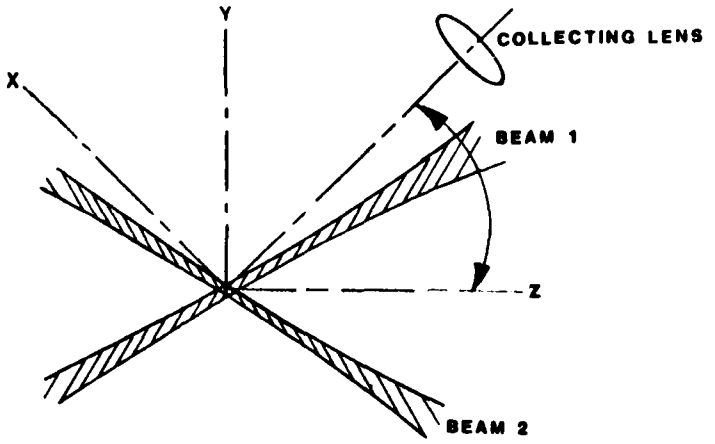

b. Doppler Signal

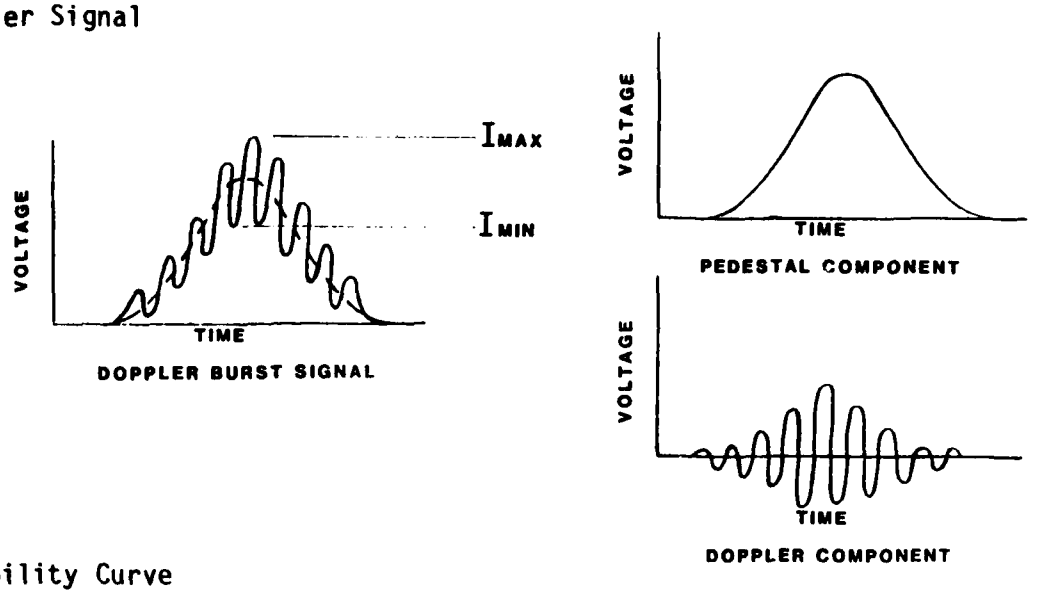

c. Visibility Curve

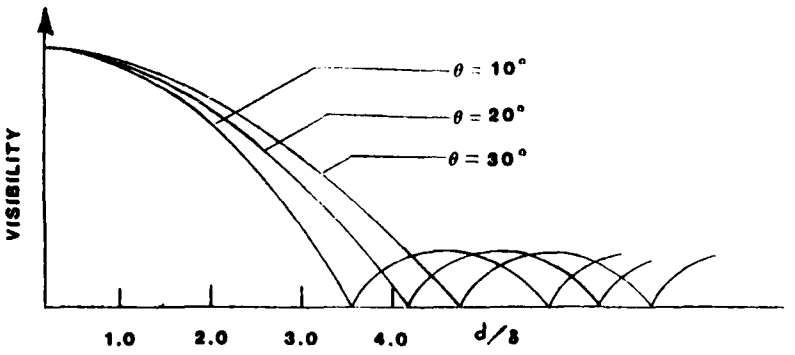

Figure 6. Particle-Sizing Interferometry

where d is the scatterer diameter, assuming the scatterers to be spherical in shape with known extinction coefficients, and ℓ is the length along the incident beam from which scattering is observed.

For broadband detection, $I_s(\theta, \lambda, d)$, $I_L(\lambda)$, and σ_λ may be integrated over the bandwidth of the detector to yield

$$I_s(\theta,d) = I_L N\ell \int_{\Delta\Omega} \frac{d\sigma(\theta,d)}{d\Omega} d\Omega \quad , \tag{10}$$

where we used the fact that the line source is narrow compared to the detection process.

The differential scattering cross section, which carries all the information about the polarization state and angular dependence of the scattered light, in addition to the scatterer diameter section, is derived by solving Maxwell's equations for the incident and scattered electromagnetic waves. For a collection of spherical dielectric scatterers, the differential scattering cross section will be

$$\frac{d\sigma_\lambda}{d\Omega} = \frac{k^4}{E_0^2} \left| \sum_j \left[\vec{\epsilon}^* \cdot \vec{P}_j + (\vec{n} \times \vec{\epsilon}^*) \cdot \vec{M}_j \right] e^{i\vec{q}\cdot\vec{x}_j} \right|^2 \tag{11}$$

where k is the wave number defined as $k = 2\pi/\lambda$, E_0 the incident electric field amplitude, $\vec{P}_j$ and $\vec{M}_j$ the vectorial electric and magnetic dipole moment of scatterer j, $\vec{n}$ the unit vector in the direction of observation, and $\vec{\epsilon}^*$ the complex conjugate of the polarization tensor. The electric and magnetic dipole moments are proportional to the cube of the scatterer diameter. The angular dependence of the scattered wave is embedded in the electric and magnetic polarization. Finally, it is important to notice that the angular distribution of the scattered light is a unique function of the scatterer diameter.

To summarize, one may regard the scattered light to be a function of the scatterer diameter d, wavelength λ, extinction coefficient k, scattering angle θ, polarization angle ϕ, and incident beam intensity I_L such that

$$I_s = f(d, \lambda, \kappa, \theta, \phi, I_L) \quad , \tag{12}$$

where the functional relationship can be recovered from Equations (2) and (3). The beauty of the intensity ratio techniques is that the range of their applications is the only limitation, unlike particle-size interferometry where the fringe size is a serious limitation to smaller particles.

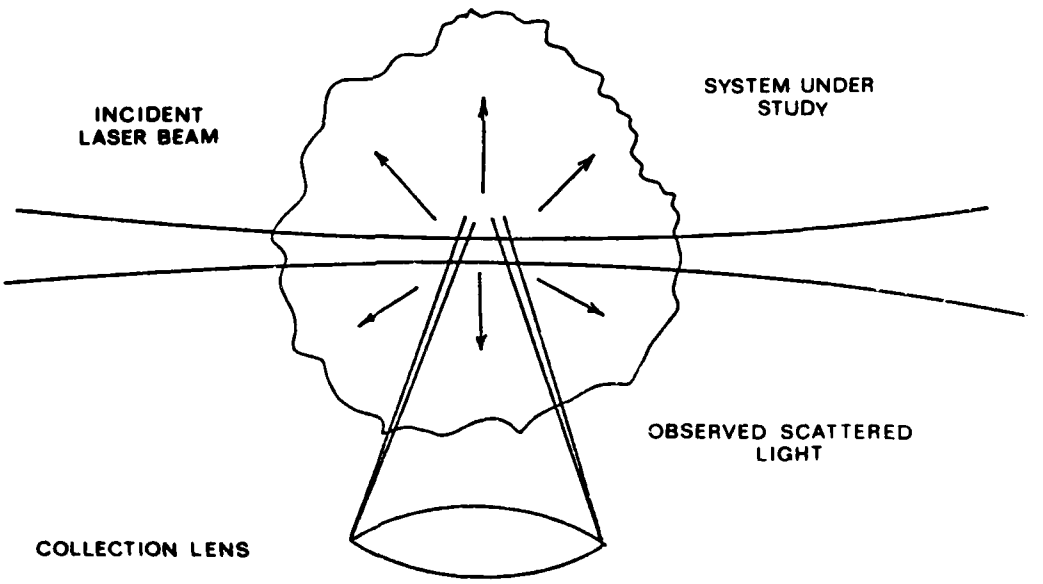

Figure 7. Intensity Ratioing

c. Polarization-Intensity Ratioing

The Lorentz-Mie theory of scattering and extinction of electromagnetic waves by small spherical particles may be applied to the flame to determine the particle sizes. If the incident light is polarized perpendicularly to the scattering plane defined by the directions of incident and scattering beams, then

$$I_{s\perp}(\lambda, \theta, d) = I_{L\perp}(\lambda) N \ell i_{\perp}(\theta, d, \lambda) \quad , \tag{13}$$

where

$$i_{\perp}(\theta, d, \lambda) = \int_{\Delta\Omega} \frac{d\sigma_{\lambda}(\theta,d)}{d\Omega} d\Omega \quad , \tag{14}$$

similar treatment can be followed for the plane of polarization parallel to the scattering plane. Therefore

$$I_{s//}(\lambda, \theta, d) = I_{L//}(\lambda) N \ell i_{//}(\theta, d, \lambda) \quad . \tag{15}$$

A treatment similar to that imposed in the previous section for intensity ratioing can yield

$$I_{s\perp}(\theta, d) = I_{L\perp} N \ell i_{\perp}(\theta, d) \quad , \tag{16}$$

and

$$I_{s//}(\theta, d) = I_{L//} N \ell i_{//}(\theta, d) \quad . \tag{17}$$

For a constant index of refraction and detection at relatively large azimuthal angle, the ratio of $I_s / I_{s//}$ is regarded as a unique function of particle size. The major advantage of this method is that it has the capability to detect a wide range of very small particles with relatively large densities.

d. Data Analysis

The strategy is to convolute the experimental measurements of polarization ratio, intensity ratio, or visibility to actual size by using the numerical results obtained from the Mie or Lorentz-Mie scattering theory. The visibility results obtained from the numerical solution of Equation(7) for particle size versus visibility are used to interpret particle-size interferometry. All the numerical results of the intensity ratio techniques are based on the solution of Equations(9-12)for the particle size-versus-intensity distribution. The numerical solution must consider the integration of the scattered light over the area of the collection lens. The numerical analysis of polarization ratioing is based on the solution of Equations(13-17). These numerical results are integrated in a software routine which is used for data acquisition and data reduction.

2. Experimental Aspects

The experimental apparatus developed for the present study to size soot particles comprises two components: an optical system (which will be first described), and a data acquisition system. The section concludes with a description of the system fine adjustment and, finally, the experimental uncertainties.

a. Optical System

Figure 8 illustrates the basic building blocks for the optical configuration used for the different techniques. A 5-Watt Spectra-Physics 165 argon-ion laser,operating in the multiline mode,is used for the source of light. The laser lines are separated by a dispersion prism. The green line (5145°A). and blue line (4880°A), are then directed to the focal volume through separate optical paths.

Figure 9 illustrates the optical system used for particle-size interferometry. The green beam is partitioned into two equal-intensity beams with a path matched beam splitter as shown in Figure 10. A system of mirrors is used to recombine the beams,which are then focused to a common point in the flow field to generate the required interference fringe pattern. The scattered light is collected by a 100 mm diameter F/2 lens and focused to photomultiplier tube PMT-5. The tube is of the type EMI 9781, having a quantum efficiency of 12-percent at the 5145°A wavelength. The supply voltage for PMT-5 is about 350 volts.

Figures 10 and 11 show the optical treatment for the small-and large-angle intensity ratio techniques respectively. The blue laser line is focussed to 110 m in diameter using a 50 mm diameter F/5 focusing lens. For small-angle intensity ratio, the scattered light is collected by a single-lens system which is masked except for small annular ring openings. The annular ring openings are selected to transmit the scattered light at two chosen scattering angles, in this case 10° and 5° off the laser axis. These masks also serve to effectively limit the length of the measurement region,resulting in higher spatial resolution The collected light is then focused to two RCA 8575 photo-

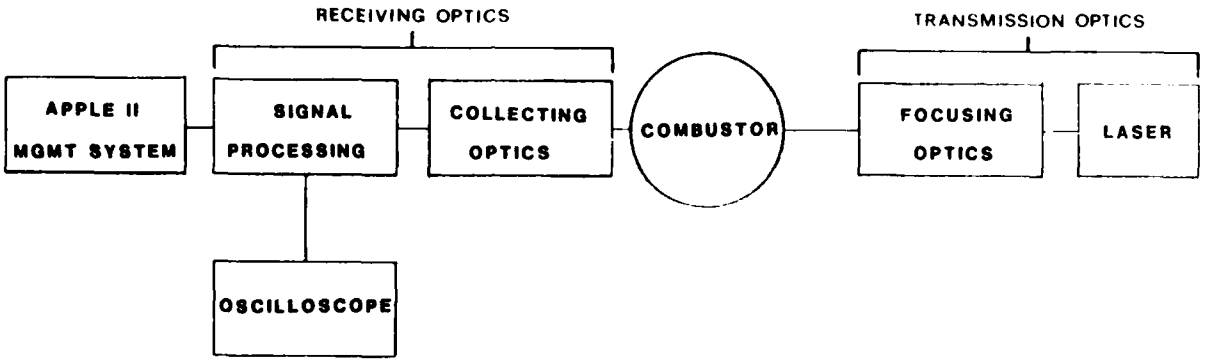

Figure 8. Optical Configuration

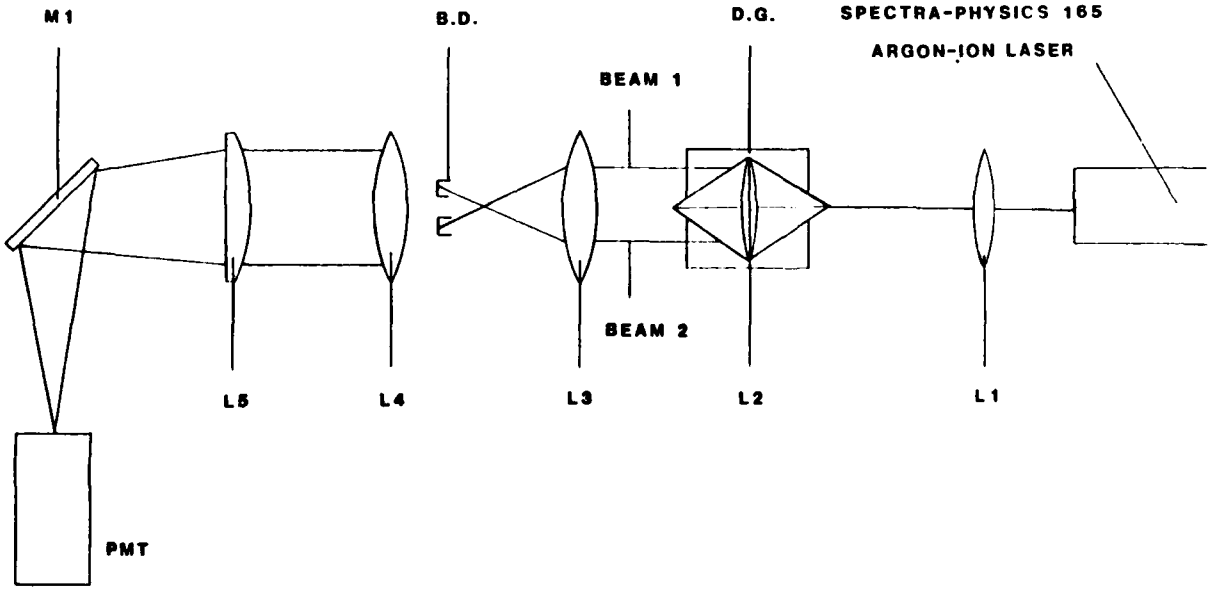

Figure 9. Particle-Sizing Interferometry

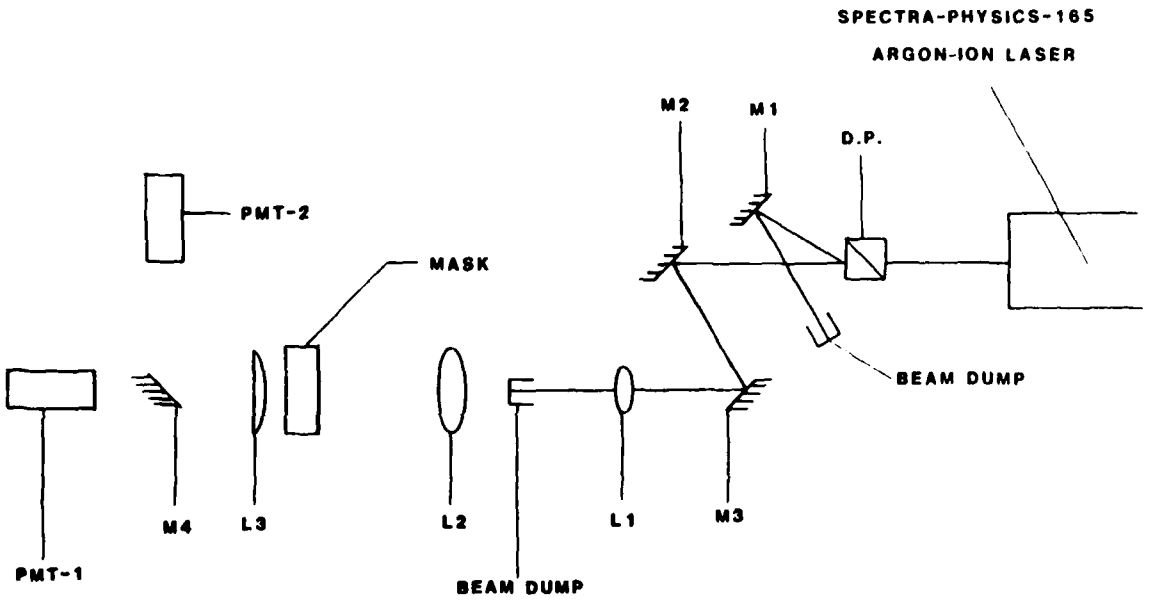

Figure 10. Small Angle Intensity Ratioing

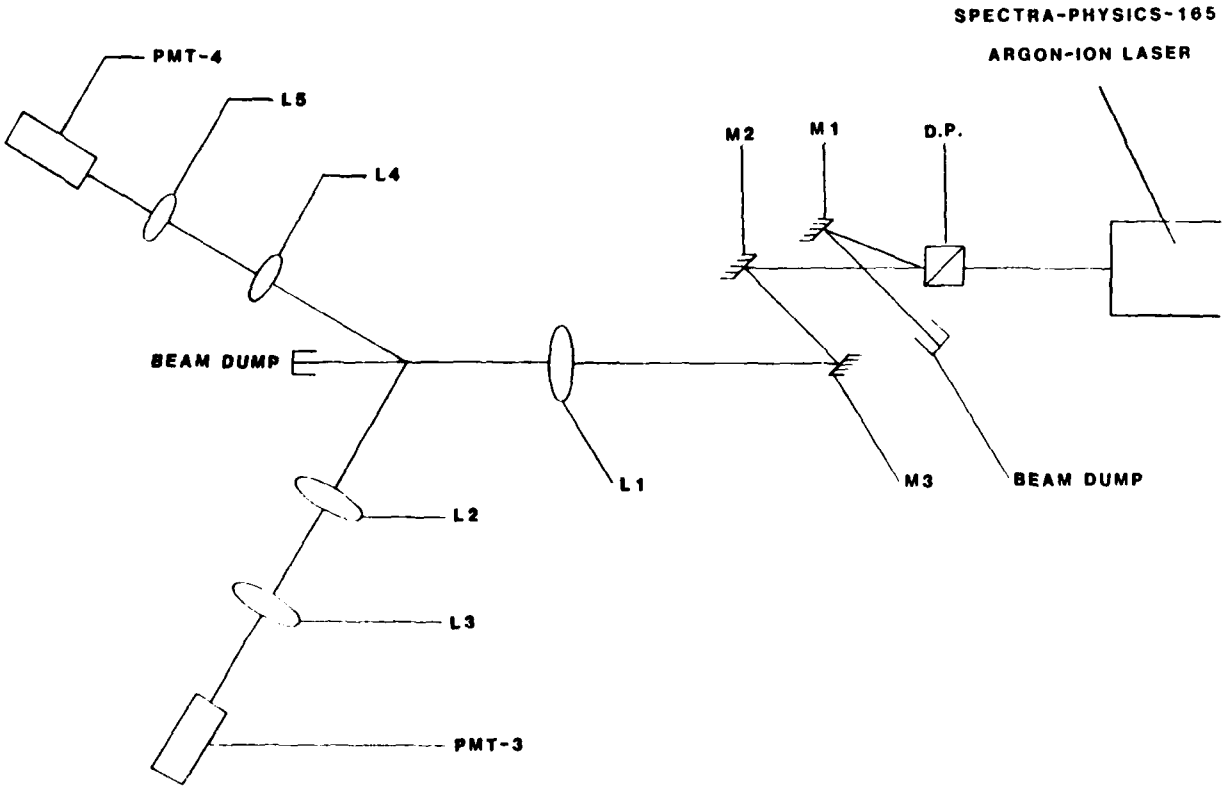

Figure 11. Large-Angle Intensity Ratioing

multiplier tubes, PMT-1 and PMT-2, having quantum efficiencies of about 15-percent at the 4880°A wavelength. The supply voltage to the tubes is about 1100 volts. For large-angle ratioing, the collected light is focused to two separate, RCA 8575 detectors, PMT-3 and PMT-4. The supply voltage to the tubes in this case is also about 1100 volts.

Figure 12 is a schematic of the optical configuration for the polarization-intensity ratio technique. The green laser beam passes through a half-wave polarization plate to rotate its polarization by 90°. The green beam and the polarized blue beam are focussed into the flame by a 38 mm diameter F/4 lens. The laser waist at the focal volume is 20 m in diameter. The scattered light is collected at 60° off the laser axis by a 45 mm diameter F/4.3 collecting lens. The collected light is then focussed into PMT-3 and PMT-4.

b. Data Acquisition

The signal output from the photomultiplier tubes is passed into a Spectron Development Laboratories (SDL) Model LA-1000 logarithmic amplifier which converts the negative current to a positive voltage and is scaled for +10 volts peak output pulse when the input current is -1 mA. The amplified signal is then fed to an Intensity Ratio Processor (SDL Model RP-1001) developed under subcontract at SDL. The RP is designed to trigger at the peak of the signal, rather than the customary signal integration processors, which has the merit of allowing for a wide dynamic range of the RP,as well as reducing the noise. The DC-level outputs of the two peaks detectors go to an analog subtractor circuit. The subtractor output signal is converted to an 8-bit binary number by the analog-digital converter (ADC) after being amplified with a gain of 5. The RP has a threshold voltage of 4 volts, to minimize the background noise, which partly determines the supply voltage to the photomultiplier tubes.

The RP is interfaced with an Apple II microcomputer as a data management system. The code "MAIN" resolves the output numerical data from the ratio processor into 62 bins, where the size distribution is determined by the number of counts in each bin. The resultant histogram is normalized between 0 and 1.0 and can be convoluted into actual size by the appropriate subroutine in MAIN. The numerical results, of the code MIE, based on the theoretical analysis (Section IVA1) and which have been computed by a HP1000, minicomputer are stored in MAIN in the form of tables.

c. Uncertainty

As the final product of the measurements is the PDFs of size distribution, uncertainty exists in that distribution due to nonisotropy and nonsphericity of the particles, index of refraction, depth of field, resolution limitations and the resulting statistical uncertainty in constructing the PDFs, and the error introduced by the convolution process.

Uncertainty due to nonisotropy, inhomogeneity, and nonsphericity of the particles may be determined by comparing the standard deviation obtained experimentally using well-calibrated particles with the theoretical standard deviation of the particles. The uncertainties in this case were about 10 percent. Particles larger than the focal volume will lead to the common depth-of-field uncertainty which reaches its maximum towards the large-size particles.

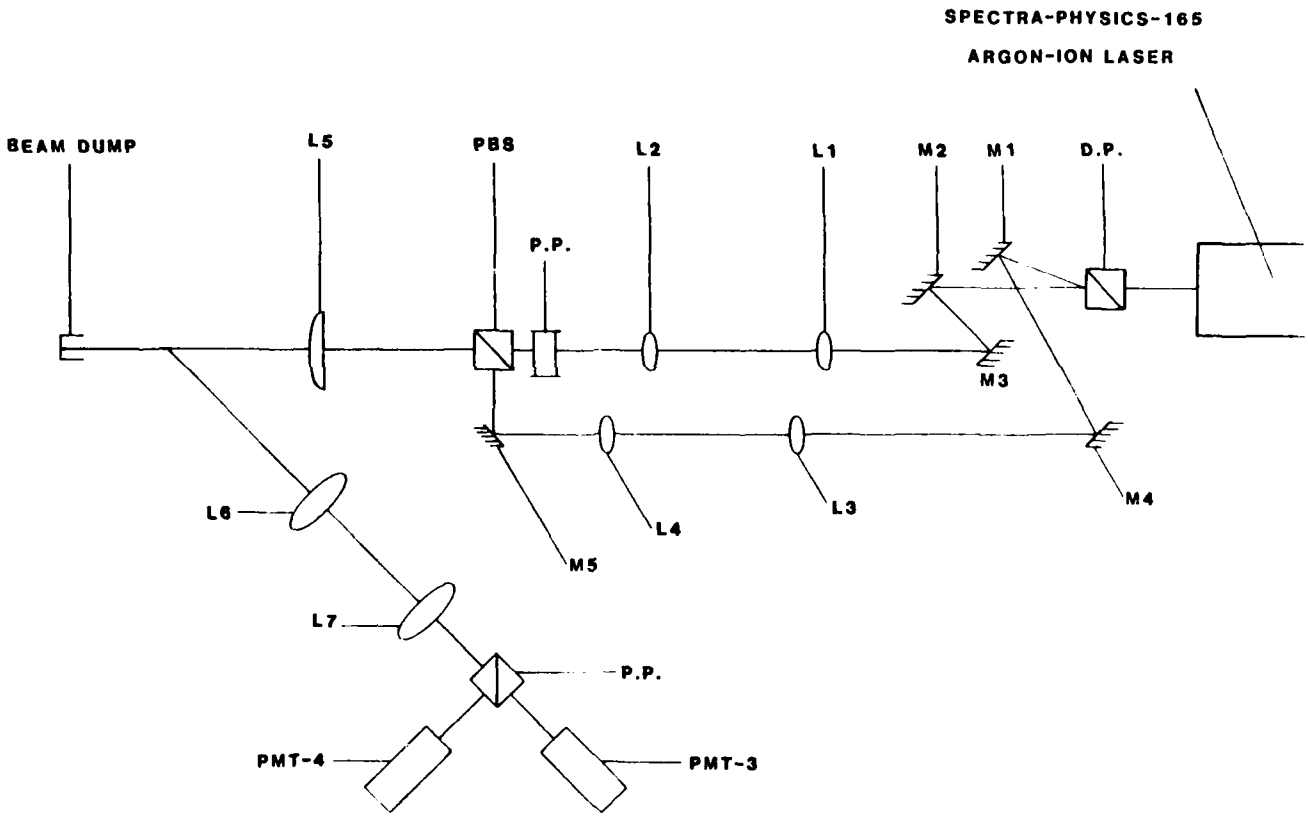

Figure 12. Polarization-Intensity Ratioing

Although the overlap region between the different techniques will eliminate the focal volume and depth-of-field uncertainties, a special study of that effect is recommended. Upper Limit Distribution Function may be used to correct for the focal volume by specifying various shape parameters which can be determined experimentally.

Regardless of the single-shot uncertainty, the statistical precision of the discrete PDF is limited by the bin size and the number of points in each bin. Since the PDF distribution obeys Poisson's statistical distribution law, the statistical precision is inversely proportional to the square root of the number of entries for each bin. The average number of valid data points is about 100,leading to a statistical bin uncertainty of about 10-percent.

The convolution error is introduced from the linear interpolation process. The convolution is accomplished by comparing the averaged value of the intensity ratio over the bin width with its theoretical counterpart to determine the size. Therefore, the convolution error which is determined by the bin value and bin size, is estimated to be within the 10-percent statistical uncertainty.

d. System Fine Adjustment

Fine adjustments of the PMT supply voltage with well-calibrated particles is essential in order that the numerical results coincide with the experimental data, which minimizes the convolution error. Polystyrene particles have been used for that purpose,as they provide accurate particle sizes with a narrow standard of deviation (as low as 3-percent of the mean).

The process of fine adjustment of the PMT supply voltage takes care of inhomogeneity, nonisothropy and monsphericity of the particles, which were assumed to be to the contrary in the theoretical analysis, as well as the uncertainty concerning the index of refraction of the particles.

B. EXTRACTIVE PROBE AND SAMPLING SYSTEM

The designs of the extractive probe and sampling system are based on the discussion presented in Sections IIE and IIF. The features selected for the present program (Table 8) were first included in the design of a prototype probe which was subsequently used in an exploratory study of probe perturbation (see Table 5, APPROACH). This experience led to a final design which culminated in the construction and use of a refined probe and sampling system. The specific design features and evaluation of both the prototype and refined are presented below. The section concludes with a description of the methods employed for the gravimetric, morphologic and composition analyses.

1. Prototype Extractive Probe and Sampling System

The prototype extractive probe and sampling system are shown in Figure 14. Stainless steel (316) was used for all surfaces exposed to the sample or the combustion atmosphere (i.e., the sample transport tube and the outside wall). For all other requirements, 304 stainless steel was used. Outside diameter for the probe was 9.5 mm (0.375 inch); inside diameter was 3 mm (0.12 inch) The overall probe length was 86 cm (34 inches) from tip to mounting plate

TABLE 8. DESIGN FEATURES OF EXTRACTIVE PROBE AND SAMPLING SYSTEM

Extractive Probe

Point Measurement. The probe must be a point-measurement design rather than a rake measurement design to provide the local measurements required for direct comparison to the optical point-wise measurements.

High-Temperature Capability. The probe must be capable of withstanding the high temperatures experienced in the flame zone, not just at the exit plane. The temperature in the reaction core can approach the adiabatic flame temperature which approaches or exceeds the safe design temperatures of many metals. Hence, the probe will require cooling to maintain its integrity.

Quick-Reaction Quenching. Since samples are to be taken from both high temperature regions and reaction zones, the probe must be capable of quickly quenching the sample. Although the convective cooling provided by cooling the probe will help meet this goal, additional quenching is selected because it simultaneously reduces the dew point of the sample and reduces the particulate number density, the latter of which suppresses the opportunity for agglomerations.

Small Size. The probe must be large enough to accommodate the design features required, yet as small as possible to minimize perturbation and permit higher spatial resolution of sampling locations.

Minimization of Particulate Deposition. The probe and transport lines should be as straight as possible. Necessary bends should be gentle (minimum bend radius of 20 cm). Transport length should be as short as possible. Diluent injection will be beneficial in preventing particulate deposition since it will decrease the overall particulate concentration and increase the velocity of the sample through the transport lines.

Isokinetic-Sampling Capability. Null pressure ports should be included to assess the error associated with null pressure measurements in a swirling flow. The principal means of set ting the probe flow for isokinetic sampling will be laser anemometry.

Prevention of Condensate Formation. The choice of dilution quenching will suppress the dew point of the sample. The probe must be cooled with hot water and the sample transport lines and the filtration bank must be heated. Instrumentation must be protected either by a water dropout or sufficient suppression of dew point so that no dropout will occur. The of the water component of the total sample volume.

Gas Sampling. A gas sampling port should be available to allow gaseous samples to be extracted coincident with the soot samples so that local equivalence ratios can be determined and anypollutants that may be precursors to soot can be analyzed. The gas sample must be taken upstream of the diluent injection to prevent variations in the composition due to the diluent. The gas stream should also be free of particulates as possible to prevent deterioration of gas analysis instrumentation.

Sampling System

Sampling System Filters. Filters must be used that are appropriate for the analyses desired. Membrane filters should be used for the morphology analysis. The gravimetric analysis can use either fiber filters or membrane filters but, for the latter caution is required to control the static charge and retain the sample. For the chemical composition either membrane or filter filters can be used and the utility of each should be assessed.

Accurate Volumetric Measurement. Accurate volumetric measurement instrumentation is necessary for the diluent gas as well as the total sample volume. (The diluent is mixed with the extracted sample. Contration calculations, as a result, require the difference between the diluent volume and the total volume to yield the net volume sampled).

Ease of Operation. Because a number of different operators are expected during the life time of the system, the sampling system must be easy to operate. A minimum of controls should be provided. Ease of filter changes as well as system cleaning is to be stressed.

with an additional 15.6 cm (5.75 inches) of sample tube before the heated sample line interfaced with the probe. Each of the considerations for the probe and sample train set forth in Table 8 are discussed below.

a. Point Measurement

The desire to sample at a point within the flame requires a small sample-tube diameter within the probe. However, long sample times and particulate deposition that result from an excessively small tube are to be avoided. Based on the reported results of the Purdue studies (Reference 60), a 3 mm ID (0.12-inch) sample tube was chosen.

b. High-Temperature Capability

To estimate the flow of cooling hot water required, a heat transfer calculation was made which simulated the inner and outer surfaces of the probe as two parallel flat plates with surface areas equal to the inner and outer probe surfaces. The separation distance, equal to 1/2 the diameter clearance of two tubes, was filled with flowing water entering at 24°C (100°F) and exiting at less than 100°C (212°F), the latter of which was selected as a limiting value to prevent internal boiling. The outer surface was set to a conservative estimate of the maximum gas temperature 1800°K (3200°R) while the inner (sample tube) plate was set to a gas stream temperature gradient varying from 1800°K to 350°K (3200°R to 630°R) to account for the cooling of the sample. Based on this approximation, a cooling water flow rate of 0.63 l/min (10 gallons/hr) was calculated as necessary to maintain the probe surface temperature below the design temperature for 316 stainless steel and the temperature of the cooling water below 100°C (212°F).

Coolant was carried through two 1.6 mm OD x 1.09 mm ID (0.063-inch OD x 0.043-inch ID) tubes inside the annulus to the probe tip. The water was returned through the remaining annular space. This method kept the overall probe diameter small by eliminating the need for triple-wall construction. Thermocouples at the cooling water inlet and exit ports were used to monitor coolant temperatures.

c. Diluent Injection

Nitrogen was used as the diluent gas because of its inert qualities and its relatively low cost. Injection into the main sample stream was through a single-injection port 0.86 mm (0.034 inch) in diameter located 3.5 cm (1.38 inches) downstream of the probe inlet.

The diluent injection serves three purposes: sample cooling, dew point suppression, and sample dilution. Even though the quick cooling provided by the diluent is desirable, it is not necessary for the diluent to cool the mixture down to the ultimate exit temperature. The degree of dilution necessary to prevent particulate deposition is unknown,although any dilution would help reduce the amount of deposition. Hence the injection rate of the diluent was based on suppression of the dew point such that water would not condense within the sampling system. The calculation is based on the fuel-to-air ratio, the fuel used, and the expected temperatures within the system. The calculated rate

a. Extractive Probe

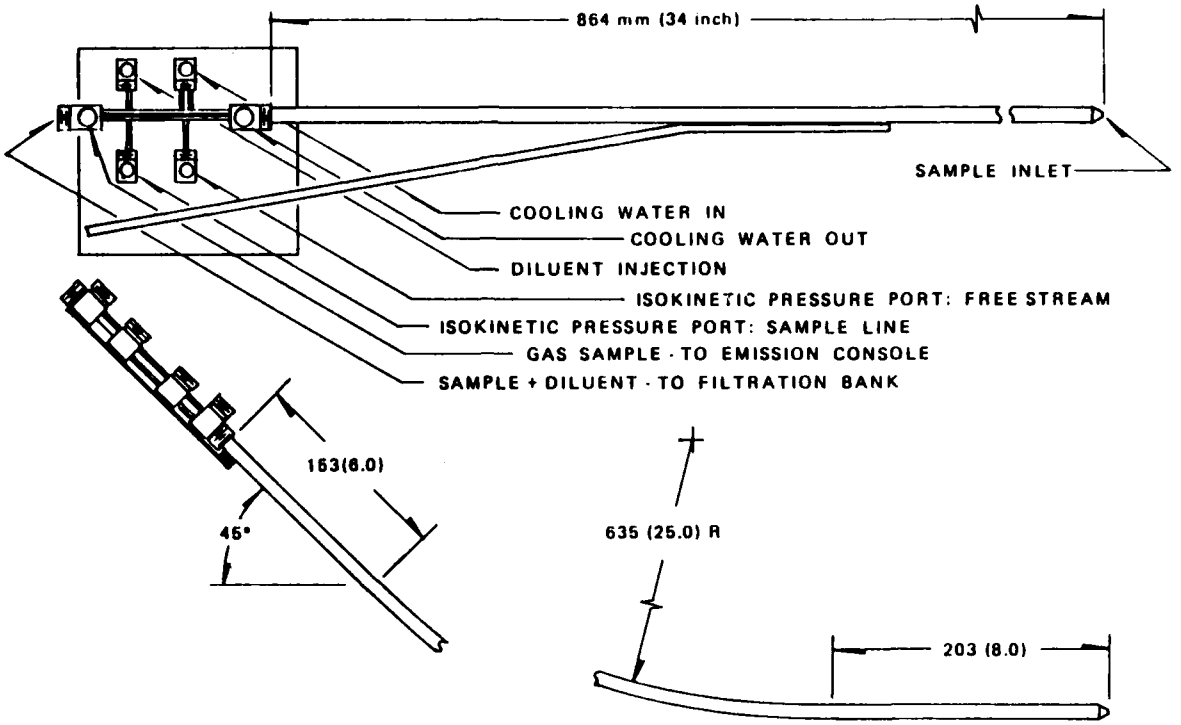

b. Probe Tip Detail

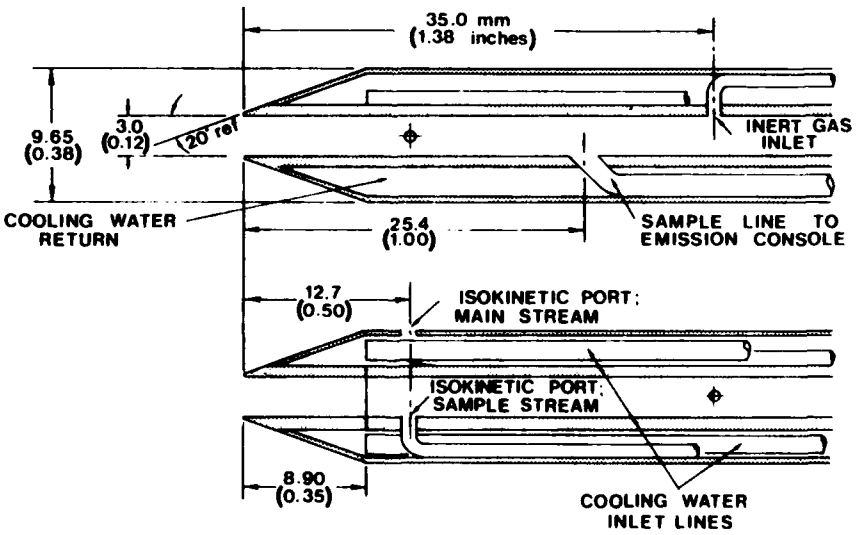

Figure 13. Prototype Extractive Probe and Sampling System

c. Sampling System

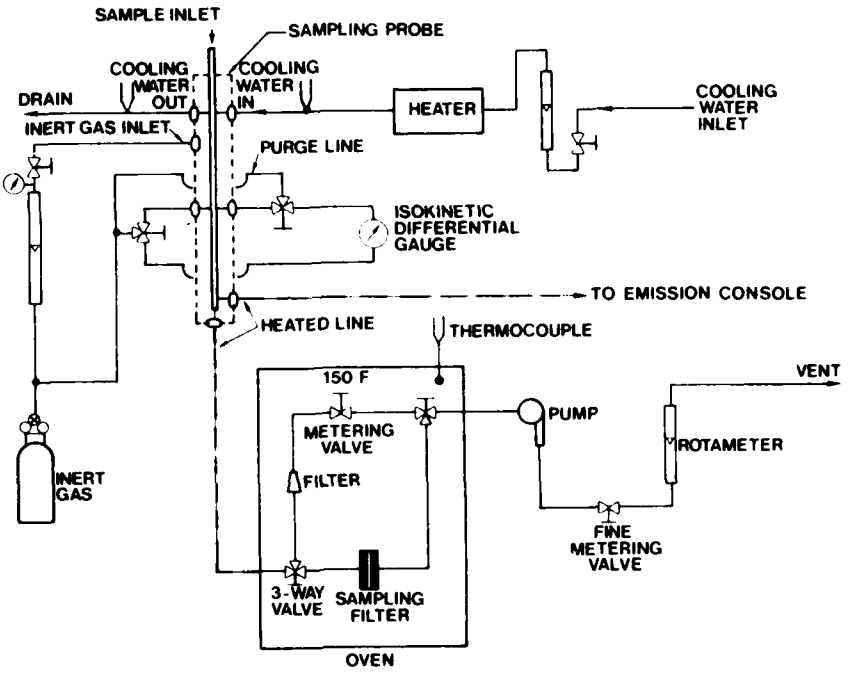

Figure 13. Prototype Extractive Probe and Sampling System (Concluded)

necessary to prevent condensation of the water in a flame with a 0.2 equivalence ratio is approximately 1 part nitrogen for every part sample.

Consideration was given to possible hydrocarbon condensation. However, all of the hydrocarbons that could appear in exhaust stream during the study had condensation temperatures less than water. Hence if water condensation is prevented, so too is the condensation of hydrocarbons.

d. Probe Size

Every effort was made to minimize the probe size while retaining the desired features. After considering the minimum sizes feasible for the coolant, gas sampling, diluent injection, and isokinetic pressure lines, an overall diameter of 9.53 mm (0.375 inch) was chosen as the smallest probe diameter possible.

e. Short Transport Length and Gentle Bends

The overall probe length of 86 cm (34 inches) was longer than desirable but necessary to provide full traversing of the combustion zone and to position the connections between the probe and sample train out of the combustor exhaust stream.

A large-radius bend 63.5 mm (25 inches) in the probe was necessary to remove the probe from the exhaust stream. All other bends in the sample train were kept at a large radius. The heated sample line between the probe and the filtration bank was 1.22 mm (4 feet) in length.

f. Isokinetic Sampling

A pressure-null system was used to set and monitor isokinetic sampling. Static pressure ports on the inner sample line and on the outer surface were located 12.7 mm (0.50 inches) back from the probe tip and oriented flush with the tube surface. The ports were positioned to minimize influences and yield true static pressures. Note that the diluent injection point was located downstream of the pressure port to minimize the effects of the diluent on the measured pressure. The tubes used to transmit the pressure information through the probe annulus and to the probe interface were 0.86 mm (0.034 inch) ID. A + 0.5 inch H_2O differential pressure gauge with 0.01 inch H_2O resolution was employed for the null-pressure measurement. The pressure lines could be backflushed if necessary.

g. Prevention of Condensate Formation

Besides the diluent injection, heated sample lines and filtration within an oven were incorporated to prevent condensation. The heated sample line, a Technical Heater's Model LP-212, was heated to 120°C (250°F) while the oven housing the filter, a Blue-M model SW-17TA, was maintained at 60°C (140°F).

h. Gas Sampling

A port for extracting gaseous samples separate from the main flow was positioned 2.54 cm (1 inch) back of the probe tip.

i. Filtration

Nuclepore membrane filters were chosen because of their applicability to scanning electron microscopy. Tests were conducted to determine the combination of primary and secondary filters that gave the best filtration with a minimal pressure drop. Filters (47 mm OD) of 5.0 μm and 0.2 μm pore size were used for the primary and secondary stages respectively. Nuclepore filter holders and multiple-holder adapters were used to construct the two-stage filtration system.

j. Volumetric Determination

The more desirable positive displacement dry test meters were not selected for the prototype in order to gain the experience appropriate for specifying the appropriate capacity. Instead Matheson rotameters with 604 and 605 meters were used for the diluent and total flow streams. A stopwatch was required for total volume determination.

k. Ease of Operation

The system operation was controlled through four control valves: water flow rate, diluent injection flow rate, total sample flow rate, and filter bypass. The water flow rate utilized a Dwyer Model RMC-13 rotameter with built-in metering valve. An emergency water shutoff was also used. The diluent and total flow rate utilized Nupor Model SS-4L fine metering valves for control. These valves provide a nearly linear flow coefficient variation over a 20-turn range and hence can provide a very fine adjustment. Two three-way ball valves were used to permit bypassing of the filter for changing while the sampling system remained running.

l. Other Features

A Thomas Model 727CM39 vacuum/pressure pump was used for the sampling system pump. Based on estimations of the pressure drop along the sample train, the specifications for this pump indicated isokinetic sampling was achievable. All the sample transport lines from the probe interface throughout the remaining sample train were 6.35 mm OD x 4.6 mm ID (0.25 inch OD x 0.18 inch ID) copper or Teflon® tubing.

2. Refined Extractive Probe and Sampling System

The prototype extractive probe and sampling system were utilized in studies involving the Large-Particle Optical System as described in Section VA. Although the overall performance of the prototype system was satisfactory, the need for a select number of improvements was indentified.

First, the cooling capacity was limited. The small transport lines throttled the cooling water flow rate so that, although the necessary 0.63 l/min (10 gal/hr) was achieved, the limited cooling capacity did not provide an adequate safety margin. Second, the pressure-null system for monitoring isokinetic conditions was found to not be suitable in a swirling flow. While it was possible to adjust the sample flow rate to yield a zero-pressure differential, concurrent measurements with a laser doppler anemometer indicated

the probe entrance velocity was significantly higher than the surrounding gas stream (See Section VA2). Also, excessively long response times resulting from the long pressure lines complicated the use of this system. Third, probe vibration was encountered. When subjected to the highly turbulent flows within the combustion chamber, the probe tip could vibrate from its desired position within the flow.

In addition to the apparent problems, diluent jetting and thermophoretic effects were evaluated. Based on the work by Holdeman and Walker (Reference 89), calculations indicated that the single diluent jet could impinge the opposite wall at its nominal operating condition (i.e., sample flow rate at isokinetic conditons and diluent injected normal to flow at a rate necessary to prevent water condensation . Calculation of the thermophoretic forces based on the work done by Waldmann and Schmidt (Reference 90) indicated that, although the particle velocity can be significant, the residence time in the high-temperature gradient region of the probe (from the probe tip to the diluent injection port) was sufficiently short that the particles moved a very minute distance towards the wall. Hence, while thermophoretic forces cannot be discounted, the force did not likely affect the sample.

The design of the refined system was initiated to eliminate the problems and deficiencies encountered with the prototype system, and to refine those features deemed adequate.

A schematic of the refined system is presented in Figure 14. An overall probe diameter of 9.5 mm (0.375 inch) was retained as the smallest feasible size that would permit incorporation of the necessary features yet keep the effects of probe perturbation and flow blockage to a minimum. The sample tube diameter of 3 mm (0.12 inch) was also retained. The overall length was reduced from 86 cm (34 inches) to 61 cm (24 inches) to reduce vibration displacement of the probe tip. Probe curvature was reduced to 51 cm (20 inches) as a result of the shortened probe and modifications to the combustor stand.

To increase the high-temperature capability of the probe, the cooling water capacity was increased by utilizing seven transport lines rather than two,as used in the prototype probe.

The diluent injection was modified to eliminate the jetting associated with the prototype probe. Thirty-two 0.79 mm (0.031-inch) diameter holes organized into 8 groups of 4 holes, and starting 1.27 cm (0.5 inch) back from the probe tip diffusely injected the diluent and eliminated jetting. The arrangement results in a more uniform quenching and a better mixing of the diluent and sample.

The effects of thermophoretic forces were reviewed with respect to the second-generation probe and found to not produce a significant disturbance to the flow.

Isokinetic null-pressure ports were not included in the design of the refined probe. The increased annular space was used to increase the cooling water capacity.

a. Extractive Probe

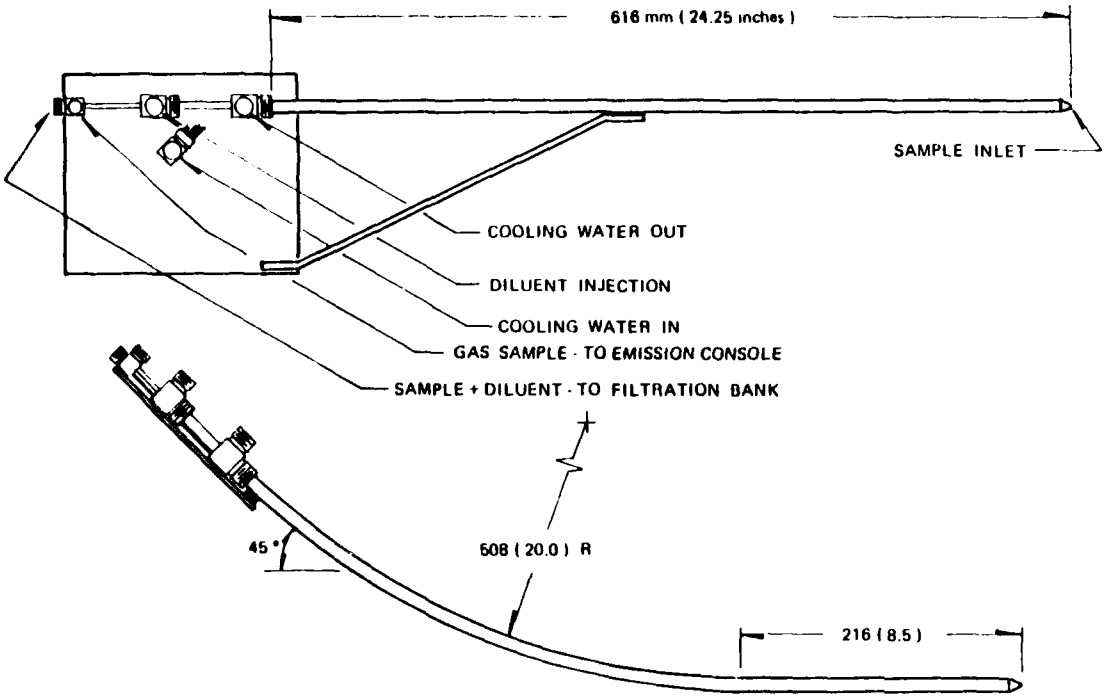

b. Tip Detail

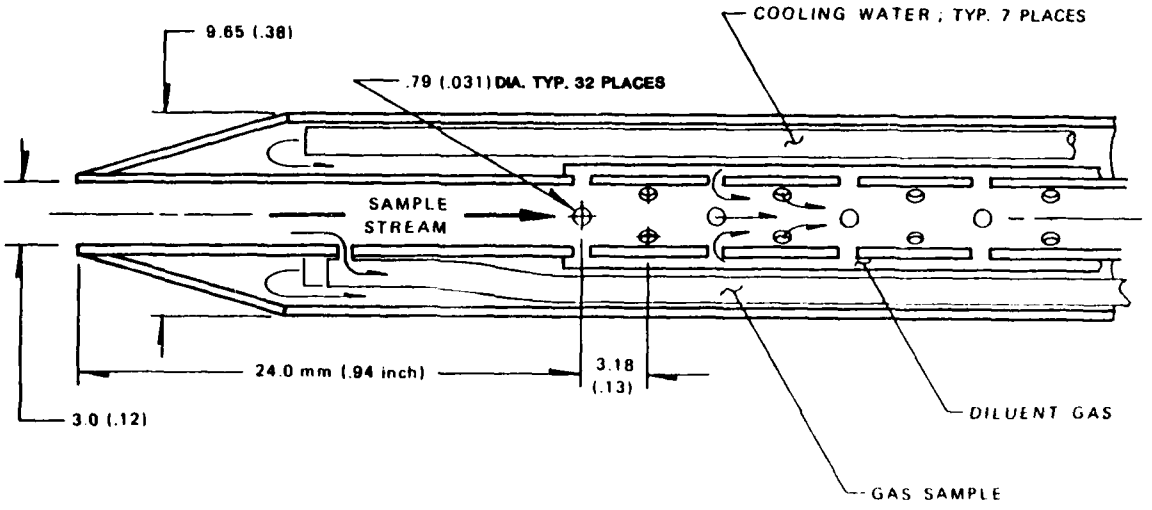

Figure 14. Refined Extractive Probe and Sampling System

c. Sampling System

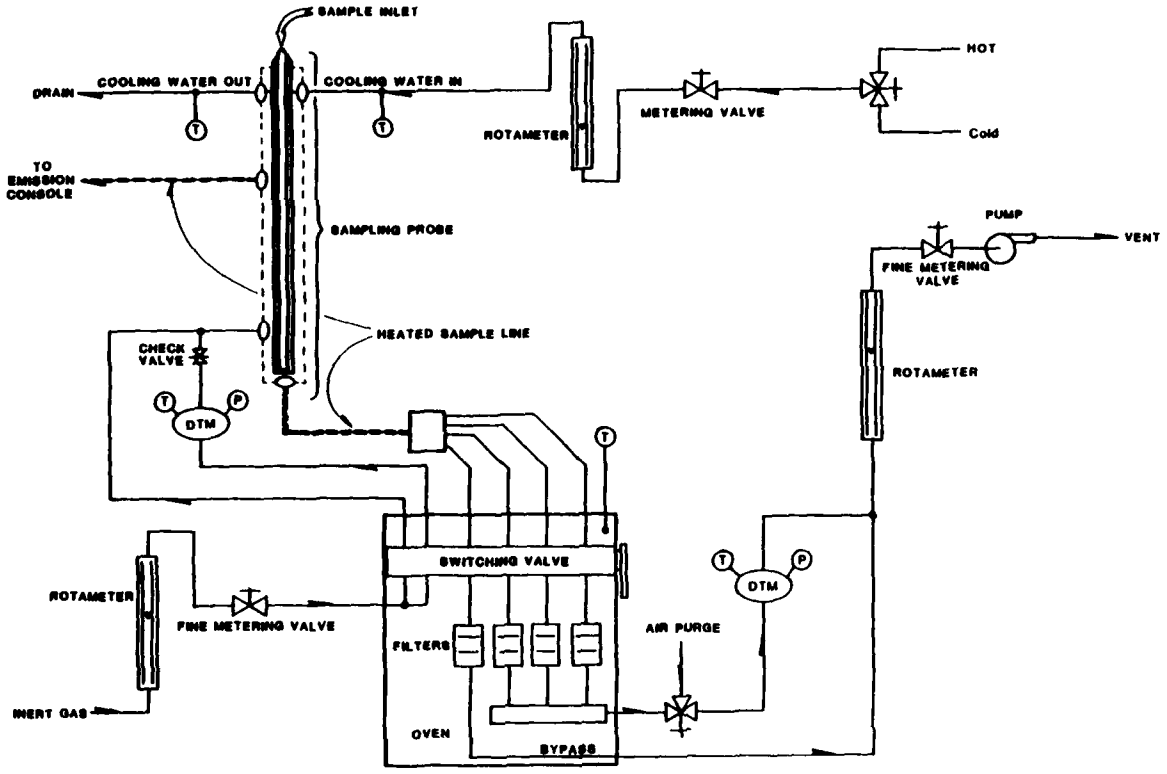

Figure 14. Refined Extractive Probe and Sampling System (Concluded)

The majority of the components utilized in the prototype sampling system were retained for the refined system including the Matheson rotameters for diluent and total sample flow rates, the cooling water rotameter, meter valves, oven and pump.

Because the prototype system had trouble attaining isokinetic sampling rates when the combustor reference velocity approached 15 m/s larger tubing 9.5 mm OD x 7.1 mm ID (0.375-inch OD x 0.28-inch ID) replaced all the old 6.35 mm OD (0.25-inch OD) tubing wherever possible.

Dry test meters (Singer Model DTM-200-1) were installed in series with the existing rotameters on the inert and total sample lines. The combination of a DTM and a rotameter is ideal; sample flowrates can be quickly set and an integrated accurate total volume can be read directly from the DTM.

Although not a serious problem in the prototype system, the need to change filters during a run, if more than one sample was desired, was awkward and time consuming. The refined system incorporated a unique filtration bank in which three filters could be installed and used in sequence eliminating the time involved with changing filters. A specially designed manifold with straight flow paths to prevent deposition gently diverts flow into one of four lines, three filtration and one bypass, as selected by toggle valves at the exit of each filter. The filter exits are manifolded together and plumbed into the total sample DTM. The bypass line joins the sample train downstream of the DTM. In the bypass mode, sample is drawn through the probe and diluent is still injected into the sample but both DTMs are bypassed, as are the filters. This mode is designed to permit intermediate volume recording of total sample and diluent. The valve and sample train designs ensure that both DTMs will be measuring volume simultaneously.

A resin holder is included in the refined system downstream of the filter exit manifold and upstream of the total sample DTM. Intended to contain a resin that absorbs gaseous polynuclear aromatic hydrocarbons, the vessel is positioned so that a sample passes through it whenever any of the three filters is in use.

The performance of the refined sampling system proved far superior to the prototype system. The improved cooling capacity of the probe permitted full traversing of the 15 m/s flame. The shortened probe length reduced the probe vibration. Increasing the sample train lines significantly increased the volumetric flow rate achievable with the sample train. The diffused inert injection proved more satisfactory, at least from a particulate deposition point of view, as very little particulate was found deposited within the probe and sample lines up to the filter. The incorporation of dry test meters on both the total sample line and the diluent injection was far simpler and far more accurate than the use of rotameters.

The initial use of the refined system (see Section VB) utilized the plastic filter holders used in the prototype system. Repeated use established that the plastic housings are vulnerable to leaks. For the final study (see Section VC), the plastic was replaced with aluminum filter holders with notable success and satisfaction of performance.

C. GRAVIMETRIC ANALYSIS

Gravimetric results are presented in terms of soot weight collected per some characteristic of the combustion process such as the fuel consumption or volume of exhaust gas corrected to STP conditions, 70°F (21°C) and 14.7 psia (101 kPa abs). For the latter, the concentration, C, is given by

$$C = \frac{\text{weight of soot collected}}{\text{volume of sample gas extracted corrected to STP}} \quad (18)$$

The key to representative and accurate soot concentrations is the accurate determination of both the soot weight collected and the volume of gas sampled.

The use of rotameters and stopwatches to calculate the sampled volume accurately and consistently was difficult. Dry test meters, with their 0.001-cubic foot (0.028-liter) resolution, allowed for accurate and consistent volume measurements. Since the dry test meters read only the diluent volume and the sample plus diluent volume, the sample volume is obtained by the difference. The volume diluent and volume of sample plus diluent are measured at different temperatures and pressures and, therefore, must be corrected to STP conditions before the difference is taken.

The weight of soot collected is the difference in the filter weight before and after sample is collected. Extreme care must be taken to ensure that the weighing conditions do not vary between the initial and final weighing.

Water absorbtion by either the collected soot, the filter substrate, or both must be monitored. Resulting from variations in the humidity, water absorption can cause variations as great as 20 percent in the calculated sample weight.

A Cahn Model 26 electromicrobalance was used to weigh the filters. Even though an ultimate resolution of 0.1 g is possible, accuracy of the remaining sampling system only warrants resolution to 10 g. Filters used for gravimetric study are placed in a 400°C (752°F) oven for 1 hour to drive off any water or other impurities that may be present on the filter (note that this temperature was only possible because of the high-temperature capability of filters.) Filters were then stored in a desiccator at least 24 hours before use. Immediately prior to use, the filter was weighed and assembled in the filter holder. The weighing chamber environment was controlled with a small quantity of dessicant and radioactive static charge eliminator. After a sample was collected, the filter was again placed in the desiccator for at least 24 hours prior to final weighing. The collected sample was not dried in the oven at 400°C; hydrocarbons trapped in the soot sample could boil off at this sustained temperature and affect subsequent chemical analysis of the sample. Weighing took place in the same environment-controlled weighing chamber.

These precautions and steps resulted in consistent and repeatable soot sample weights.

D. MORPHOLOGICAL ANALYSIS

The morphological analysis of the soot samples was conducted on a Hitachi S-500 scanning electron microscope. Samples of soot collected on nuclepore filters were desiccated for at least 24 hours prior to preparation.

To eliminate any possible biasing, a random segment of the filter, approximately 5 mm x 5 mm, was cut out and attached with silver colloid adhesive to a mounting stud. After drying in a 70°C (158°F) oven for 5 minutes, samples were flash cold-plated and then desiccated for 24 hours prior to analysis.

Typically, a random but characteristic segment of the mounted sample was found and two photographs, one at 2,000x and one at 10,000x magnification, were taken. This was true for both primary and secondary filters unless no evidence of soot was visible or unless some particular feature warranted further investigation.

E. COMPOSITION ANALYSES

Three analyses were employed to investigate the composition of the soot particles. First, via a series of solvent extractions, the soluble organic fraction was obtained and then analyzed by gas chromatography and mass spectroscopy. Second, an elemental analysis was performed on a second sample with a Perkin-Elmer model 240B C-H-N analyzer. Finally, atomic absorption was used for those samples which contained the additive, ferrocene, to determine the amount of iron incorporated into the soot.

1. Polycyclic Aromatic Hydrocarbon Analysis

After collection of the sample, the filter was stored in a dessicator at room temperature. The dessicator was covered with aluminum foil to block out light and prevent photodegradation of the PAH.

The soot extraction was carried out with the filter folded in half and placed in an extraction thimble (Whatman 33 mm x 80 mm) which was contained inside a Soxhlet apparatus. The filter was extracted with 200 ml of dichloromethane for 20-24 hours. During this period, fresh solvent vapors from the flask rise through the sidearm and up into the condenser. As they condense, the solvent drips into the extraction thimble containing the filter. The liquid rises to a given level, at which time the automatic siphon starts. The extracted material accumulates in the flask as more pure vapor boils off to repeat the process. All of the solvents used were distilled in glass purity.

The extract was then evaporated to dryness at room temperature under reduced pressure in a rotary evaporator, a means of rapidly concentrating solvents without affecting the reaction product. The DMSO separation procedure (Reference 67) used to isolate the PAH component precluded the continued use of dichloromethane due to the miscibility of the two solvents. Therefore, the residue was resuspended in 10 ml cyclohexane. In some instances, however, the cyclohexane would not dissolve all the residue, so after the solution was transferred to a 125 ml separatory funnel, the flask was rinsed with 2 ml dichloromethane, which was then added to the cyclohexane.

The cyclohexane was then extracted with three 15 ml portions of fresh DMSO in the separatory funnel. Slightly greater than equivolume amounts of DMSO were used to improve the PAH recovery from the cyclohexane phase. The DMSO fractions were collected in a 250 ml separatory funnel to which two volumes of distilled water were added. The DMSO/ water solution was then back-partitioned four times with 100 ml of pentane to recover the now-separated PAH. The pentane was then evaporated to dryness with the residue resuspended in 2 ml dichloromethane. A schematic chart of the separation procedure appears in Figure 15.

The dichloromethane soot extract was initially analyzed by a Hewlett-Packard 5830A gas chromatograph with a flame ionization detector (FID). Quantitative analysis of individual PAH was accomplished by peak area integration with a standard solution of naphthalene, phenanthrene, chrysene, and benzo[ghi]perylene used to calibrate the FID response. Each chromatographic peak in a sample run was compared to the standard compound with the closest retention time. A 30 m (98.4-foot) x 0.30 mm (0.012-inch) J & W fused silica SE-54 capillary column was used throughout these experiments. A splitless mode of injection was used with 50:1 inlet purge and a helium carrier flow rate of 1 ml/min. After a 2 ml injection of sample at 20°C to reconcentrate the solutes at the head of the column, the gas chromatograph was programmed from 50°C to 290°C at the rate of 2°C/minute.

Limited identification of individual compounds was accomplished with a Hewlett-Packard 5992A gas chromatograph/mass spectrometer (GC/MS). Identification above naphthalene was not possible as the column-ionizer interface, a glass capillary restrictor, is not temperature-controlled. Structural assignments of individual PAH were made from mass spectral data and relative gas chromatographic retention indices. Over 200 PAH have been characterized with this relative retention indices scheme (Reference 82) which uses the four PAH standards previously mentioned.

2. Elemental Analysis

A Perkin-Elmer model 240B C-H-N analyzer was used to determine the carbon/ hydrogen ratio of the soot before and after the Soxhlet extraction. An 11.5 mm (0.45-inch) diameter section of filter was removed with a metal cork borer, weighed to the nearest microgram, and then wrapped in a piece of 52-mesh platinum gauze which serves as a catalyst in the instrument combustion process. It is necessary to only use a section of the filter as the instrument is overranged with samples containing more than 3 mg of carbon. The platinum gauze containing the filter is fitted into a quartz sample ladle which is then placed in the instrument combustion tube.

The system is purged with helium for 90 seconds, followed by a 30-second flush of the combustion train by oxygen. The sample is then introduced into the combustion chamber, and the analysis proceeds automatically. Combustion occurs at 980°C, with the reduction of combustion gases over copper being at 675°C. The microquartz fiber filter was selected due to its ability to withstand the combustion temperature without melting, whereas a glass fiber filter would be fused into a glass bead, possibly trapping some of the sample. The combustion products are then flushed by helium through a series of thermal conductivity detectors. Water and carbon dioxide are removed by traps located

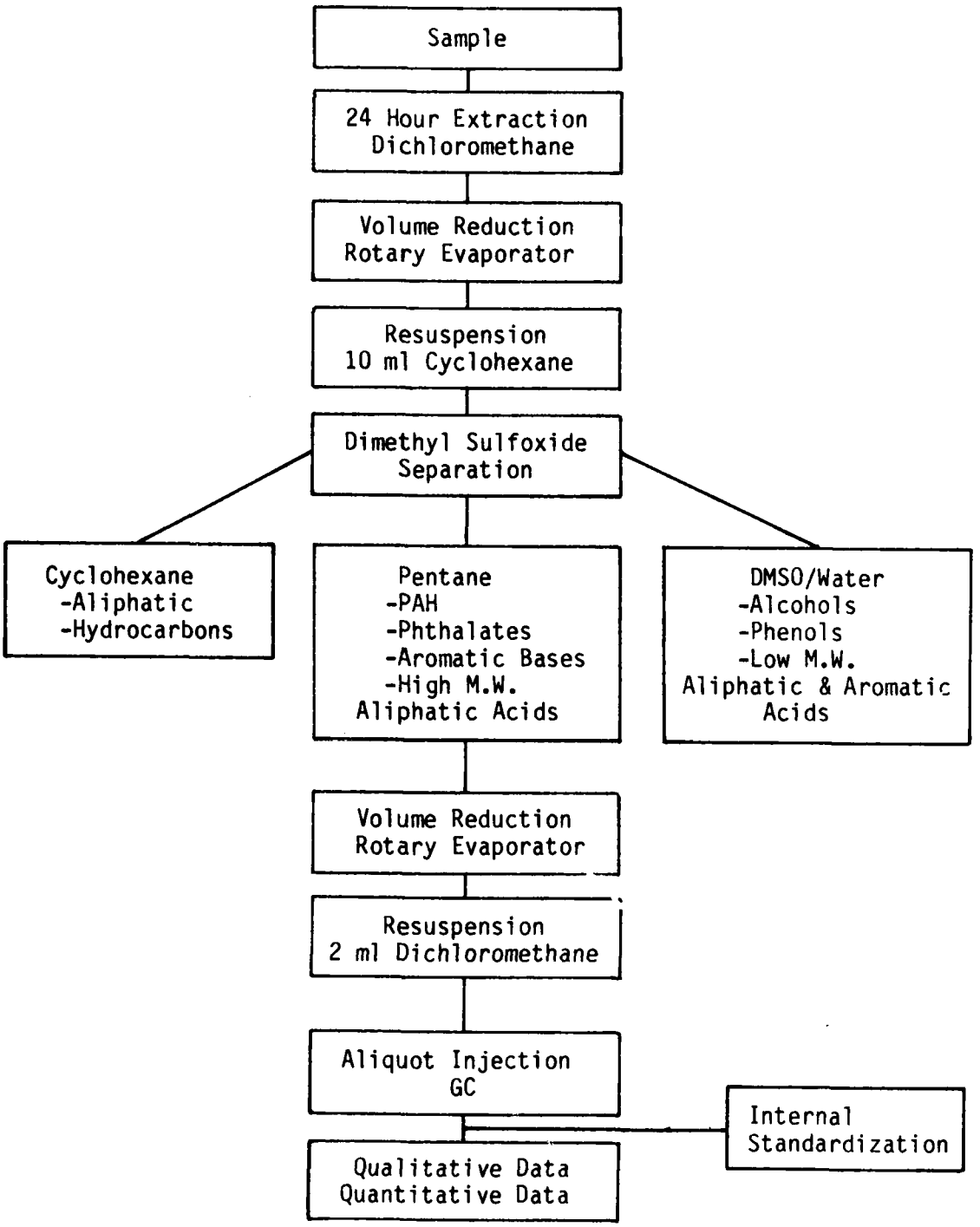

Figure 15. Separation Procedure

between the sensing and reference detector cells in the respective hydrogen and carbon detector circuits. The remaining sample passes through the nitrogen sensing cell where any difference from helium flowing through its reference cell is recorded as nitrogen.

Five sections from four blank filters were used to obtain the average weight of the filter sections and the background values of carbon and hydrogen. The results were averaged, with these mean values being subtracted from the results obtained from sections containing sample. In this manner, the amount of carbon and hydrogen in the soot could be determined.

3. Ferrocene Analysis

The amount of additive incorporated into the soot was determined by quantitatively analyzing the samples for iron, using a Perkin-Elmer Model 403 absorption spectrophotometer. As this analysis was performed after the Soxhlet extraction, both the organic extract and the insoluble fraction remaining on the filter were analyzed for iron content. Thus, the sample collected was extracted as before, but after evaporating the soluble fraction to dryness, the residue was resuspended in 5 ml dichloromethane. One milliliter was removed, evaporated, and resuspended in 10 ml of methyl-isobutylketone (MIBK), an organic solvent which does not interfere with the iron absorbance wavelength of 248.3 nanometers. The extracted filter was subsequently divided in half with one part for the iron analysis and the other for elemental analysis. A filter half was then soaked sequentially in hot, concentrated nitric acid and sulfuric acid for approximately 30 minutes to remove any iron oxide (FeO, Fe_2O_3). The acid was then transferred to a 10 ml volumetric flask and diluted to the mark with deionized water. The absorbance signals obtained from the prepared solutions were then compared to those obtained from a series of iron standards. In this manner, the iron concentration of the solutions was determined, and after taking into account the dilution factors, the iron present on the filter and in the soluble extract could be calculated.

F. COMPLEX FLOW MODEL COMBUSTOR

1. Experimental Facility

A schematic of the experimental facility is presented in Figure 16 for the two configurations employed: gaseous-fuel injection, and liquid-fuel injection. An explanation of the air system is documented elsewhere (Reference 91).

The gaseous-fuel injection system (Figure 16a) was used for propane and ethylene. The construction is of conventional design with the use of a rotameter bank for flow metering.

The fuel supply for the liquid-fuel injection system (Figure 16b) consisted of nitrogen pressurized, plated steel tanks (total capacity of 7.4 liters, 2.0 gallons) which provided a steady flow of fuel to the nozzle without the pulsations encountered with gear pumps. The fuel passed through a Type 95A Balston filter (grade C) and a Nupro 7 sintered metal filter to remove any particulate contaminants before the fuel was injected into the combustor. The fuel was metered with calibrated flowmeters (Matheson 603) by varying the atomizing air pressure. Increasing the air pressure decreased the fuel flow rate and vice versa.

For prevaporized operation, the liquid flow was directed to a prevaporizer (Figure 16c) constructed from a block of cast aluminum approximately 1 cubic foot in volume. The block was drilled to accommodate the insertion of eight calrod-type heater rods that were used to maintain a nominal block temperature of 200°C (400°F). The aluminum was cast over two spiraling coils of 6.35 mm (0.25-inch) OD 316 stainless steel. One of the coils was used to preheat the atomizing gas (nitrogen) required for the twin-fluid atomizer. The nozzle (Spraying Systems J Series, Round Spray, 2050 Fuel Cap, 6747 Air Cap) was selected to provide a narrow angle (~12°), well-atomized spray. The nozzle was installed just above the aluminum block and mounted on a 1.27 cm (0.5-inch) OD tube directed straight down and into the block. At the bottom of the block, this injection tube connected to the 6.35 mm (0.25-inch) OD coil.

2. Combustor Configuration

The following two combustor configurations were utilized during the present study (see Section III, APPROACH): Centerbody and Dilute-Swirl. The former was the first employed. The latter evolved through a series of evaluations conducted in a parallel, AFOSR study.

a. Centerbody Combustor

The centerbody combustor (Figure 5a) was operated with either an 80 mm (3.15-inch) ID or 52 mm (2.0-inch) ID quartz tube. The diameter of the internal centerbody in both cases was 44 mm (1.73 inches) OD and 28 mm (1.1 inches), respectively. A recirculation zone generated by 60° swirl vanes (Swirl number of 1.4 as calculated using Reference 92) served to stabilize and concentrate the flow in the center of the combustor. The swirl vane location, approximately one centerbody diameter upstream of the centerbody face, was established to suppress recirculation back to the annular wall. Either gaseous or liquid fuels were introduced through a nozzle at the face of the centerbody.

b. Dilute-Swirl Combustor

The Dilute-Swirl Combustor (DSC) configuration is presented in Figure 5b. It consisted of an 80 mm ID cylindrical tube. A set of swirl vanes (57 mm OD) was concentrically located within the tube around a 19 mm OD centrally positioned fuel delivery tube. Dilution and swirl air were metered separately. The dilution (i.e., nonswirling) air was introduced through flow straighteners in the outer annulus. The swirl air passed through a set of swirl vanes which imparted an angle of turn to the flow, 60° in the present case. Either liquid or gaseous fuels were introduced through a nozzle at the end of the central tube. The exit plane of the fuel injector was set at the same axial location as the exit plane of the swirl air to provide a clean, well-defined boundary condition for modeling.

The DSC duct can be a quartz tube or, in the case of the present study, a stainless steel duct with flat, glass quartz side windows to provide the optical quality required by the Expanded Particle Optical System. The windows were approximately 2.54 cm (1 inch) in width and 22.9 cm (12 inches) in length.

a. Gaseous-Fuel Injection

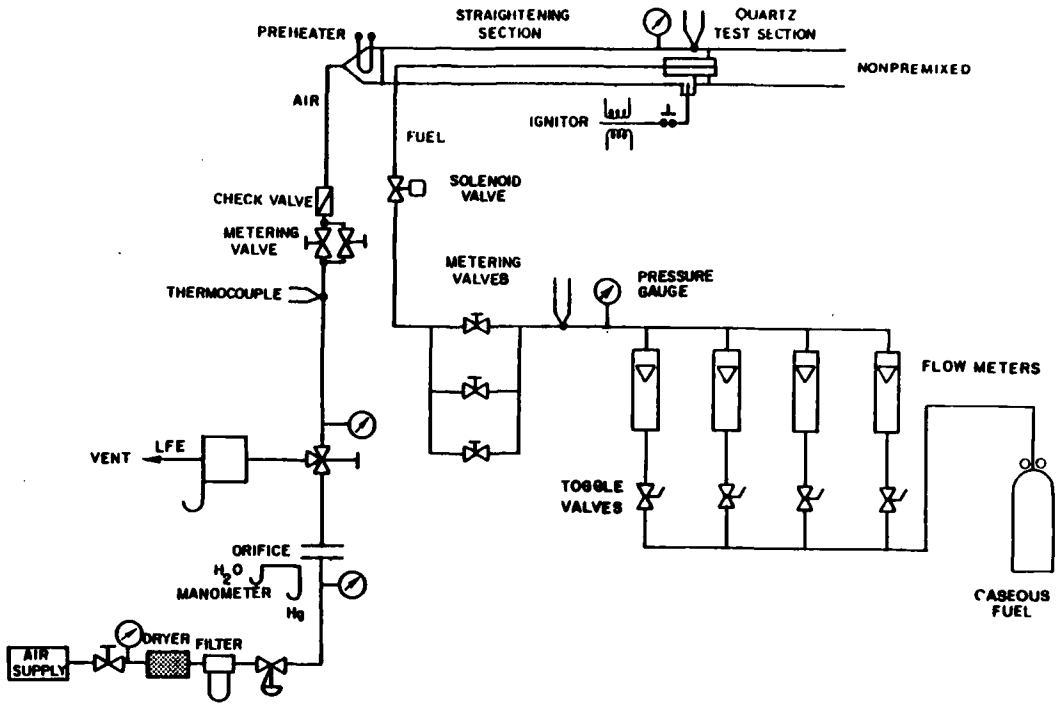

b. Liquid-Fuel Injection

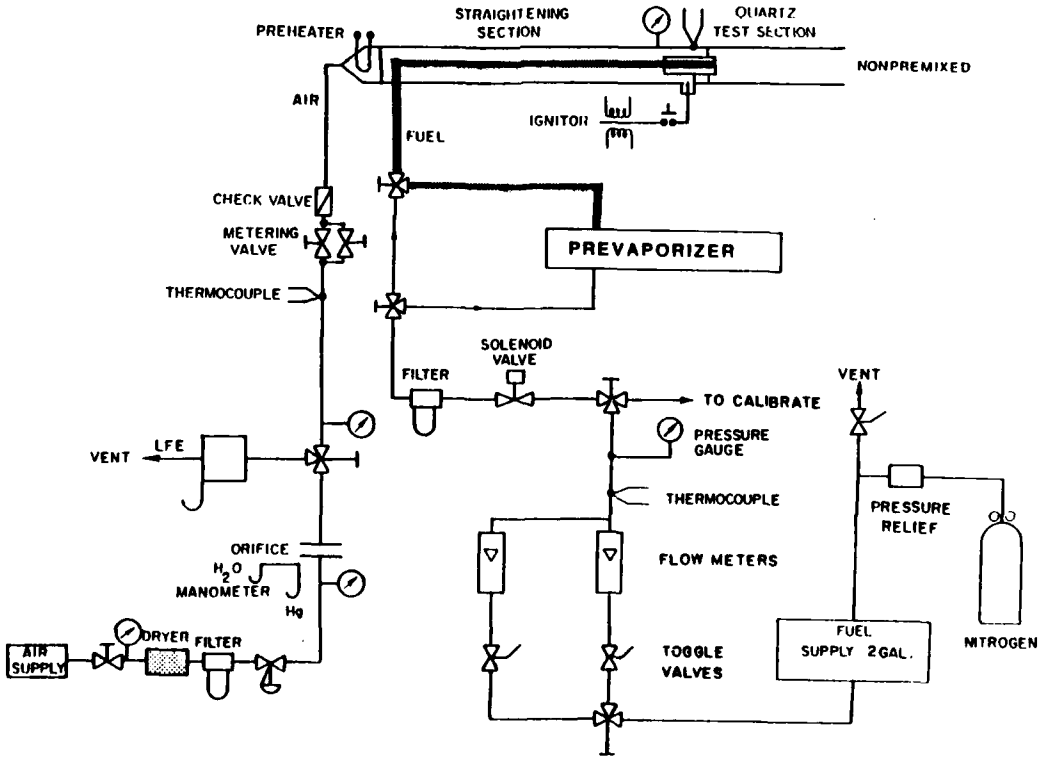

Figure 16. Combustor Facility

c. Liquid-Fuel Prevaporizer

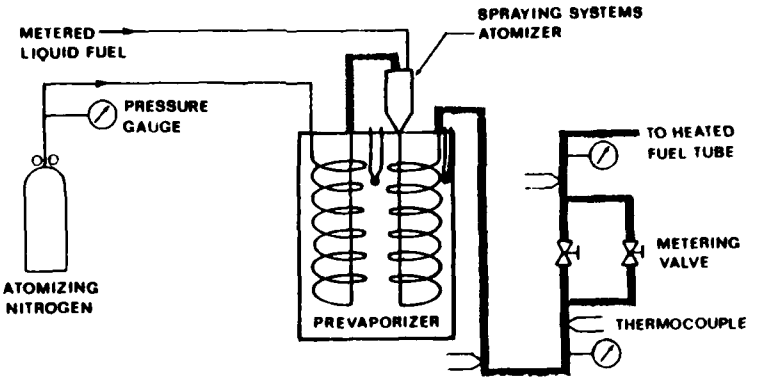

Figure 16. Combustor Facility (Concluded)

SECTION V

EXPERIMENTS

The experiments were conducted in parallel with the evolution of the diagnostic and analytical methods following the approach described in Section III. Results for the Large-Particle Optical System and prototype extractive probe are presented first. Second, results are presented using the refined extractive probe and sampling system to assess the effect of fuel molecular structure on the physical and chemical properties of soot. Finally, a demonstration and evaluation of the performance of the Expanded-Particle Optical Probe is described.

A. LARGE-PARTICLE OPTICAL SYSTEM

1. Introduction

An evaluation and validation of the Large-Particle Optical System was first conducted for both cold and hot flow. During the evaluation, comparative tests were run against the prototype extractive probe, and evidence of extractive probe perturbation was observed. As a result, an exploratory study of extractive probe perturbation was also conducted. Both the evaluation and probe perturbation studies are described below.

2. Verification and Validation

The evaluation of the Large-Particle Optical System was conducted in the centerbody combustor operated with a 51 mm (2-inch) ID duct and a central fuel jet with a 1.3 mm (0.052-inch) diameter (Figure 5b). Both gaseous propane and ethylene were used as the fuels. Performance of the optical system was evaluated under both cold-flow and hot-(reacting) flow conditions.

a. Cold Flow

Under cold-flow conditions, two specified-size polystyrene particles 4.8 μm (7.7 percent SD) and 0.5 μm (0.5 percent SD) were selected so that each of the two optical-sizing techniques (particle-size interferometry and small angle intensity ratioing) could be tested. A nebulizer was used to inject seed particles into the main air flow 2 meters upstream of the centerbody. At this location, it was experimentally determined that water droplets produced by the nebulizer completely evaporated, leaving dry polystyrene particles. No fluid was injected through the jet.

Particle-sizing interferometry was used to observe the 4.8 μm diameter particles. A fringe spacing of 7.3 μm was established thus making the instrument sensitive to particles between 2 to 8 μm. Measurements were obtained at an axial location 6d downstream of the centerbody (where d is the diameter of the centerbody).

The measurements are shown in Figure 17a. The most probable size measured was 3.2 μm, well outside the specified size error limit (4.8 μm, 7.7 percent SD). This caused concern over the accuracy of the instrument and led to a subsequent inspection of the particles using a scanning electron microscope

a. 4.8 μm

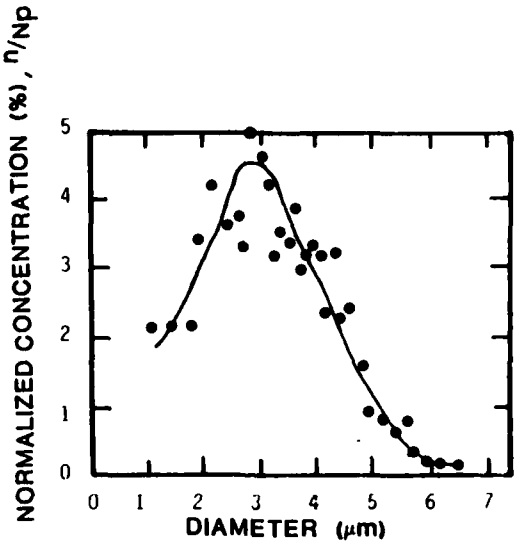

b. 0.5 μm

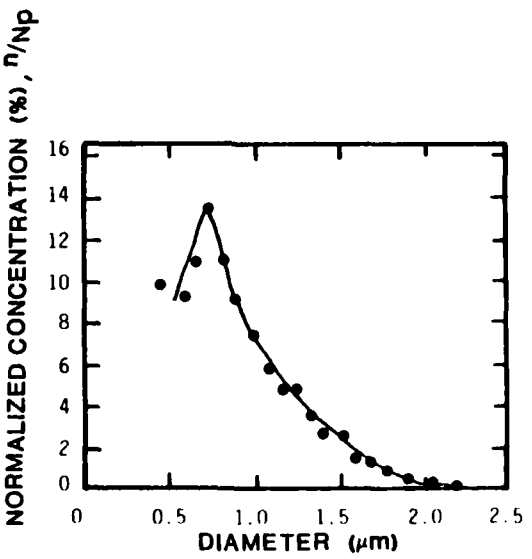

Figure 17. Size Distribution of 4.8 μm and 0.5 μm in Cold Flow.

(SEM). Based on SEM photography of nine such particles, the average size was determined to be 3.6 μm (11 percent SD). The most probable size measured with the interferometry technique (3.2 μm) deviates by 12 percent from the SEM measurement, which is acceptable at this preliminary stage.

To measure the 0.5 μm particles, the scattering intensity-ratioing technique was used. The two scattering angles selected were 6° and 12°, thus making the instrument sensitive to particles between 0.4 and 2.2 μm. Measurements were obtained under the same conditions as in the previous cold-flow case. The most probable size measured was 0.7 μm (Figure 17b). Although this is larger than the stated size of 0.5 μm (0.5-percent SD), SEM observations of a small number of extracted particles indicated an average size somewhat larger than 0.5 μm. In the present instrument, 0.5 and 0.7 μm correspond to intensity ratios of 0.9 and 0.79, respectively. Therefore, a 12-percent change in the relative gains of the two detectors could account for the discrepancy. The accuracy of the intensity-ratioing technique was monitored by using standard size particles for day-to-day calibration. In the present case, the greatest error occurs at the small-size end of the ratioing-size curve (e.g., at 0.5μm, the error is about 60-percent). At the large-size end (e.g., at 2μm), the error is below 10-percent.

Finally, the data rate calculated from the scanning electron micrographs of the filtered seed verified that the measured data rate was correct within experimental uncertainty.

b. Hot Flow

The hot-flow results are presented in Figure 18. The sampling location selected was 5d downstream of the centerbody. The combustor was operated with either propane or ethylene in the fuel jet at an overall equivalence ratio (ϕ) of 0.25, and relatively low reference velocity of 0.65 mps. The latter was required to generate particles larger than the 0.4 μm lower limit threshold of the intensity ratioing technique. Higher intensity flames produced particle size distributions below 0.4 μm for the two fuels tested.

The ethylene flame is shown to produce proportionately more large particles (e.g., 1-2 m) than the propane flame. This production was confirmed by SEM photographs of extracted samples. For the 20-minute samples presented, large particulates were observed on the 5 μm primary filter for ethylene, with relatively few small particulates on the 0.2 μm secondary filter. The reverse is found for propane. The size distribution inferred from the SEM photographs was consistent with the optical results.

3. Extractive Probe Perturbation Assessment

A major concern with the use of physical probes in complex flows is the perturbation of the probe on the flowfield. The optical probe provides a unique opportunity to explore probe perturbation. To this end, a study was conducted to address probe perturbation as a function of extractive probe location, reference velocity, and extractive probe sample flow rate. The goal was to address two questions associated with the use of extractive probes -

a. Propane

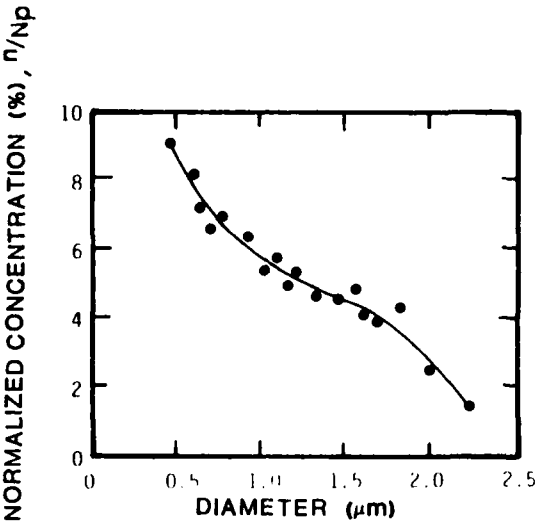

b. Ethylene

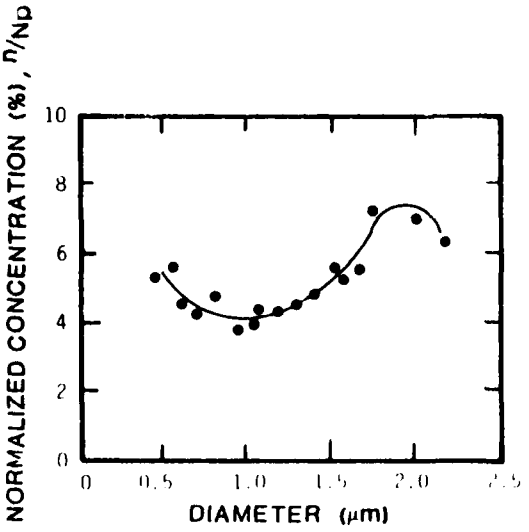

Figure 18. Size Distribution of Soot Particles in Propane and Ethylene Flames

- Representativeness of sample. Is the extracted sample representative of particulate at the probe entrance or do the processes of extraction, transport, and subsequent deposition of the particulate on a filter transform the morphology and number density of the soot?

- Flow perturbation. Does the presence of the probe in the flow perturb the local conditions (e.g., temperature, aerodynamics, chemistry) and thereby produce a condition at the probe entrance different from that which occurs in the absence of the probe?

These questions are especially important in flows, such as those that occur in gas-turbine combustors, boilers, and furnaces, where the aerodynamics includes swirl and flow reversal.

The test conditions selected for the perturbation study are itemized in Table 9. An equivalence ratio of 0.37 was chosen to provide conditions suitable for good optical measurements. The sampling points were located in the wake of the zone of recirculation (6d) and within the zone of recirculation (3 1/2d).

TABLE 9. EXTRACTIVE PROBE PERTURBATION TEST CONDITION

Reference Velocity,[a] U_{ref} (m/s)	Overall Equivalence Ratio,[b] ϕ	Sampling Location,[c] (x/d)
5.5	0.37	6, 3 1/2
7.5	0.37	6

a cold-flow velocity referenced to duct diameter, 51 mm (2-inch)
b actual overall fuel-to-air ratio divided by stoichiometric ratio
c x,d: Refer to Figure 6

To assess the perturbation produced by the extractive probe, the position of the extractive probe was changed relative to the optical probe. The probe was removed axially in incremental steps while the optical probe remained fixed. In addition, radial profiles of data rate and particle size distribution were obtained optically with and without the extractive probe in the flame.

a. Nonreacting Flow with Seeding

The study was initiated by seeding the nonreacting flow of the annular jet with 0.48 μm polystyrene particles, and comparing the measured

optical data rate to that recorded as the extractive probe was removed axially from the optical probe volume.

The cold-flow study was conducted at 7.5 mps and at an axial sampling station of x/d = 6. The intensity-ratioing data rate (n) decreased as the extractive probe was withdrawn (Figure 19) by more than 200 times the levels with the extractive probe present. The relatively low data rate in the absence of the extractive probe is due to the strong centrifugal force on the particles caused by the swirl. When the probe is present, this force is reduced and particles can more freely diffuse radially toward the centerline. The radial diffusion of the particles becomes evident by examining Figure 19b. Two observations are noteworthy. First, the profile without the probe exhibits a very small data rate in the center which increases radially. This shows that diffusion is quite small and that very few particles are able to reach the central core of the combustor. However, in the presence of the probe, radial diffusion is enhanced. This is supported by the flat data profile in the figure. Secondly, because of experimental difficulties, radial measurements were not obtained beyond r/R = 0.5; thus, a particle rate balance could not be performed.

b. Reacting Flow

The presence of the extractive probe produced an impact on the optically measured data rate that ranged from a small to a substantial effect depending on the operating conditions. For example, at 5.5 mps and ϕ = 0.37, and at the sampling station x/d = 6, the data rate remained relatively constant (Figure 20a) as the extractive probe was separated from the optical probe. The radial profiles (Figure 20b) also remain similar with and without the probe.

The factor of two difference (Figure 20b) in data rate at r/R = 0 is not significant and within the reproducibility at ϕ = 0.37. For example, a twofold change in data rate was observed for small changes (e.g., $\Delta\phi$= 0.01) in mixture ratio. The lack of change in these measurements is attributed to the relatively small axial and radial gradients in flow properties at this sampling location as a result of the upstream recirculation and mixing.

No observable change in the optically measured particle size was recorded as the extractive probe was removed from the optical probe. For verification, the optically measured particle size distribution was compared to scanning electron micrographs of the filtered sample with no unexplained discrepancy.

Closer to the centerbody (x/d = 3 1/2), the results are dramatically different (Figure 21a). Here, the sampling station is located within the recirculation zone. The data rate increases more than 70-fold as the probe is withdrawn from the optical sampling volume, with the steepest gradient in data rate occurring within two centerbody diameters of the sampling station. The change is likely a result of a substantial perturbation of the local flow field with a concomitant change in mixing, chemistry, and temperature due to the intrusion of a solid, cold body into a zone of reverse flow. It is noteworthy that the effect on data rate levels off to the without-probe condition at approximately six centerbody diameters downstream of the recirculation zone.

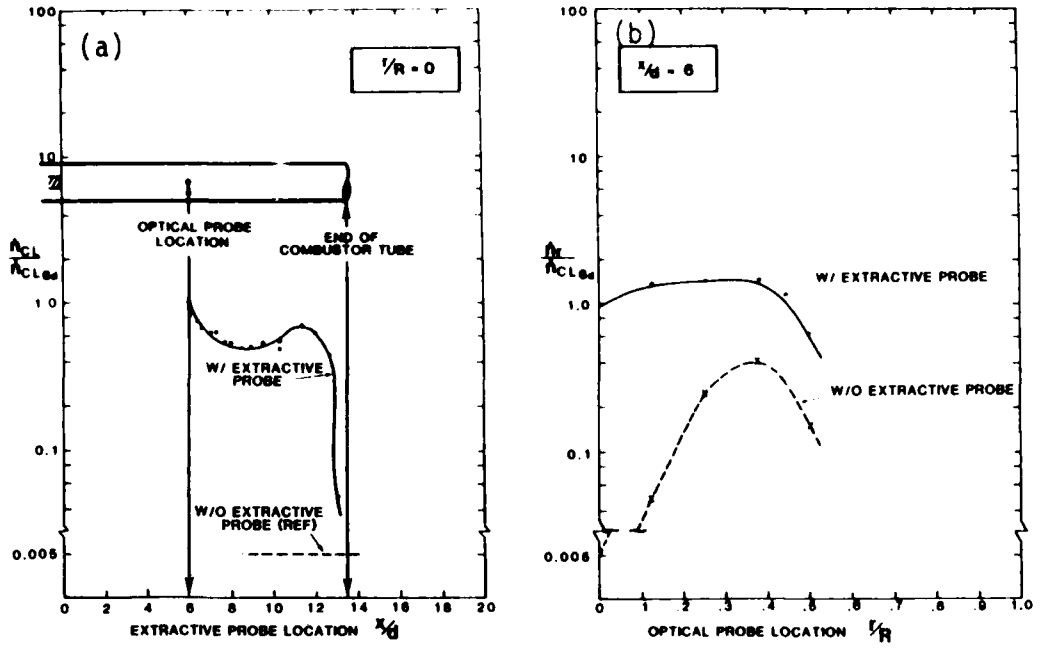

Figure 19. Extractive Probe Perturbation -- Nonreacting Flow with Seeding (x/d = 6, U_{ref} = 7.5 mps, 0.48 μm particles)
(a) Removal of Extractive Probe
(b) Optical Probe Radial Traverse

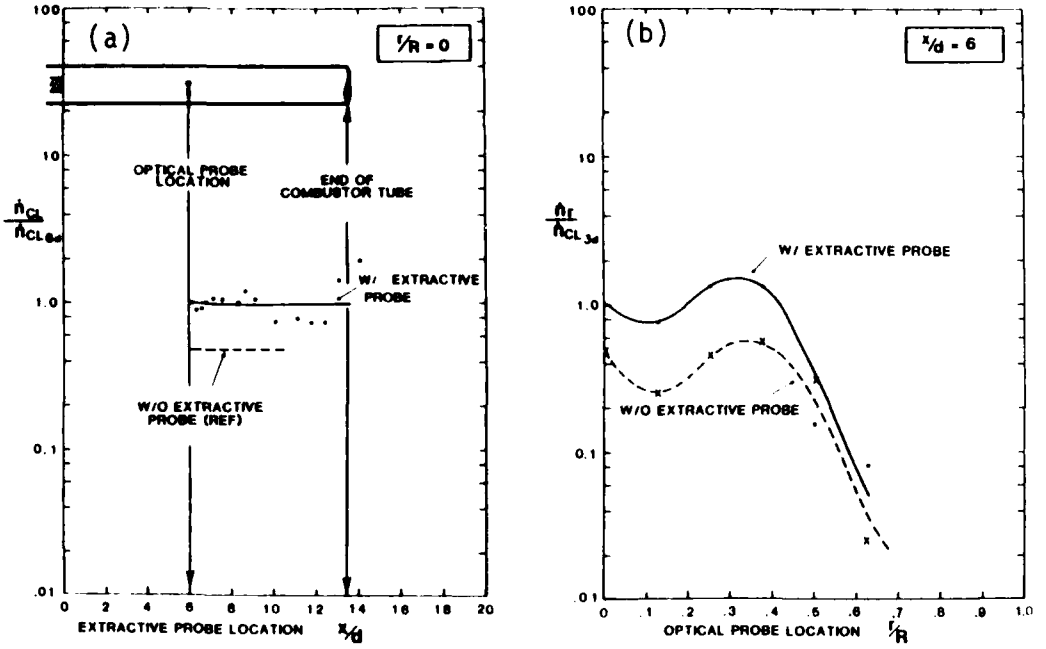

Figure 20. Extractive Probe Perturbation -- Reacting Flow (x/d = 6, U_{ref} = 5.5 mps)
(a) Removal of Extractive Probe
(b) Optical Probe Radial Traverse

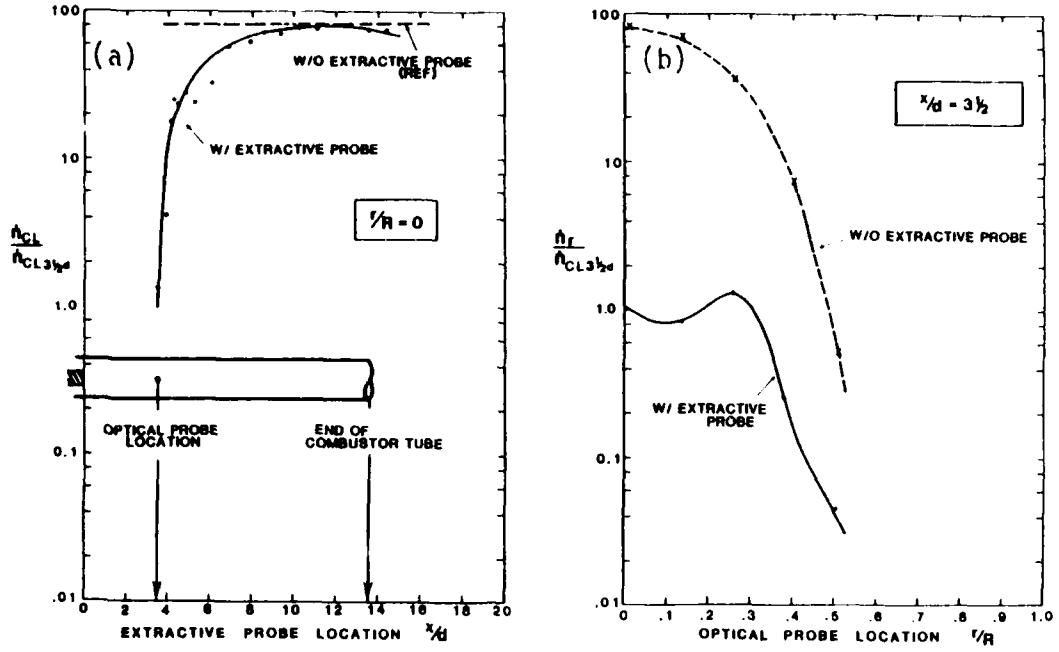

Figure 21. Extractive-Probe Perturbation -- Reacting Flow (x/d = 3 1/2, U_{ref} = 5.5 mps)
(a) Removal of Extractive Probe
(b) Optical Probe Radial Traverse

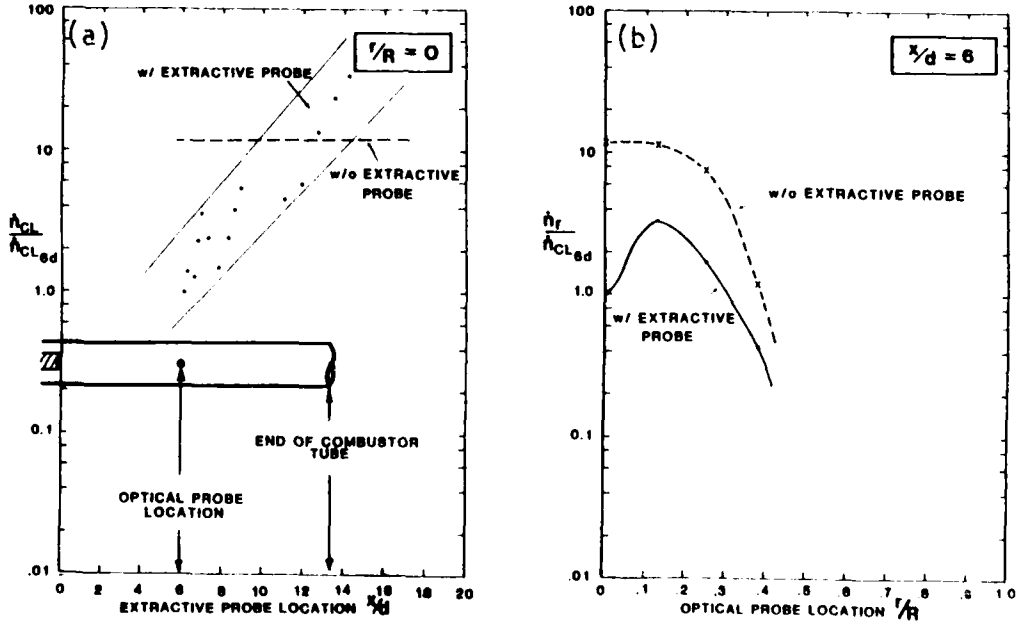

Figure 22. Extractive-Probe Perturbation -- (x/d = 6, U_{ref} = 7.5)
(a) Removal of Extractive Probe
(b) Optical Probe Radial Traverse

The substantial probe perturbation is further evidenced in the radial profiles (Figure 21b). Here, the profile with the probe present resembles the previous case (Figure 20b). However, the profile without the probe is markedly different, having a distinct maximum data rate on the centerline and decreasing monotonically along the radius.

Increasing the reference velocity from 5.5 to 7.5 mps produces an even more dramatic impact even though the sampling volume was located in the wake of the recirculation zone (x/d = 6). Again, the data rate increases about 40-fold as the probe is removed from the sampling volume (Figure 22a). However, for this case there is an appreciable scatter in the measurements. This is attributed to a small but perceptible change in flame structure, probably due to blockage, as the extractive probe is moved from one location to another. In particular, the flame compressed, and the wake region moved upstream as the extractive probe was moved toward the centerbody. The extractive probe perturbation was therefore not limited just to local changes (as in the previous two cases), but extended to dominate flame behavior throughout the combustor. This gross impact on data rate notwithstanding, the change in particle size in the range measured optically was not appreciable. The radial profiles (Figure 22b) resemble the last case (5.5 mps, ϕ = 0.37, x/d = 3 1/2), showing both the large increase in data rate and large change in the presence of the probe.

c. Extractive-Probe Flow Rate

In a final test, the effect of variation in the extractive probe flow rate on data rate was optically assessed. Tests were first conducted for the case of nonreacting flow by seeding with 0.48 μm polystyrene spheres and the effect of sample flow rate on the optically measured data rate at the extractive probe entrance was recorded. For a 7.5 mps reference velocity, the data rate increased 40-percent at the maximum flow rate (Figure 23), consistent with theories relating to nonisokinetic effects; namely, the higher flow rate promotes the radial convection of small particles into the sampling volume.

For reacting flows, the effect of extractive probe flow rate on the optically measured data rate was shown to depend on the operating condition and sample volume location. The extractive probe perturbation results provide some explanation of these trends. At 5.5 mps, ϕ = 0.37, and x/d = 6, the perturbation of the extractive probe is minimal and the effect of an increase in sample flow rate is to increase the data rate to the same degree observed in the nonreacting flow tests. At 3 1/2d, the sampling volume is in the recirculation zone. An increase in sample flow rate had no effect on data rate, which indicates that the flow aerodynamics fully control the local flow properties. Finally, at 7.5 mps, and x/d = 6, the blockage of the probe dominates and, because the blockage is influenced by sample flow rate, an increase in flow rate was observed to produce a perceptible change in flame structure and, as a result, a substantial change in data rate.

d. Summary

The results represent an exploratory investigation into the ·mple perturbation associated with extractive probe sampling for soot. The use · nonintrusive optical measurement techniques focused at the entrance of an · tive probe provided a unique and independent measurement of number density . data rate) and particle size.

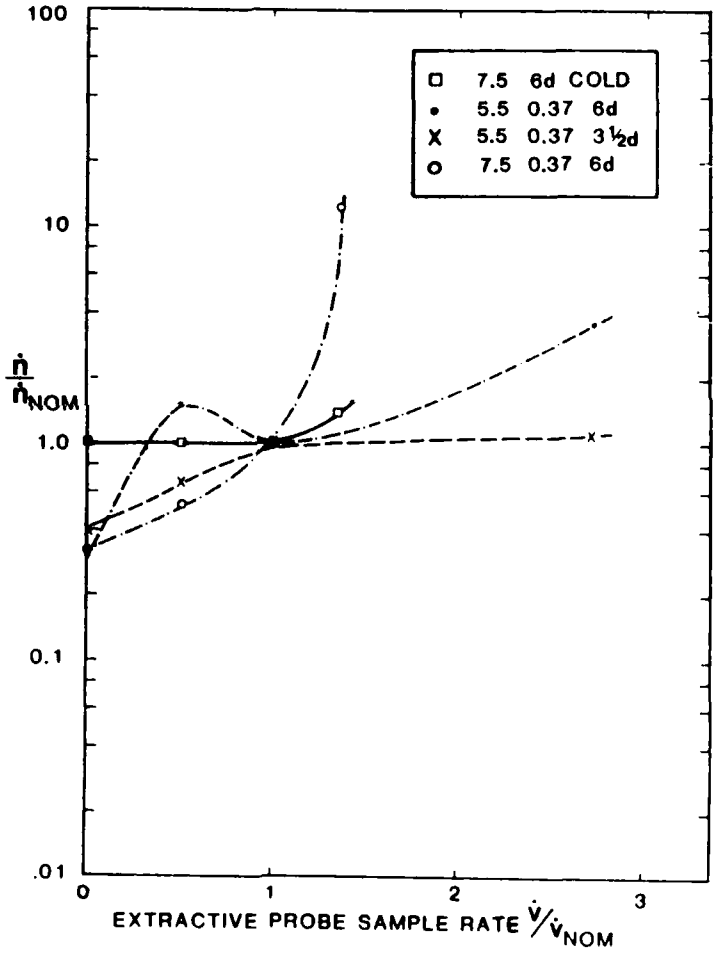

Figure 23. Extractive Probe Conditions--Effect of Sampling Flow Rate on Optically Measured Data Rate

The effect of the physical presence of the extractive probe varied from no significant impact on data rate and particle size (in the particle size range measured) to a dramatic effect on data rate. The dramatic perturbation occurred when the sampling volume was located in the recirculation zone, or when the reference velocity was increased beyond the value (5.5 mps in the present case) above which the blockage produced by the extractive probe became significant.

The results reported here are undoubtedly specific to the combustor configuration employed, and the size and design of the extractive probe used. In addition, the results are limited by the small-particle size cutoff for the optical technique. As a result, the effect of extractive-probe conditions and perturbation on soot particle formation, and on formed soot particles in the size range considered to be heavily populated ($0.02\ \mu m \leq d_p \leq 0.3\ \mu m$) requires the expanded optical capability provided by an expanded range instrument. This notwithstanding, the present results reveal:

- The type of problems associated with extractive probes.
- Questions that must be raised in the interpretation of data from extractive and optical probes.
- The type of experiments necessary to develop and test methods employed to measure soot in gas turbines, boilers, and furnaces.

B. FUEL MOLECULAR STRUCTURE AND ADDITIVE EFFECTS STUDY

1. Introduction

This study was initiated during the period allocated to expanding the capability of the optical system to smaller particulate resolution. The goal was to evaluate the extractive probe and sampling system, and acquire the first data to (1) assess the validity of the ASTM Smoke Point Test in predicting the sooting characteristics of fuels in complex flow, and (2) assess the effect of fuel molecular structure and smoke suppressant additives on the physical and chemical nature of soot. The approach was to use shale-derived JP-8 as the reference fuel, and to blend the five pure hydrocarbon liquids, described in Section III. Isooctane served as the baseline fuel as it represents a major component of JP-8 and serves as the reference fuel in the ASTM Smoke Point Test. The five remaining fuels consisted of shale-derived JP-8 and mixtures of isooctane with either decalin (decahydronaphthalene), toluene, tetralin (1,2,3,4 tetrahydronapthalene), or 1-methylnaphthalene.

The amount of hydrocarbon blended with the isooctane was selected to yield the same ASTM smoke point as that attained with the shale-derived JP-8. The amount of hydrocarbon blended with isooctane was determined by first preparing a curve of smoke point versus volume percent isooctane (Figure 24). Table 10 summarizes the composition and the actual smoke point found for each blend. Although not equivalent, the smoke points are well within the achievable accuracy of the smoke point test $\pm$ 1 mm (Reference 27).

A single ferrocene additive concentration of 0.05-percent by weight

was chosen as being the most effective based on data in Naval Air Propulsion Test Center reports (Reference 21). Test cell smoke abatement work with ferrocene in the J52-P-6B, J57-P-10, and TF30-P-6C gas turbine engines demonstrated this concentration as optimizing an overall reduction in mass emissions. With metal additives, a trade-off does exist, as the additive itself contributes to the mass emissions. Therefore, the additive must be effective in a low enough concentration so that a reduction in the overall mass emissions can occur.

The study was performed in the 80 mm (3-inch) centerbody combustor with liquid fuel injected at the face of a centerbody using a flush-mounted twin-fluid atomizer (Spraying Systems J-Series, Round Spray, 2050 Fuel Cap, 67146 Air Cap).

TABLE 10. COMPOSITION AND SMOKE POINTS OF FUEL BLENDS

Fuel	Smoke Point[a]		Change
	Without Additive mm	With Additive mm	%
Isooctane	43.0	>50.0	+16
Shale JP-8	23.0	24.7	7
Blend 1 86% Decalin 14% Isooctane	24.3	28.3	16
Blend 2 21% Toluene 79% Isooctane	24.0	26.3	10
Blend 3 8% Tetralin 92% Isooctane	25.3	30.0	29
Blend 4 5% 1-methylnaphthalene 95% Isooctane	22.2	35.0	58
Mean	23.8	28.9	
Standard Deviation	1.2	4.0	

[a] Distance above base of burner at which sooting first occurs

The combustor was operated at an overall equivalence ratio of 0.2, a reference velocity of 15 m/s, and at atmospheric pressure throughout the experiment. Operation at atmospheric pressure, although not representative of gas turbines, was necessary to allow a comparison of sooting propensity between the ASTM-D-1322 Smoke Point Test and a complex flow at a common pressure. Combus-

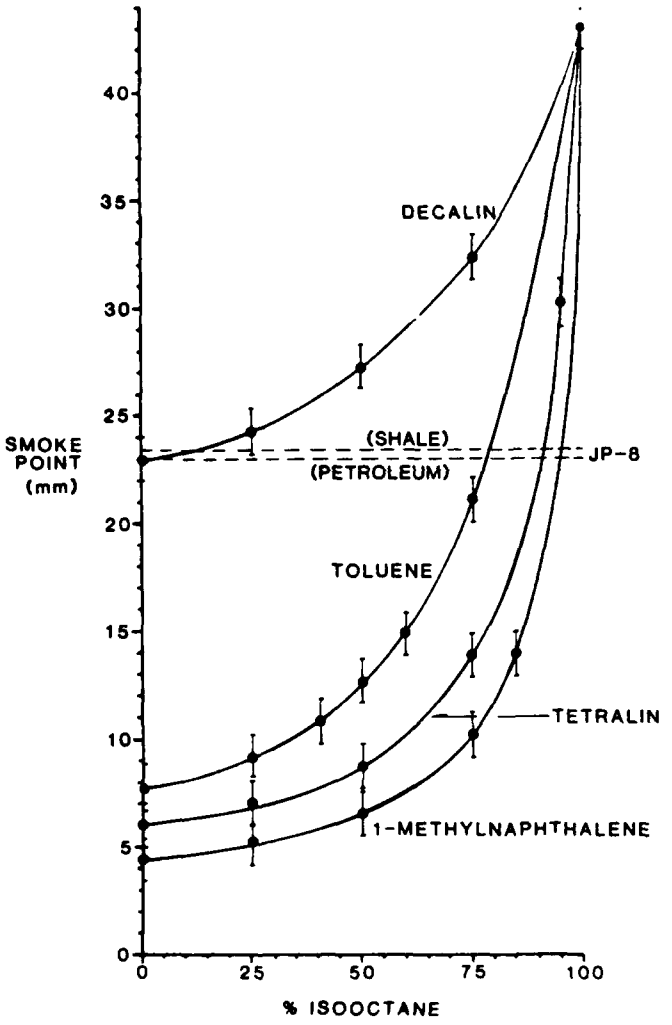

Figure 24. Smoke Point Versus Volume Percent Isooctane

tion of fuels of varying sooting propensity at different pressures has indicated, however, that even though the sooting increases with pressure, the relative sooting intensity among the different fuels remains the same (Reference 6).

The results from each phase of the analysis of soot samples withdrawn from the flame are presented in the following four sections. The PAH section entails a comparison of the chromatographs obtained from the filter and resin extracts with respect to the fuel molecular structure and the amounts and types of PAH present. These results are then related to the currently proposed mechanisms for the formation of soot. The ferrocene section utilizes the gravimetric data from the samples collected to ascertain the effectiveness of the ferrocene additive. The addition of a uniform amount of ferrocene, on a weight basis, to each of the fuels also allows an assessment of the reproducibility of the sampling location for the different fuels by comparing the amount of iron recovered in each sample. The predictive value of the ASTM Smoke Point Method is evaluated in the next section by comparing the smoke points found for each of the fuels with the soot gravimetric data attained. Finally, the elemental analysis section presents the carbon percentages of the soot samples attained before and after each extraction along with the limitations of the method.

2. Polycyclic Aromatic Hydrocarbons

A comparison of the gas chromatographs from the filter and resin extracts is shown in Figure 25. As can be seen from the retention times of the PAH standards, the retention of PAH on a capillary column increases nearly linearly with molecular weight. Wilmhurst (Reference 93) has demonstrated, however, that the aliphatic carbons in the PAH molecules contribute less to the overall retention than the aromatic carbons. Thus, the alkylated PAH show some deviation from the expected linearity, but the overall order in which the compounds are eluted provides a rough indication of their molecular weight.

Taking into account the attenuation factor involved in each chromotograph, it is evident that a greater preponderance of vapor-phase organics were collected up to a point approximately halfway between the retention times of phenanthrene and chrysene. After this point, the presence of any PAH fell off dramatically. A similar result has been noted in studies involving PAH in auto exhaust (Reference 66), in which filters were found to collect 90-percent of the PAH less volatile (greater molecular weight) than pyrene and only 25 to 50-percent of the PAH more volatile than pyrene. The relative retention index of pyrene is 351.22 (Reference 80) which corresponds to a location halfway between phenanthrene and chrysene. Any PAH associated with the soot was found to be present at trace levels with the large peaks being identified as adipates and phthalates upon GC/MS analysis. These contaminants are common plasticizers whose presence is attributed to the Dow-Corning high-temperature lubricant used as a sealant at the glass junctions of the Soxhlet extraction apparatus.

Identification of the compounds via GC/MS analysis was compromised by a limitation of the instrument. The instrument is capable of the less sensitive split mode of injection in which only a fraction of the injected sample is carried into the column. Thus, trace components are not present at the same concentration attained in the GC analyses, which uses splitless injections, resulting in a number of compounds being at a concentration below the limit of

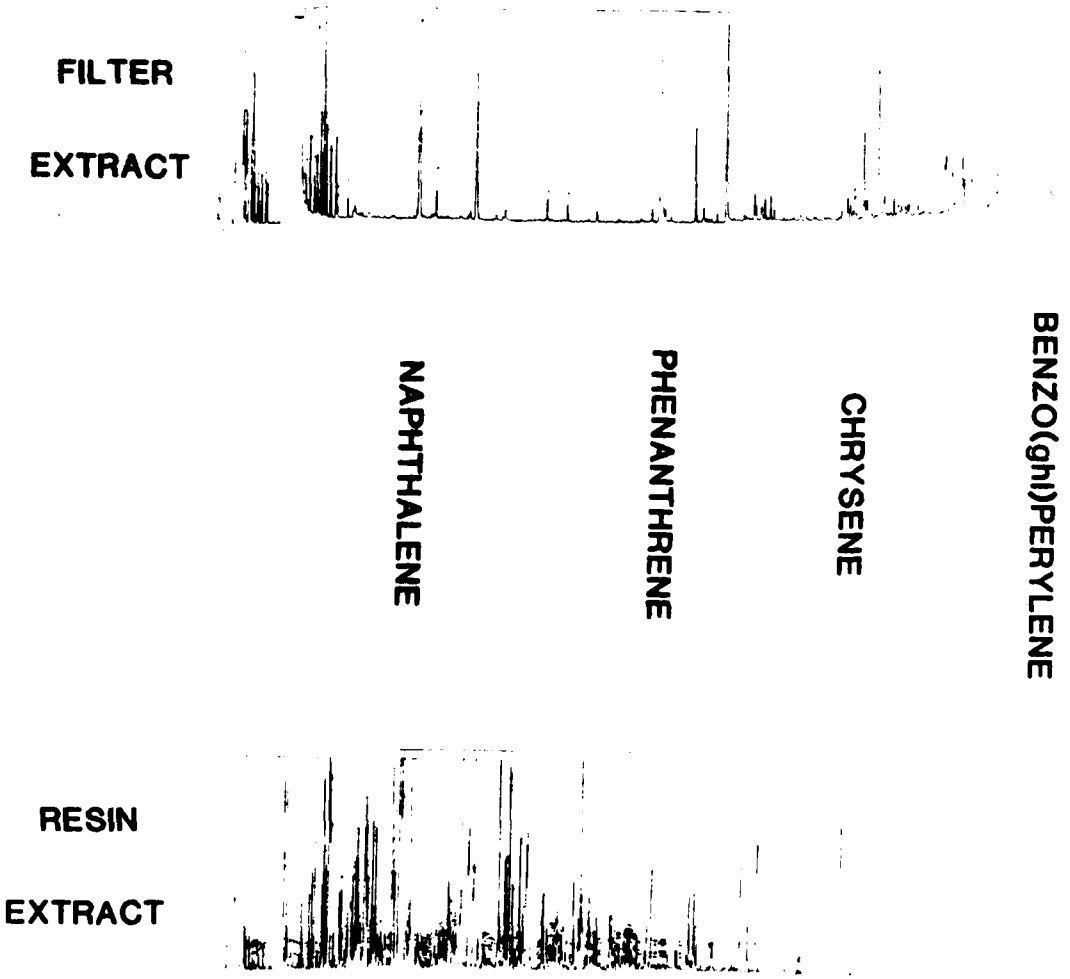

Figure 25. Gas Chromatographs of Filter Extract (2 ml Injection) and Resin Extract (0.5 ml Injection) from Soot Generated in the Toluene Blend Flame

detection. Although the compounds present from the main extract were more concentrated than the filter extract, they eluted in such abundance that the resolution was compromised and insufficient separation for analysis was attained.

A tabulation of the compounds found in the filter extracts from the various fuels is presented in Table 11. Even though the fuel blends were predominantly isooctane, the presence of aromatic groups in the fuel contributes significantly to the presence of higher molecular weight PAH. Although small quantities of high molecular weight PAH are present from the saturated hydrocarbons isooctane and decalin, there are far fewer compounds present.

These findings are in agreement with the simplified soot formation mechanism proposed by Graham, et al. (Reference 94) which is shown in Figure 26. Aromatic hydrocarbons can follow two mechanistic paths,depending on the temperature. Below 1800°K, the condensation of the aromatic rings into a graphite-like structure is favored, while above this temperature, the fuel molecules are fragmented into small hydrocarbon radicals which then polymerize to form larger, hydrogen-deficient molecules which eventually nucleate and produce soot. Based on shock-tube studies of soot formation, Graham has concluded that the condensation route is much faster than the fragmentation/ polymerization route. Aliphatic hydrocarbons predominantly follow the slower fragmentation/polymerization mechanism, thereby exerting a less dominate effect on the production of soot than the aromatics.

The addition of ferrocene to the fuel blends has no apparent effect on the composition of the soot organic extract. As mentioned previously, the iron is thought to be occluded in the soot particle and to act in the later regions of the flame. If this is the case, the formation of the PAH soot precursors would be unaffected by the iron additive as it operates within the soot molecule and not by affecting the concentration of flame hydrocarbon ions. It is difficult to ascertain, however, whether the PAH molecules are directly associated with the soot molecules in the flame or are an artifact of the sampling procedure. The rapid quenching of the combustion gases upon entering the probe may cause the condensation of some PAH on surrounding particulate matter.

One must also recognize three factors which may potentially cause PAH losses during the sampling process and analytical procedure. First, the filter plus adsorbent sampler may not be able to completely trap the gaseous or particulate-associated PAH, resulting in sample penetration. Although the effluent was not tested for hydrocarbon content, penetration appears unlikely as the XAD-2 resin was found to change from white to yellow in the region of hydrocarbon adsorption. This discoloration never extended the length of the resin sample holder and was judged to be indicative of sufficient resin for complete retention of the sample. Second, losses due to wall deposition are minimized through the nitrogen dilution and heated sample line. Finally, some losses may occur due to photodegradation or reactions between collected PAH and other components during the sample collection and extraction. Thus, it is difficult to assess the representativeness of the sample, although the measures taken would appear to be adequate.

TABLE 11. TABULATION OF COMPOUNDS FOUND IN SOOT FILTER EXTRACTIONS

Compound Name	Retention Indices[a]	Soot PAH Content — Fuel: Isooctane w/o Add.	Isooctane w/[f] Add.	86% Decalin 14% Isooctane w/o Add.	86% Decalin 14% Isooctane w/[f] Add.	21% Toluene 79% Isooctane w/o Add.	21% Toluene 79% Isooctane w/[f] Add.	8% Tetralin 92% Isooctane w/o Add.	8% Tetralin 92% Isooctane w/[f] Add.	5% 1-methyl 95% Isooctane w/o Add.	5% 1-methyl 95% Isooctane w/[f] Add.	JP-8 w/o Add.	JP-8 w/[f] Add.
Naphthalene	200.00		(3.8)[g]			(0.8)	(0.8)						
	206.67±.14[b]	(4.2)		(0.7)		(0.3)				(0.4)			
	252.73±.25[c]					(0.2)	(1.1)						
	285.98±.29[c]		(50.2)		(8.8)		(11.6)		(0.7)				
	290.98±.01[c]		(3.7)				(0.6)						
	298.75±.24[c]				(4.4)								(3.3)
Phenanthrene	300.00		(63.0)			(7.1)				(1.0)			
	303.32±0[c]												(0.5)
	318.15±.09[c]				(6.4)		(10.6)						
	343.79±0[c]						(0.8)						
	348.77±.11[c]		(6.0)		(1.0)		(0.6)						
	396.90±.20[d]					(1.4)	(1.4)	(1.4)	(1.3)	(1.7)	(1.4)	(0.9)	(1.8)
Chrysene	400.00		(39.0)		(3.9)	(4.4)	(2.2)	(1.0)		(0.6)			(4.0)
	407.40±.04[d]											(0.2)	
	445.99±0[d]					(0.6)							
	451.47±.19[e]							(0.7)					
	452.99±.21[e]	(4.0)				(3.8)	(0.9)	(5.1)	(1.4)	(2.0)	(1.7)	(0.8)	
	483.56±0[e]				(1.6)								
	491.69±.13[e]					(1.4)		(1.6)		(0.6)			
Benzo[ghi] Perylene	500.00	(5.5)	(20.3)		(2.6)	(4.7)	(2.0)	(4.3)	(2.8)	(2.2)	(1.5)	(0.4)	(2.7)
	503.18±.15[e]					(0.7)		(1.9)		(0.6)			

[a] retention indices are the relative positions of the compounds retention times to the PAH Standards. The PAH standards are assigned values corresponding to the number of aromatic rings in the standard.
[b] reported as naphthalene equivalent
[c] reported as phenanthrene equivalent
[d] reported as chrysene equivalent
[e] reported as benzo[ghi]perylene equivalent
[f] DMSO separation procedure not carried out on these runs. (no interfering aliphatic peaks)
[g] Number in parenthesis = μg PNA/mg Soot/M[3] recovered; blank indicates no evidence of species

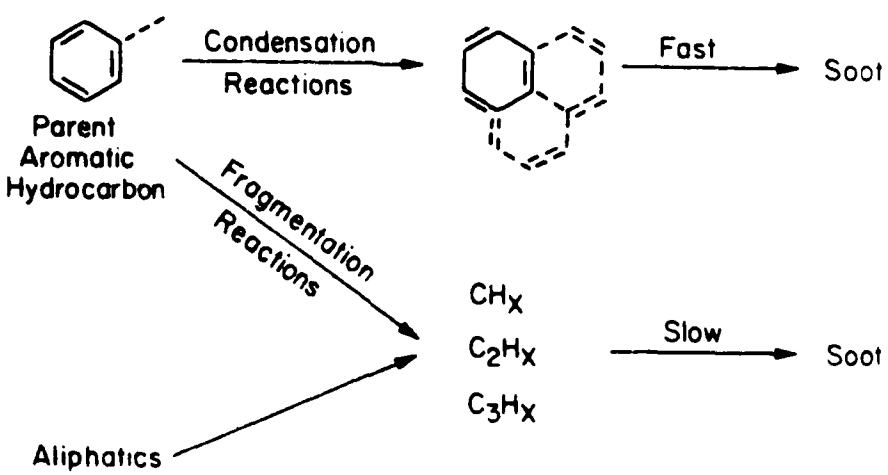

Figure 26. A Simplified Mechanism for Soot Formation (Reference 94)

The analytical procedure was successful in extracting the soluble organics associated with the soot although some modifications are necessary to improve the GC and GC/MS analysis. The trace levels of PAH appear to necessitate further sample concentration from a volume of 2 ml to 100 ml using a micro Kuderna Danish technique. In this way, the signal-to-noise ratio will be improved 20x, thereby increasing the number of PAH within the instruments limits of detection. The types of compounds associated with the soot can then be better evaluated, and the necessity of the dimethyl sulfoxide step used to isolate the PAH can be better assessed. The chemical separations do involve some minor losses, which may be significant for those compounds present at trace levels. The resin extracts indicate that the precleaned XAD-2 resin may have to be extracted with dichloromethane before use, as a substantial background was still found to be present.

3. Ferrocene

The addition of ferrocene to the fuel had no effect on the basic flame shape but did result in a more luminous flame. As the iron analysis occurred after the Soxhlet extraction, it was necessary to examine both the soluble and insoluble fractions for iron content. The results are presented in Table 12 and indicate that less than 1 percent of the total amount of iron recovered was found in the soluble fraction. The trace amount of iron found in the soluble fraction is consistent with the ferrocene being oxidized during the combustion process to either wuestite (FeO) or hematite (Fe_2O_3). The weight of iron determined from atomic absorption spectrophotometry was reported as iron oxide (50 percent FeO and 50 percent Fe_2O_3) and subsequently subtracted from the gross sample weight to yield the actual amount of soot collected. The composition of iron oxide was assumed, as a direct analysis was not performed and the ratio is dependent on the combustor operating conditions. By choosing an equivalent composition of the iron oxides, the corrected values can only be in error by at most 5 percent, which is well within the experimental uncertainty.

A comparison of the amount of iron found on the filter to the theoretical value calculated from the fuel flow rate and percentage of the total flow sampled (Table 13) indicates a high degree of reproducibility in the amount of iron recovered for a constant sampling location and fuel ferrocene concentration. The 1-methylnaphthalene blend, however, is seen to deviate significantly from the mean value obtained from the other fuels and is indicative of a possible operator error in the amount of additive used in the fuel blend. With the possible exception of this one blend, these results are consistent for an aerodynamically similar flow within the combustor for each of the different fuel types. The gravimetric results are, therefore, also taken as being characteristic of the fuel blend without any aerodynamic biasing of the sample occurring.

As shown in Table 14, no significant difference in the soot weight concentration was found between the ferrocene and nonferrocene runs with the pure isooctane, and the decalin and toluene blends. In direct contrast, the soot weight concentration of the tetralin and 1-methylnaphthalene blends increased 50 percent in the presence of ferrocene while the soot weight concentration of the chemically complex JP-8 decreased 60 percent. Based on the proposed mechanism for soot reduction with ferrocene presented earlier, the

effect of ferrocene is likely to be a function of the temperature, residence time, and chemical structure of the soot matrix. Since the temperature field and residence times are relatively uniform for each run due to the narrow range of fuel-heating values and consistent aerodynamics, the gravimetric results suggest that the effect of the ferrocene additive is strongly tied to the chemical structure of the soot matrix.

TABLE 12. IRON CONTENT OF SOLUBLE AND INSOLUBLE FRACTIONS OF SOOT EXTRACTS FROM FUELS CONTAINING 0.05-PERCENT FERROCENE

Fuel	Soluble Fraction (μg)	Insoluble Fraction (μg)	Iron Corrected To Oxides of Iron[a] mg	mg/m^3
Blank	--	9	--	--
Isooctane	<1	225	.306	.57
86% Decalin 14% Isooctane	<1	237	.322	.77
21% Toluene 79% Isooctane	<1	252	.342	.62
8% Tetralin 92% Isooctane	<1	259	.352	.68
5% 1-methyl-naphthalene 95% Isooctane	<1	467	.634	1.15[b]
Shale JP-8	<1	147	.200	.75
Mean				.68±.08

[a] Assumed composition of oxides of iron to be 50-percent FeO and 50-percent Fe_2O_3
[b] Value not used in calculating the mean and standard deviation

The use of the microquartz fiber filters, which contain trace amounts of iron (Reference 95), proved to be suitable as background values from blank filters (Table 12) typically accounted for less than 5 percent of the iron detected. The recovery of iron from the filter is only assumed to be complete, however, and may need to be assessed by impregnating a clean filter with a known amount of wuestite and hematite and subjecting it to the same analytical procedure. An alternative method would be to compare the results of identical

samples by first using neutron activation analysis and then atomic absorption spectrophotometry.

TABLE 13. COMPARISON OF ACTUAL AND THEORETICAL QUANTITIES OF IRON COLLECTED ON THE FILTER FROM SAMPLED FLOW

Fuel	Amount of Ferrocene (grams)	Amount of Iron (mg)	Percent of Flow	Iron Recovered		Percent of Theoretical
				Theoretical (mg)	Actual (mg)	
Isooctane	2.096	629	.198	1.24	.225	18
86% Decalin 14% Isooctane	2.230	669	.155	1.04	.237	23
21% Toluene 79% Isooctane	2.208	662	.207	1.37	.252	18
8% Tetralin 92% Isooctane	2.160	648	.186	1.20	.259	22
5% 1-methyl-naphthalene 95% Isooctane	2.144	643	.203	1.30	.467	36[a]
Shale JP-8	0.714	232	.260	.60	.147	24
Mean						21 ± 2.8

[a] Value not used in calculating the mean and standard deviation

4. Elemental Analysis

The collection of particulate matter on a fibrous filter media necessitated an accurate determination of the background carbon and hydrogen values as well as an average weight of the filter aliquots. As can be seen from Table 15, the standard deviation of filter aliquot weights was only approximately 1-percent of the total aliquot weight, but represented a 20-percent error in determining the amount of sample if 15 mg was collected. One-hour sampling periods only provided samples on the order of 1-5 mg depending on the fuel. Consequently, the weight of sample on the filter aliquot could not be determined accurately as it was not significantly greater than the deviations in filter aliquot weights and required an assumption of homogeneous sample distribution to be made. In this manner, a sample weight could be calculated by multiplying the weight of the total sample collected by the area percentage of the filter aliquot. With this value, the percentage of carbon present could then be obtained. The background values of hydrogen proved to be of the same

order as that present in the sample, thereby prohibiting any determination of the amount of hydrogen present in the samples.

TABLE 14. SOOT WEIGHT CONCENTRATION FROM FUELS WITH AND WITHOUT FERROCENE

Fuel	Soot Collected without Ferrocene (mg/m^3)	Soot Collected with Ferrocene (mg/m^3)	Change in Weight Concentration
Isooctane	1.06	1.33	0
86% Decalin 14% Isooctane	5.37	5.37	0
21% Toluene 79% Issoctane	6.74	7.34	0
8% Tetralin 92% Isooctane	4.10	5.88	+50%
5% 1-methyl-naphthalene 95% Isooctane	5.12	7.92	+50%
Shale JP-8	23.52	9.10	-60%
Mean	5.33	6.62	
Standard Deviation	1.09	1.20	

The percentage of carbon found in each sample before and after a Soxhlet extraction appears in Table 16. Different samples collected under identical conditions were used in evaluating the percentage of carbon present. The toluene blend with additive had two different samples analyzed for carbon to provide an idea of the repeatability of the carbon percentage values. The results indicate a high degree of variability, although this could be attributed to the imperfect method of calculation as well as the different samples. The scatter in the data indicate no definite trends with regard to the percentage of carbon other than the lower values obtained from the fuels containing the ferrocene additive. This stands to reason as these samples also contain iron oxide which lowers the percentage of the total sample that is carbon. The standard deviations of the mean values indicate no similarity among the fuel blends with respect to carbon content. There is also no apparent trend attributable to fuel molecular structure which would demonstrate an increasing carbon content in the soot with increasing aromaticity in the fuel. The relatively small samples obtained, however, were not sufficiently greater than

AD-A137 208 EFFECTS OF FUEL SPECIFICATION AND ADDITIVES ON SOOT FORMATION(U) CALIFORNIA UNIV IRVINE COMBUSTION LAB G S SAMUELSEN ET AL. DEC 83 AFESC/ESL-TR-83-17 2/2

UNCLASSIFIED F08635-79-C-0158 F/G 21/5 NL

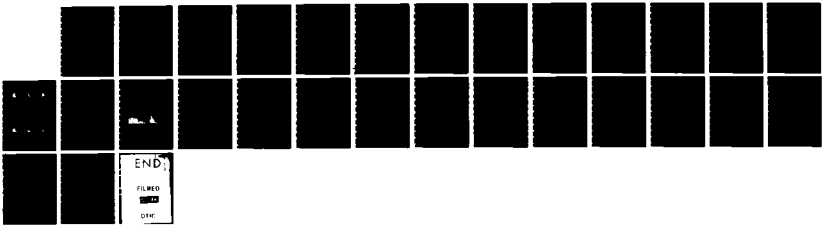

END

FILMED

DTIC

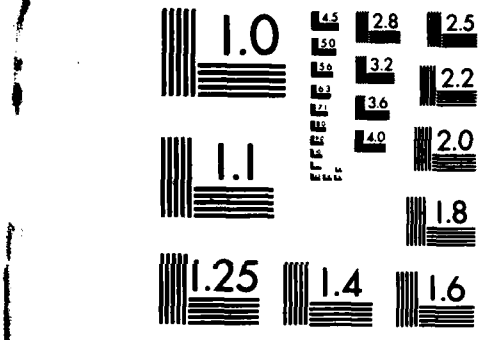

the variations in weight of the filter aliquots or the hydrogen backgrounds to allow an accurate analysis. Thus, the method only becomes a viable approach when sufficient quantities of sample can be obtained.

TABLE 15. FILTER BACKGROUND VALUES OF CARBON AND HYDROGEN

Filter/Section[a]	Carbon (μg)	Hydrogen (μg)	Weight (mg)
1 A	4.72	59.98	9.567
B	5.43	60.45	9.604
C	7.55	62.07	9.568
D	4.72	61.84	9.657
E	4.72	61.84	9.490
2 A	3.78	60.22	9.474
B	4.25	59.75	9.597
C	3.78	59.98	9.398
D	2.36	57.90	9.332
E	8.78	60.91	9.591
3 A	2.36	62.30	9.579
B	1.89	60.68	9.550
C	2.83	62.07	9.659
D	3.30	60.68	9.538
E	3.78	60.22	9.607
4 A	3.78	59.98	9.365
B	1.89	62.07	9.470
C	3.30	60.45	9.411
C	3.30	60.68	9.632
E	1.42	61.84	9.404
Mean	3.65	60.80	9.5247
Standard Deviation	1.41	1.10	0.100

[a] 11.5 mm diameter aliquots

An alternate and viable method for sampling soot in flows with relatively low soot concentration would entail the use of the nuclepore filter employed for scanning electron microscopy. In this way, a sample could be collected on smooth filtering media and then removed with the confidence of recovering the entire sample.

TABLE 16. SOOT PERCENTAGE CARBON BEFORE AND AFTER SOXHLET EXTRACTION

Fuel	Before Extraction		After Extraction	
	Without Additive	With Additive	Without Additive	With Additive
Isooctane	89%	50%	51%	18%
86% Decalin 14% Isooctane	88	61	45	38
21% Toluene 79% Isooctane	93	43	95	39
8% Tetralin 92% Isooctane	59	40	89	41
5% 1-Methyl-naphthalene 95% Isooctane	63	34	88	38
Shale JP-8	98	47	100[a]	36
Mean	81.7	49.3	73.6	35.0
Standard Deviation	16.4	12.5	23.6	8.5

[a] Method of calculation indicated more carbon than theoretical weight of filter aliquot

5. ASTM Smoke Point

The smoke points attained with each fuel containing ferrocene appear in Table 10 with the gravimetric results appearing in Table 14. The average smoke point exclusive of the baseline fuel, isooctane, is 23.8 mm with a standard deviation of 1.2 mm which is roughly equivalent to the established experimental error of $\pm$ 1 mm reported for the smoke lamp with a single operator (Reference 27). The gravimetric results of the four fuel blends averaged 5.33 mg/m^3 with a standard deviation of 20 percent which is very similar to the deviation found with the iron loading on the filters from the fuels containing ferrocene. A 20-percent variation in soot loading is therefore considered not to be significantly different from the established range of experimental fluctuations. The chemically complex shale JP-8, however, resulted in a soot concentration greater than 400 percent of the average of the fuel blends. The significant increase in soot loading, not predicted by the smoke point test, must be attributed to differences between the two modes of combustion. The fact that the simple fuel blends reflected the smoke point results indicates that the differences are probably attributable to some factor affecting the chemistry.

The addition of 0.05-percent by weight ferrocene to the fuels resulted in increases to all of the smoke points ranging from 7 percent for shale JP-8 to 58 percent for the 1-methylnaphthalene blend. The standard deviation from the mean of 4.0 (Table 10) is four times greater than the acceptable level of error if the additive were to affect each fuel equally and is indicative of a chemical role governing the effectiveness of the iron (ferrocene) in oxidizing the soot. Whereas the smoke points portend a decrease in soot emissions for all of the fuels, the additive was found to markedly increase the emissions for the tetralin and 1-methylnaphthalene blends, and have no significant effect on the others except for the JP-8 which demonstrated a 60-percent reduction in soot emissions.

In a turbulent diffusion flame with complex aerodynamics, a number of factors affect the flame chemistry which are not represented with the laminar diffusion flame used in the smoke point lamp. Although the simple fuel blends with nearly identical smoke points gave similar performances in the combustor, the chemically complex JP-8 and the ferrocene-containing fuels gave a range of results totally dissimilar to those anticipated from the ASTM Smoke Point Tests. The two additive blends which yielded 50-percent increases in soot emissions possess dicyclic aromatic structure. Even though tetralin does not initially possess dicyclic aromatic structure, Benjamin, et al. (Reference 96) have reported that naphthalene is a major product of the pyrolysis of tetralin. These fuel blends thus contained aromatics in excess of the 3-percent specification which currently exists for Jet-A (Table 1) and, as mentioned previously, produce more soot than the hydrogen correlation. These results suggest that fuel molecular structure must be a consideration in the development of new fuel specifications for future fuels.

6. Summary

Simple fuels of varying molecular structure as well as a chemically complex shale-derived JP-8 were utilized to assess the effect of fuel molecular structure on the chemical properties of soot. The simple fuels were blended so as to yield an equivalent smoke point with the JP-8,enabling an evaluation of the ASTM Smoke Point Method to be performed by burning these liquid fuels in a laboratory combustor possessing complex aerodynamics. Gas chromatographic analyses of the filter and resin extracts resulted in the following observations:

- A greater proliferation of PAH species in the soot occurs with aromatic fuels, with the quantities of PAH following the percentage of aromatics in the fuel.
- PAH associated with the soot primarily consisted of the less volatile, higher molecular weight species and were only present at trace levels.
- A large number of low molecular weight species are present in the vapor phase with essentially no compound eluting from the resin extracts after a relative retention time of 350.
- Ferrocene has little apparent effect on the quantities and types of PAH present.

Gravimetric determinations of the collected soot samples in conjunction with the atomic absorption analyses of their iron content demonstrated that the ferrocene additive was effective in reducing only the soot concentration arising from the combustion of shale JP-8. In the remaining cases, ferrocene had either no effect or a significant adverse effect leading to the conclusion:

- The chemical structure of the soot matrix appears to govern the effectiveness of the iron additive in oxidizing the soot.

Gravimetric determinations of collected soot samples from JP-8 and fuels blended to yield the same ASTM Smoke Point as the JP-8 study revealed the following:

- The ASTM Smoke Point Method can be misleading in the prediction of the smoking tendency associated with fuels burned in complex flows.

- The ASTM Smoke Point Method failed to predict the effect of the ferrocene additive in a complex flow.

- Mixtures of pure aromatic hydrocarbons in isooctane, blended to produce the same ASTM Smoke Point as shale JP-8, produced similar soot loadings in a complex flow. The chemically complex JP-8, however, produced a soot concentration a factor of four higher in the same complex flow.

- The inconsistency between the ASTM Smoke Point Test and the complex flow results is attributed to the dependency of sooting on flame temperature and residence time on the one hand, and the role of aerodynamics dictating the turbulent diffusion of oxygen, the temperature field, and the distribution of residence times in a complex flow field on the other.

The results are indicative of the complexity of the problem of soot formation in gas turbines. Fuel molecular structure has been shown to play a dominant role in the formation of soot, the quantity and type of PAH species produced, and the effectiveness of the smoke suppressant, ferrocene. The current ASTM Smoke Point Test for aviation fuels appears to be inadequate and may necessitate the use of alternative specifications such as the hydrogen and dicyclic aromatic content of the fuel, as well as the testing of fuels under actual complex flow conditions.

C. EXPANDED-PARTICLE OPTICAL SYSTEM

1. Introduction

The Expanded-Particle Optical System was tested using the 80 mm (3-inch) Dilute-Swirl Combustor (DSC) module (Figure 5c). Cold flow runs were conducted to verify and validate the system, and hot flow runs were conducted to assess performance of the optical system under reacting conditions, and to obtain first insights into the distribution of soot size and number density throughout the flow field as a function of fuel molecular structure.

2. Verification and Validation

Calibration of the intensity ratio techniques -- 10°/5°, 60°/20° and polarization ratio -- was performed using latex particles with known diameters and comparing the measurements with the theoretical curves for latex particles. Specified-size particles were seeded into the combustor, while running cold, and monitored using the different sizing techniques. Several sizes of polystyrene spherical particles (Dow Diagnositcs, Indianapolis, IN) were used. Table 17 summarizes the different sizes of the polystyrene latex particles, their standard deviation, and the range of each optical technique. All the measurements were performed at two reference velocities, U = 7.5 m/s and 15 m/s. As with the large particle optical system tests (Section VA), a seeding nebulizer was located about 2 meters upstream of the combustor module. The seed material was introduced in the annular jet and swirl inlet air stream. No fluid was injected through the fuel jet.

a. Large-and Small-Angle Intensity Ratio

Nonreacting flow results for the small-angle intensity ratio technique are shown in Figure 27 for the location x/D = 1.5, r/R = 0. The graph (Figure 27a) is a normal sample count versus intensity ratio in logarithmic scale. The gains of the photomultiplier were selected to provide the correct signal height. The theoretical predictions and experimental results coincide at the upper limit of the range of the technique (Figure 27b) and differ slightly at the lower limit of the range.

TABLE 17. POLYSTYRENE LATEX PARTICLES

Technique	Size (μm)	Standard Deviation (μm)	Velocity (m/s)
1. Particle size interferometry	3.3	0.12	7.5, 15
2. Small-angle intensity ratio	1.74 1.32	0.016 0.053	7.5, 15
3. Large-angle intensity ratio	0.481 0.33	0.0018 0.004	7.5, 15
4. Polarization intensity ratio	0.198 0.109	0.0036 0.0027	7.5, 15

Results of large-angle intensity ratio technique (60° and 20° off the laser axis) were performed at the same axial and radial locations as the small-angle intensity ratio technique (Figure 28). The photomultipliers were

a. Raw Data

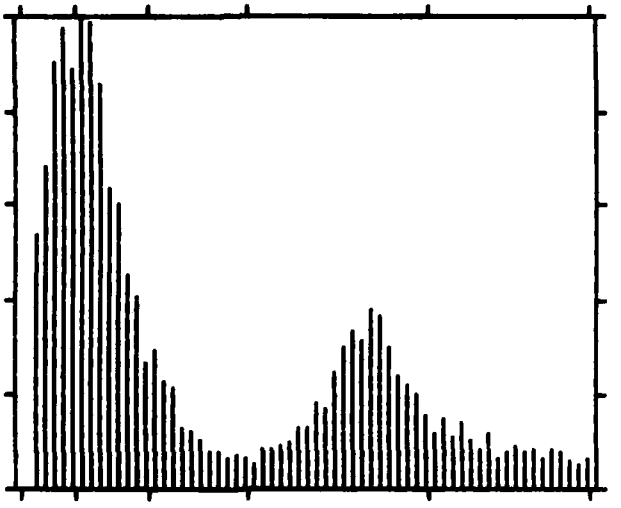

GRAPH OF NORMALIZED RAW COUNTS VERSUS
LOGRITHMIC INTENSITY RATIO FROM 1 TO .1

DATE: 12-17-81
SERIES: BOTH RUN: 6
COMMENT: D=.481/2.25 KNOBS=188/150 LASER=0.500 RADIAL=CENTER V=7.5

MAX RAW COUNT = 764
TOTAL RAW COUNT = 12492
SAMPLE TIME: 208.35 SECONDS

LISTING OF RAW COUNTS

RATIO	BIN COUNT	RATIO	BIN COUNT
.946	410	.31	139
.913	519	.299	128
.881	691	.289	188
.85	747	.278	232
.82	680	.268	254
.791	764	.259	238
.763	755	.25	292
.736	655	.241	280
.71	488	.232	232
.685	463	.224	184
.661	346	.216	171
.637	309	.209	153
.615	205	.201	120
.593	226	.194	87
.572	175	.187	113
.552	165	.181	83
.532	101	.174	108
.513	96	.168	81
.495	81	.162	64
.478	59	.156	91
.461	60	.151	48
.444	49	.145	60
.429	52	.14	67
.414	47	.135	57
.399	38	.13	65
.385	63	.126	51
.371	62	.121	65
.358	70	.117	60
.345	75	.113	46
.333	98	.109	41
.321	98	.105	47

Figure 27. Cold-Flow Verification Data -- 10°/5° Ratioing

b. Comparative Data

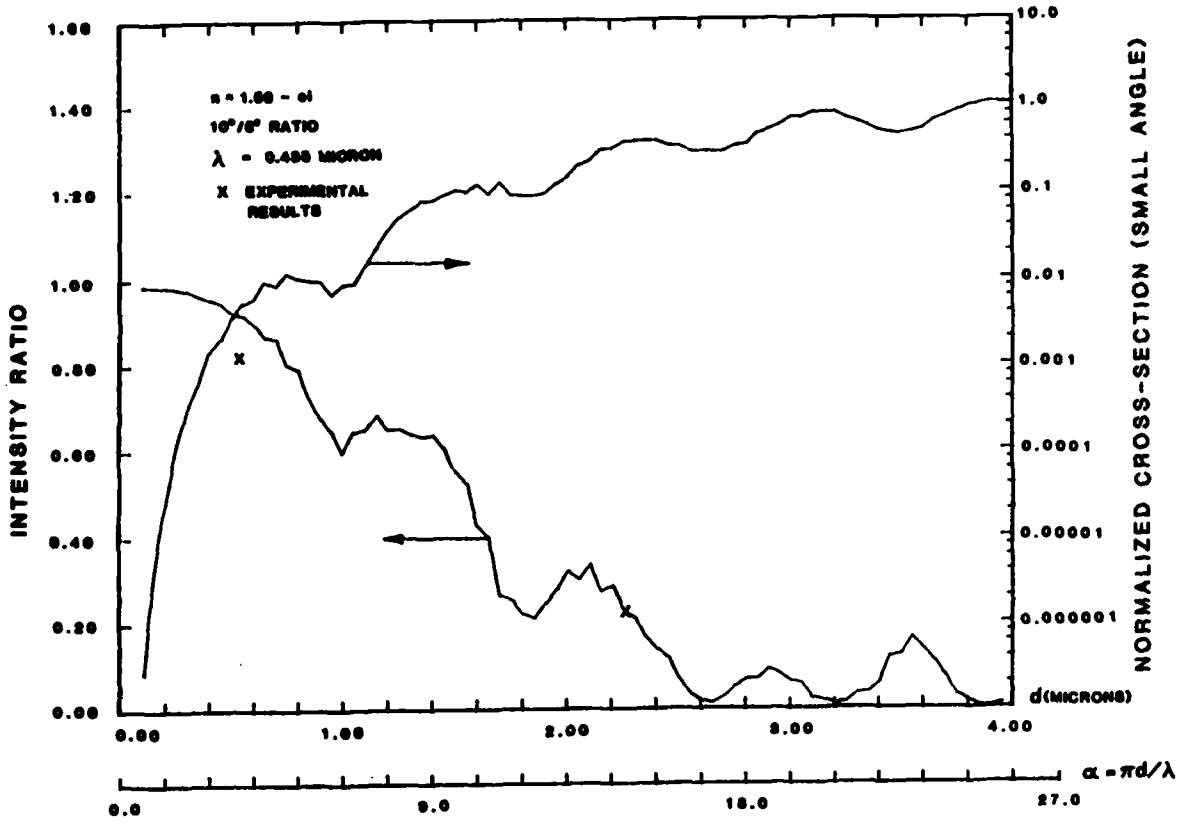

Figure 27. Cold-Flow Verification Data — $10^{\circ}/5^{\circ}$ Ratioing (Concluded)

again adjusted to provide the correct signal height. Coincidence between the experimental and theoretical prediction verifies the performance of the technique.

b. Polarization Ratioing

Particles were introduced into the laser probe in a tightly convergent air jet at about 10 m/sec in order to increase the detected signal above the threshold of the ratio processor. The low signal level results from the reduced seed particle number density when the seeds were introduced with the main combustor air flow. The observed polarization intensity ratio (Figure 29) was consistent with the theoretical predictions except for the very smallest size, 0.109 μm. It is believed that these particles may agglomerate in the concentrated water/particle solution such that the inferred size is different. However, the agreement from the other sizes provides a validation of the technique.

3. Optical Probe and Model Combustor Performance

The performance of the Expanded-Particle Optical System in a reacting flow and the performance of the Dilute-Swirl Combustor (DSC) were evaluated in a combined survey study over a variety of operating conditions, fuels, and fuel injection methods. The variables and parametric variations employed are presented in Table 18.

a. Dilute-Swirl Combustor

For the conditions listed in Table 18, the DSC performance was satisfactory and indicated that the configuration is suitable for fuel effects studies in complex flows. The reaction zone is well behaved (symmetrical, no periodic motion) with high intensity.

Although the combustor was operated lean overall, the mixture ratio in the recirculation ("primary") zone was richer in fuel due to the local injection of fuel into the swirl-stabilized region. For the 50/50 split between swirl air and dilution air, the mixture ratio in the primary zone can be estimated as twice that of the overall mixture ratio. Hence, for an overall equivalence ratio of 0.3, the primary zone equivalence ratio will be approximately 0.6.

The stability limit of the combustor as evidenced by blowout was found to fall between $\phi = 0.5$ and $\phi = 0.6$ for the fuels and injection modes listed in Table 18*. The overall equivalence ratios ($\phi = 0.2, 0.3$) employed in the present experiment were selected for consistency with the prior experiments conducted in the centerbody configuration.

---

*In an independent but complementary study conducted under Air Force Office of Scientific Research (AFOSR) support, an optimization study demonstrated that the stability limit of the DSC can be extended to overall equivalence ratios exceeding $\phi = 0.8$ without blowout by optimizing nozzle performance through custom design. The maximum limit has yet to be established.

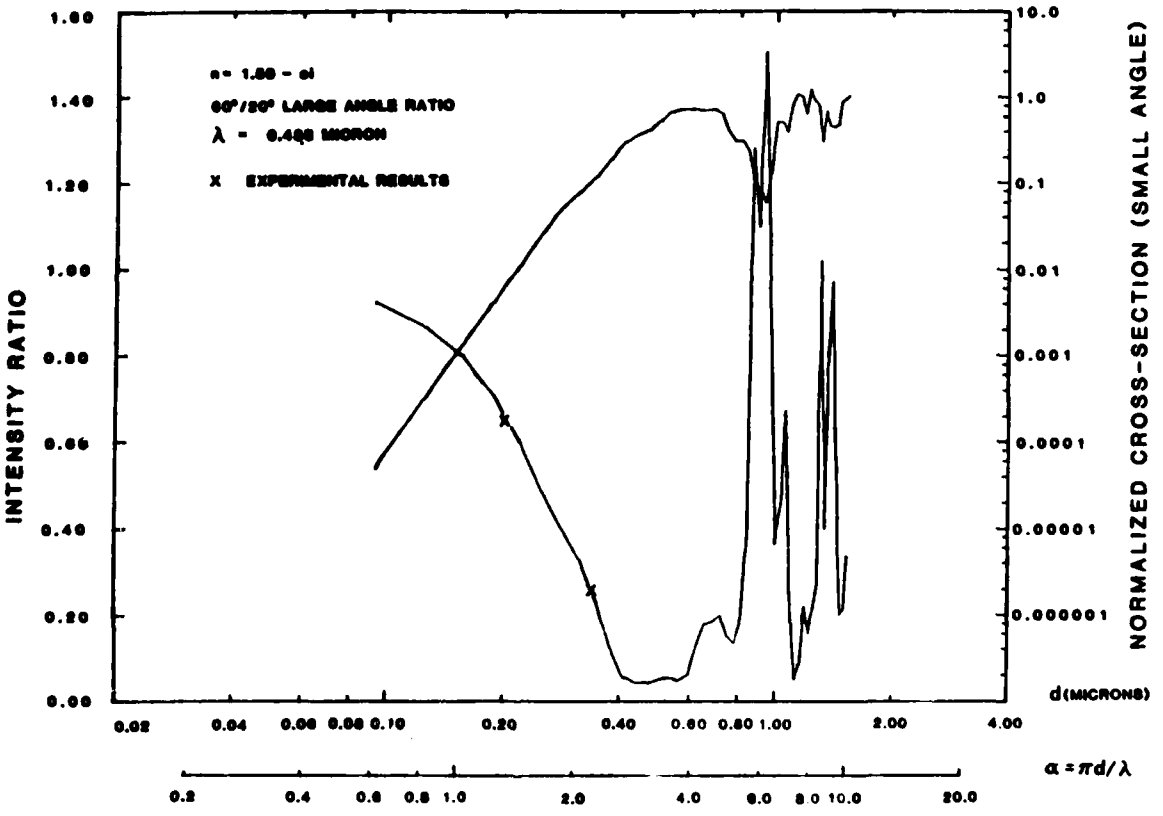

Figure 28. Cold-Flow Verification Data -- 60°/20° Ratioing

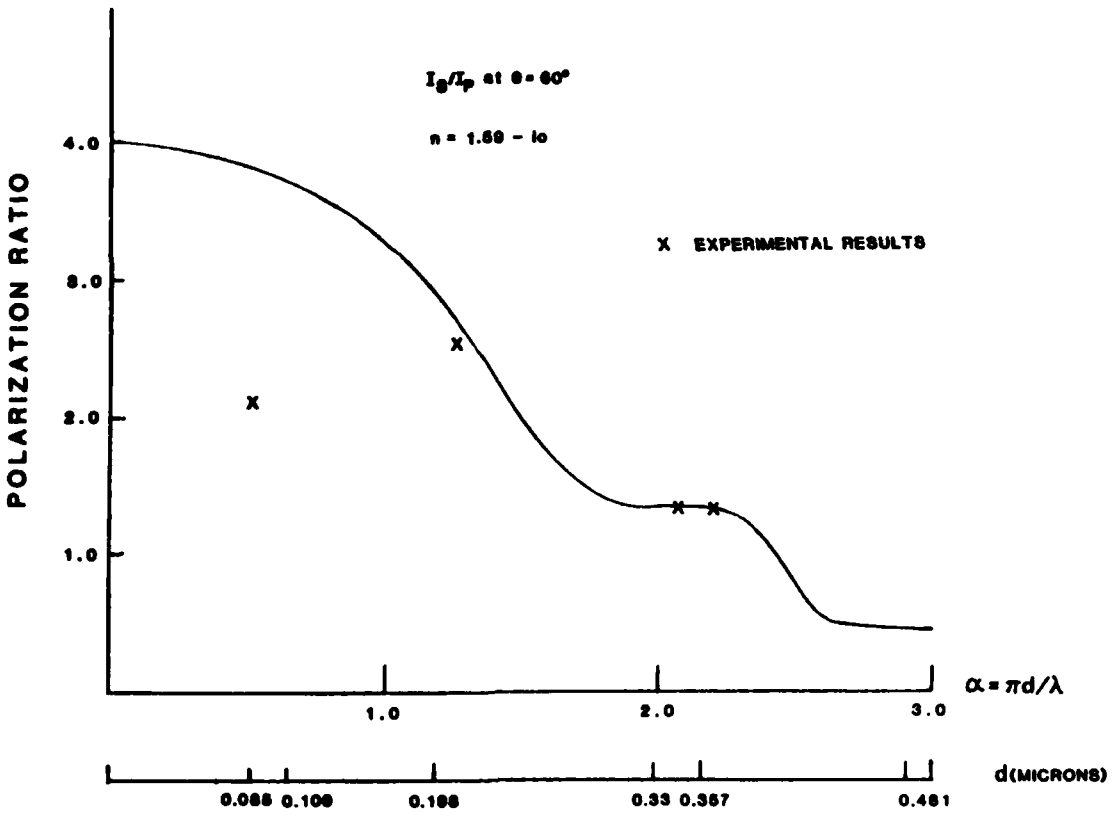

Figure 29. Cold-Flow Verification Data -- Polarization Ratioing

TABLE 18. DSC AND EXPANDED OPTICAL SYSTEM TEST CONDITIONS

Fuel	Injection State	Nozzle[a]	Reference Velocity, U_{ref}[b] (m/s)	Overall Equivalence Ratio, ϕ[c]
Propane	gaseous	WDA (35.0)80°[d]	7.5,15	0.2, 0.3
Ethylene	gaseous		7.5,15	0.2, 0.3
100% Isooctane	prevaporized		7.5,15	0.2, 0.3
14% Isooctane 86% Decalin	prevaporized		7.5,15	[illegible], 0.3
79% Isooctane 21% Toluene	prevaporized		7.5,15	[illegible] 0.3
92% Isooctane 8% Tetralin	prevaporized		7.5,15	0.2, 0.3
95% Isooctane 5% 1-methyl-naphthalene	prevaporized		7.5,15	0.2, 0.3
100% Isooctane	liquid	30610[e]	7.5,15	0.2
14% Isooctane 86% Decalin	liquid		7.5,15	0.2
79% Isooctane 21% Toluene	liquid		7.5,15	0.2
92% Isooctane 8% Tetralin	liquid		7.5,15	0.2
95% Isooctane 5% 1-methyl-naphthalene	liquid		7.5,15	0.2

[a] Delavan Nozzle Model
[b] Cold-flow velocity referenced to duct diameter, 80 mm (3 inch)
[c] Actual overall fuel-to-air ratio divided by stoichiometric ratio
[d] Pressure Atomized
[e] Twin-Fluid Air-Assist

The principal deficiency encountered in the performance of the DSC occurred for liquid fuel injection using the twin-fluid atomizer. Although performance was satisfactory from visual observation, the optical measurements established that droplets could penetrate the primary zone before evaporation was complete. This condition was exacerbated for the liquid blends with a higher boiling fraction. For example, the isooctane/tetralin blend exhibited incipient droplet impaction on the duct wall. Using the optical measurements, the droplet penetration could be substantially reduced by optimizing the performance of the twin-fluid atomizer. Atomization quality can be further improved by nozzle design refinement, so that droplet evaporation will be complete within the primary zone for isooctane and various blends. However, for a base fuel with a higher boiling point base fuel (e.g., dodecane), or high concentrations of high-boiling point fractions in a high-volatile base fuel, droplet penetration may be unavoidable in an 80 mm (3-inch) duct geometry.

b. Expanded-Particle Optical Systems

For each of the conditions listed in Table 18, radial profiles of soot particle size and data rate were obtained with the Expanded-Particle Optical System at three axial locations (x/D = 1.2, 1.8, and 2.6). Measurements were conducted with each particle-sizing system independently: 10/5°, 60/20°, and polarization ratioing. A representative set of results is presented in Figure 30. The size distribution at the three axial locations is shown at two of the outer radial points surveyed.

For the surveys conducted (Table 18), very few,if any,counts were recorded at radial points internal to the flow. Virtually all the significant data counts were recorded at the outer radial locations (Table 19). At the axial location closest to the nozzle (x/D=1.2), significant counts were recorded at one radial location closer to the centerline as well. These results suggest that the aerodynamics of the flow field, in particular the strong swirl component, transport the soot formed in the recirculation zone outward radially to the wall region of the duct.

The data rate decreased at axial stations downstream of x/D = 1.2. This is indicative of the burnout of the soot particlulate. However, the size distribution did not change appreciably between the axial stations.

The sooting propensity was higher at elevated fuel loadings, and higher at the elevated reference velocity (Table 19).

The sooting propensity in the DSC configuration was substantially lower than that observed in the swirl-stabilized centerbody configuration at similar overall equivalence ratios. This is attributed to the more efficient evaporation of fuel in the DSC where fuel is injected (Figure 6) into the shear region of the recirculation zone with an attendant improvement in the mixing and processing of the fuel. Hence, the levels of soot produced at the fuel loadings listed in Table 18 can be characterized as "light" and of low number density.

For the fuels and conditions surveyed, the size distributions peaked within the range of the 60/20 intensity ratio dynamic range (0.08 to 0.6 μm) with the maximum generally occurring around 0.2 μm. Electron micrograph samples collected on 0.08 μm pore nuclepore filters,using the extractive probe,

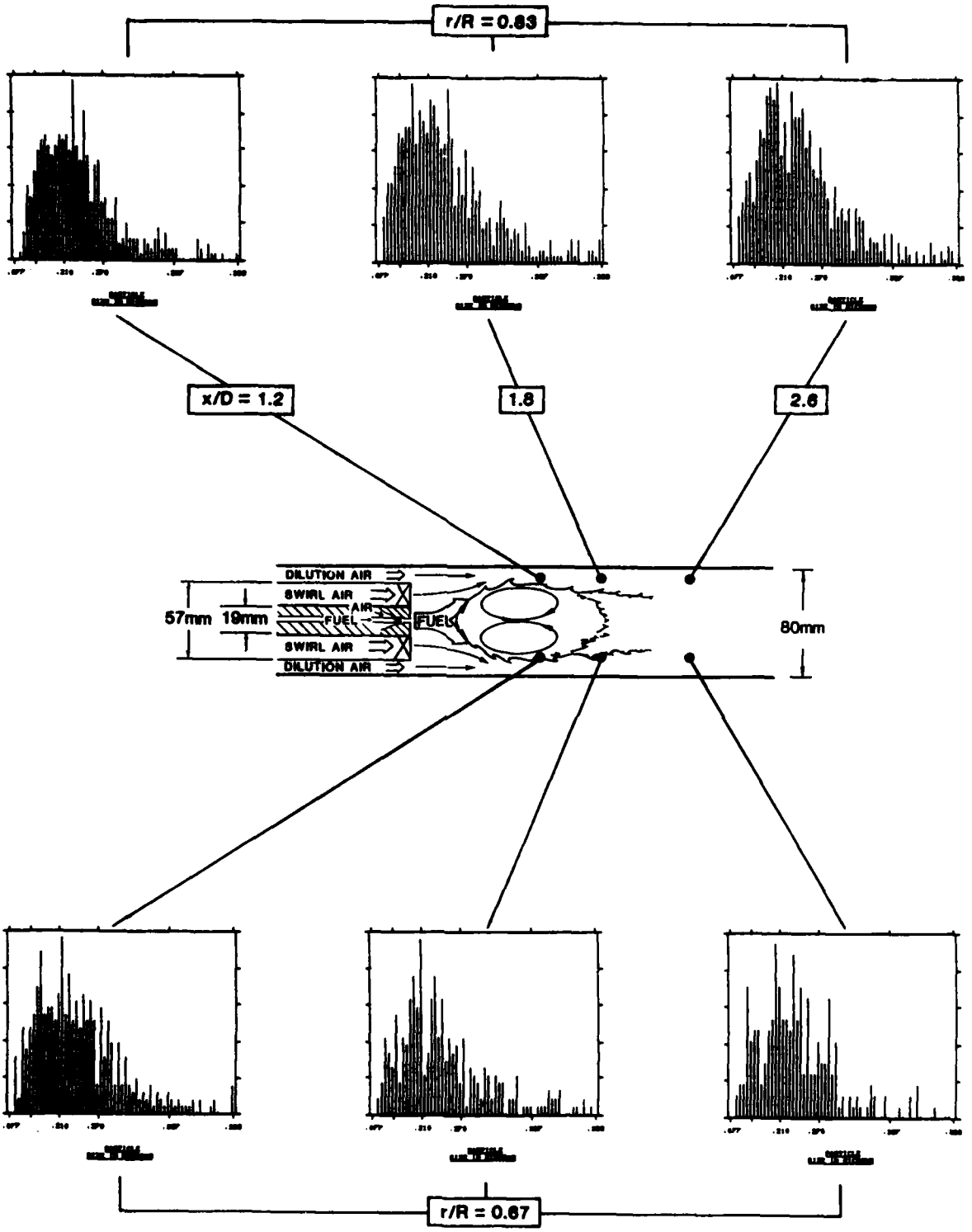

Figure 30. Hot-Flow Demonstration Data -- 60°/20° Ratioing (Prevaporized Isooctane, U_{ref} = 7.5 mps, ϕ=0.3)

were consistent with the optically measured size distribution though the resolution of the scanning electron microscope and focused deposition of the particulate about the 0.08 μm pores precluded a definitive measurement of the mean soot particle size.

Data collected for the 10/5 intensity ratio technique were consistent with data collected with the 60/20 intensity ratio technique. An example is presented in Figure 31. The 10/5 data are an extension of the 60/20 distribution and represent a detailed "blow-up" of the 60/20 tail. The data rates for the two sets of data are 7.55 Hz and 12.72 Hz respectively.

The data extend into a region below the lower limit (0.08 μm) of the 60/20 ratioing technique. Collection of data in this region using polarization ratioing was generally precluded due to the low number density of the particulate. In Figure 32, polarization ratioing data are shown for a condition where the number density was just sufficient to produce a response. The dynamic range of polarization ratioing (0.05 to 0.373) appears to be well suited for the size range of particulate encountered.

TABLE 19. HOT-FLOW DEMONSTRATION DATA -- ISOOCTANE DATA RATES (Hz)

Condition	Radial (r/R)	Axial (x/D)		
		1.2	1.8	2.6
U_{ref}=7.5 mps ϕ=0.3	0.83	10.91	10.52	7.56
	0.67	5.87	3.78	3.12
	0.50	2.92	1.57	0.84
	0.33	0.58	0.30	0.19
	0.17	0.08	0.03	0.02
	0.00	0.02	0.01	0.04
U_{ref}=7.5 mps ϕ=0.2	0.83	5.22	4.08	5.00
	0.67	2.81	2.15	1.61
	0.50	1.55	0.82	0.32
	0.33	0.24	0.14	0.05
	0.17	0.00	0.03	0.00
	0.00	0.00	0.00	0.00
U_{ref}=15 mps ϕ=0.2	0.83	51.76	35.51	26.72
	0.67	37.26	23.06	14.67
	0.50	12.84	8.92	3.22
	0.33	3.03	1.55	0.55
	0.17	0.50	0.20	0.25
	0.00	0.03	0.00	0.01

a) 60/20 Data (12.72 Hz)

b) 10/5 Data (4.55 Hz)

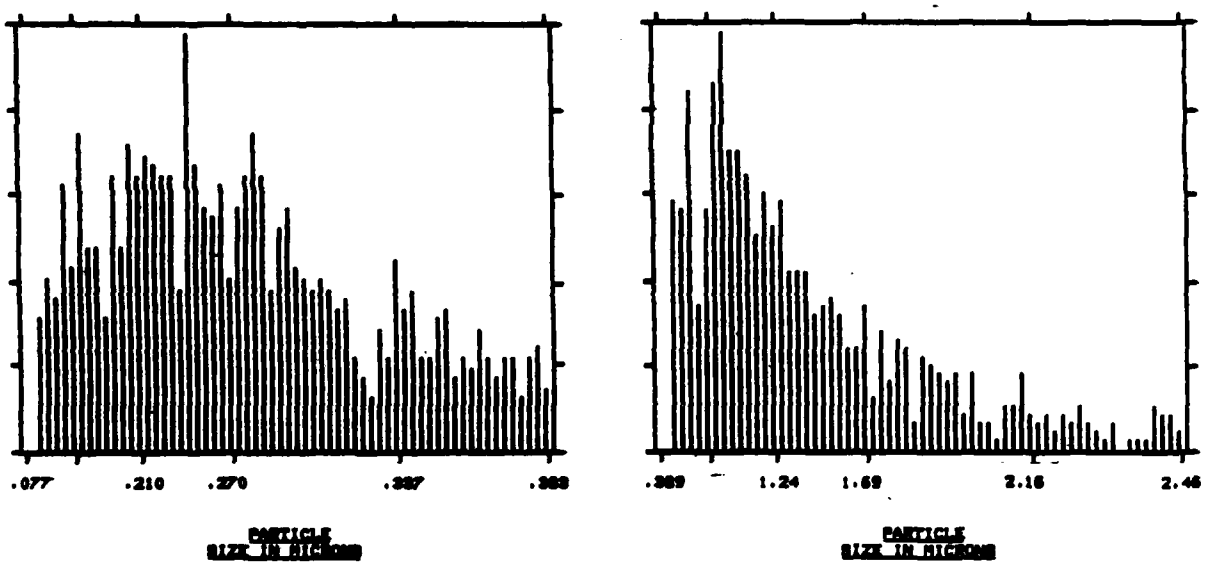

Figure 31. Hot-Flow Demonstration Data -- 10°/5° and 60°/20° Consistency (Prevaporized Isooctane/Tetralin, U_{ref}=7.5 mps, ϕ=0.3)

The sooting propensity of the isooctane blends was higher than the pure isooctane. Gravimetric data collected with the extractive probe at the exit plane are presented in Table 20. The gravimetric readings for the blends are approximately 50 percent higher than the pure isooctane, and little difference occurs for the blends which were blended to yield the same ASTM smoke point as a shale-derived JP-8 (Table 10). These results, obtained in the DSC, are consistent with those found in the centerbody combustor (Table 14). However, the DSC results are an order of magnitude lower in weight concentration which is attributed to the more efficient mixing and fuel processing associated with the DSC as well as the prevaporized fuel preparation. These results are also consistent with the optically measured data rates for the isooctane blends in contrast to the pure isooctane (Table 21).

c. Summary

The performance of both the DSC and Expanded Optical System were satisfactory and indicate that both systems will be suitable for fuels effects studies of soot production. The peak soot size was found to be around 0.2 μm, with data rates ("sooting propensity") increasing with fuel-loading, reference velocity, and the addition of ring compounds to the pure isooctane base. The large-angle scattering technique (60/20) is the most suitable for single-particle realizations in the size range encountered, whereas polarization ratioing is attractive due to the lower size resolution and broader dynamic range. However, polarization ratioing requires a higher number density than that encountered in the very lean operation adopted for the present study, and has yet to be fully tested.

TABLE 20. HOT-FLOW DEMONSTRATION DATA -- EXTRACTED SOOT WEIGHT CONCENTRATION[a]

Fuel	Weight Concentration (mg/m^3)
100% Isooctane	0.14
79% Isooctane 21% Toluene	0.20
92% Isooctane 8% Tetralin	0.22
95% Isooctane 5% 1-methylnapthalene	0.19

[a] Prevaporized, U_{ref}=7.5 mps, ϕ =0.3

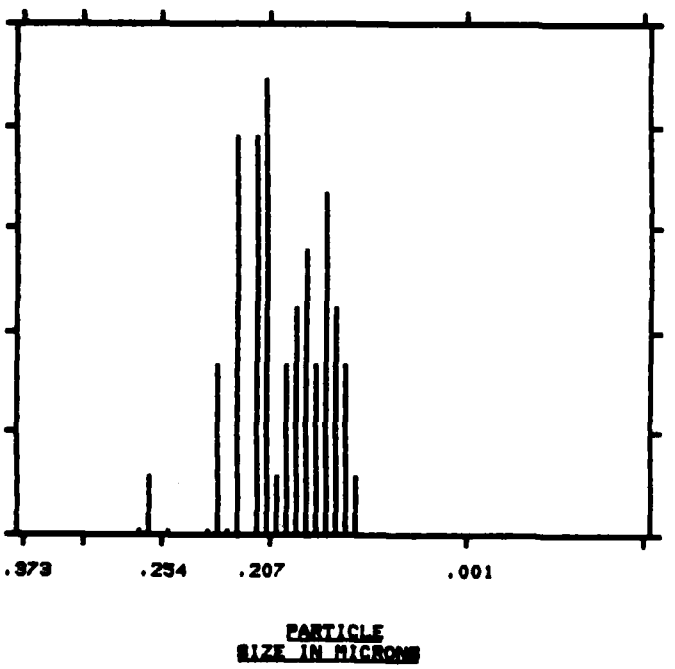

Figure 32. Hot-Flow Demonstration Data -- Polarization Ratioing Data (Prevaporized Isooctane/Toluene, U_{ref}=15 mps, ϕ=0.3)

TABLE 21. HOT-FLOW DEMONSTRATION DATA -- REPRESENTATIVE DATA RATES (Hz)

Fuel[a]	Radial (r/R)[b]	Axial (x/D) b		
		1.2	1.8	2.6
Isooctane	0.83	10.91	10.52	7.56
	0.67	5.87	3.78	3.12
	0.50	2.92	1.57	0.89
	0.33	0.58	0.30	0.19
	0.17	0.08	0.03	0.02
	0.00	0.02	0.01	0.04
Isooctane/ Tetralin	0.83	c		
	0.67	18.14	13.72	6.42
	0.50	11.45	10.20	4.85
	0.33			
	0.17			
	0.00	1.19	1.36	1.48

[a] Prevaporized, U_{ref}=7.5 mps, ϕ=0.3
[b] R and D are the duct radius and diameter respectively
[c] Data were acquired at three radial locations for the blends

SECTION VI

CONCLUSIONS

1. An optical, laser-based probe developed and demonstrated under the present study performed satisfactorily in the nonintrusive measurement of (1) calibrated polystyrene seed particles in nonreacting flows, and (2) soot particulate in reacting flows. The utility of such an instrument was demonstrated in assessing (1) the perturbation of an extractive probe, and (2) the effect of fuel properties on the sooting propensity (size distribution, data rate) in a complex flow.

2. A complex flow model combustor, the Dilute-Swirl Combustor (DCS), was successfully operated on gaseous fuels, prevaporized liquid fuels, and direct injection of liquid fuels. The configuration is adaptable to a range of operating conditions, and provides clear optical access axially and radially for visualization and optical measurements of sooting and velocity. The atomization quality of liquid fuels will have to be improved if droplet penetration of the recirculation zone, detected with the optical probe, is to be minimized.

3. For the combustor conditions addressed in the present study,

   - The peak soot particle size measured for all the fuels was approximately 0.2 μm.
   - Propane and prevaporized isooctane were relatively "clean," with either little or no optically detected or extracted soot.
   - JP-8 had the highest soot propensity.
   - Blends of isooctane with various saturated and unsaturated ring compounds, blended to the same ASTM Smoke Point of JP-8, each produced similar amounts of soot though significantly less than the JP-8.

4. The ASTM Smoke Point Method does not represent the sooting propensity of a fuel in a complex flow field such as a gas-turbine combustor. Moreover, the ASTM Smoke Point Method does not predict the performance of an additive (ferrocene) in a complex flow field.

5. For one set of conditions evaluated in the present experiment (liquid-injected, one-atmosphere, swirl-stabilized centerbody combustor), ferrocene suppressed the soot production of a JP-8 fuel, but increased the sooting propensity (promoted agglomeration) of isooctane doped with unsaturated double-ring aromatics representative of those probable in shale- and coal-derived fuels. In addition, the chemical complexity of the polynuclear aromatic hydrocarbons (PAH) in the soot particulate corresponded to the complexity of the chemical structure in the fuel blend.

6. An extractive sampling probe can significantly perturb the local flow field. The local soot data rate can vary by orders of magnitude, the extent of variation depending on reference velocity and location of the extractive probe within the complex flow field.

7. The methods developed and demonstrated under the present program (non-intrusive optical probe, model complex flow combustor) provide the capability of detailed flow field mapping of the local number density and size distribution of soot particulate under conditions representative of gas turbine combustors: high intensity with a strong coupling between the aerodynamics and fuel distribution. Such a capability is appropriate and necessary to (1) determine the impact of fuel and additive properties on the size, number density, and composition of soot, (2) assess the effectiveness of tailoring the combustion process to control the production of soot, (3) establish whether a simulated fuel, produced by blends of pure hydrocarbons, can be formulated to represent the sooting propensity of refired fuels, and (4) evaluate the perturbation of an extractive probe on the properties of the flow sampled.

REFERENCES

1. Churchill, A.V., DeLaney, C.L. and Lander, H.R., "Future Aviation Turbine Fuels," J. Aircraft, Vol. 15, No. 11, 1978.

2. Lefebvre, A. H., "Pollution Control in Continuous Combustion Engines," Fifteenth International Symposium on Combustion, pp. 1169-1180, The Combustion Institute, 1975.

3. Arcoumanis, D.C., "Water Analog of the Opposed Jet Combustor: Velocity Field Measurements and Flow Visualization," Master of Science Thesis, UCI Combustion Laboratory Report UCI-ARTR-80-5, Mechanical Engineering, University of California, Irvine, 1980.

4. Szetela, E.J. Lohmann, P. and Smith, A.L., "Analysis of the Impact of the Use of Broad Specification Fuels on Combustors for Commercial Aircraft Gas Turbine Engines," AIAA/SAE/ASME 15th Joint Propulsion Conference, 1979.

5. MacFarlane, J.J., Holderness, F.H. and Whitcher, F.S., "Soot Formation Rates in Premixed C_5 and C_6 Hydrocarbon Flames at Pressures up to 20 Atmospheres," Combust Flame, Vol. 8, No. 3, 1964.

6. Schirmer, R.M., "Effect of Fuel Composition on Particulate Emissions from Gas Turbine Engines," Emissions from Continuous Combustion Systems, edited by W. Cornelius and W.G. Agnew, Plenum Publishing Corp., 1972.

7. Hoult, D.P. and Ekchian, A., "Soot Formation in a Turbulent Swirl-Stabilized Laboratory Combustor," ASME 80-GT-77, 1980.

8. Norster, E.R. and Lefebvre, A.H., "Effects of Fuel Injection Method on Gas-Turbine Combustor Emissions," Emissions from Continuous Combustion Systems, edited by W. Cornelius and W.G. Agnew, Plenum Publishing Corp., 1972.

9. Lefebvre, A.H., Mellor, A.M., Peters, J.E., "Ignition/Stabilization/Atomization - Alternative Fuels in Gas Turbine Combustors," Alternative Hydrocarbon Fuels: Combustion and Chemical Kinetics, edited by C.T. Bowman and J. Birkeland, Progress in Astronautics and Aeronautics, Vol. 62, pp. 137-159, AIAA, 1978.

10. Gleason, C.C. and Bahr, D.W., "Fuel Property Effects on Life Characteristics of Aircraft Turbine Engine Combustors," ASME 80-GT-55, 1980.

11. Blazowski, W.S., "Combustion Considerations for Future Jet Fuels," Sixteenth International Symposium on Combustion, pp. 1631-1639, The Combustion Institute, 1977.

12. Bryan, R., Godbole, P.S. and Norster, E.R., "Some Observations of the Atomizing Characteristics of Air Blast Atomizers," Cranfield International Symposium Series, Vol. 11, Edited by E.R. Norster, Pergammon Press., 1971.

13. Mellor, A.M., "Gas Turbine Engine Pollution," Prog Energy Combust Sci, Vol. 1, 1976.

14. Longwell, J.P. Editor, "Jet Aircraft Hydrocarbon Fuels Technology," NASA Conference Publication 2033, 1978.

15. Lorenzetto, G.E. and Lefebvre, A.H., "Measurements of Drop Size on a Plain-Jet Airblast Atomizer," AIAA Journal, Vol. 15, No. 7, 1977.

16. Naegeli, D.W. and Moses, C.A., Effects of Fuel Properties on Soot Formation in Turbine Combustion," SAE Paper No. 781026, 1978.

17. Wright, F.J., "The Formation of Carbon Under Well-Stirred Conditions," Twelfth International Symposium on Combustion, pp. 867-875, The Combustion Institute, 1969.

18. Blazowski, W.S., "Dependence of Soot Production on Fuel Blend Characteristics and Combustion Conditions," ASME 79-GT-155, 1979.

19 Toone, B., "A Review of Aeroengine Smoke Emission," Cranfield International Symposium Series, Vol. 10, Combustion in Advanced Gas Turbine Systems, edited by I.E. Smith, Pergamon Press, 1968.

20. Shayeson, M.W., "Reduction of Jet Engine Exhaust Smoke with Fuel Additives," SAE Paper No. 670866, 1967.

21. Klarman, A.F., "Evaluation of the Extended Use of Ferrocene for Test Cell Smoke Abatement; Engine and Environmental Test Results," Navy Report No. NAPTC-PE-110, 1977.

22. Howard, J.B. and Kausch Jr., W.J., "Soot Control by Fuel Additives," Prog Energy Comb Sci, Vol. 6, 1980.

23. Haynes, B.S., Jander, H. and Wagner, H.G., "The Effect of Metal Additives on the Formation of Soot in Premixed Flames," Seventeenth International Symposium on Combustion, pp. 1365-1374, The Combustion Institute, 1979.

24. Bulewicz, E.M., Evans, D.G. and Padley, P.J., "Effect of Metallic Additives on Soot Formation Processes in Flames," Fifteenth Internationl Symposium on Combustion, pp. 1461-1470, The Combustion Institute, 1975.

25. Cotton, D.H., Friswell, N.J. and Jenkins, D.R., "The Suppression of Soot Emission from Flames by Metal Additives," Combust Flame, Vol. 17, 1971.

26. Dukek, W.G., "Fuel Combustion Quality by Laboratory Tests," Presented to CRC Group on Combustion Characteristics of Aviation Turbine Fuels, NASA-Lewis Research Center, 1978.

27. ASTM, "Standard Method of Test for Smoke Point of Aviation Turbine Fuels," ASTM D1322-80, 1980 Annual Book of ASTM Standards, Philadelphia, American Society for Testing and Materials, Vol. 21, p. 720, 1980.

28. ASTM, "Standard Method of Test for Luminometer Numbers of Aviation Turbine Fuels," ASTM D1740-80, 1980 Annual Book of ASTM Standards, Philadelphia, American Society for Testing and Materials, Vol. 22, p. 13, 1980.

29. ASTM, "Standard Method of Test for Hydrocarbon Types in Liquid Petroleum Products by Fluorescent Indicator Adsorption," ASTM D1319-80, 1980 Annual Book of ASTM Standards, Philadelphia, American Society for Testing and Materials, Vol. 21, p. 704, 1980.

30. ASTM, "Standard Method of Test for Naphthalene Hydrocarbons in Aviation Turbine Fuels by Ultraviolet Spectrophotometry," ASTM D1840-80, 1980 Annual Book of ASTM Standards, Philadelphia, American Society for Testing and Materials, Vol. 22, p. 105, 1980.

31. ASTM, "Standard Method of Test for Hydrogen in Petroleum Fractions," ASTM D1018-80, 1980 Annual Book of ASTM Standards, Philadelphia, American Society for Testing and Materials, Vol. 21, p. 512, 1980.

32. ASTM, "Standard Method of Test for Refractive Index and Refractive Dispersion of Hydrocarbon Liquids," ASTM D1218-80, 1980 Annual Book of ASTM Standards, Philadelphia, American Society for Testing and Materials, Vol. 21, p. 626, 1980.

33. ASTM, "Standard Method of Test for Amiline Point and Mixed Aniline Point of Petroleum Products and Hydrocarbon Solvents," ASTM D611-80, 1980 Annual Book of ASTM Standards, Philadelphia American Society for Testing and Materials, Vol. 21, p. 314, 1980.

34. ASTM, "Standard Method of Test for Estimation of Hydrogen Content of Aviation Fuels," ASTM D3343-80, 1980 Annual Book of ASTM Standards," Philadelphia, American Society for Testing and Materials, Vol. 23, p.249, 1980.

35. Kittredge, G.D. and Streets, W.L., "Gas Turbine and Jet Engine Fuels," Phillips Petroleum Co. Research Division Report 2760-60R, Feature No. 6040, 1960.

36. McClelland, C.C., "Effects of Jet Fuel Constituents on Combustor Durability," Naval Air Engineering Center Report, NAEC-AEL-1736, AD# 404084, 1963.

37. Friswell, N.J., "The Influence of Fuel Composition on Smoke Emission from Gas-Turbine-Type Combustors: Effect of Combustor Design and Operating Conditions," Combust Sci Technol, Vol. 19, 1979.

38. Gleason, C.C. and Martone, J.A., "Fuel Character Effects on J70 and F101 Engine Combustor Emissions," ASME 80-GT-70, 1980.

39. Naegeli, D.W. and Moses, C.A., "Effect of Fuel Molecular Structure on Soot Formation in Gas Turbine Engines," ASME 80-GT-62, 1980.

40. Glassman, I. and Yaccarino, P., "The Temperature Effect in Sooting Diffusion Flames," Eighteenth International Symposium on Combustion, pp. 1175-1183, The Combustion Institute, 1981.

41. Naegeli, D.W., Dodge, L.G. and Moses, C.A., "Effect of Flame Temperature and Fuel Composition on Soot Formation in Gas Turbine Engines," WSS/CI Paper 81-35, Presented at 1981 Fall Meeting Western States Section, Combustion Institute, 1981.

42. Dalzell, W.H., William, G.C., and Hottel, H.C., "A Light-Scattering Method for Soot Concentration Measurements," Combust Flame, Vol. 14, 1970.

43. D'Alessio, A., Di Lorenzo, A., Sarofim, A.F., Baretta, F., Masi, S., and Venitozzi, C., "Optical and Chemical Investigation on Fuel-Rich Methane-Oxygen Premixed Flames at Atmospheric Pressure," Fourteenth International Symposium on Combustion, pp. 941-953, The Combustion Institute, 1973.

44. Bro, K., "The Optical Dispersion Quotient Method for Sizing of Soot in Shock-Induced Combustion," Ph.D. Dissertation, Purdue University, 1978.

45. Wertheimer, A.L., Symposium on Advances in Particle Sampling and Measurement, EPA, 1978.

46. Penner, S.S., and Chang, P., "On the Determination of Log-Normal Particle-Size Distribution Using Half Widths and Detectabilities of Scattered Laser Power Spectra," JOSRT 20, pp. 447-460, 1978.

47. Driscoll, J.F., Mann, D.M., and McGregor, W.K., "Submicron Particle Size Measurements in an Acetylene-Oxygen Flame," Combust Sci Technol., Vol. 20, 1979.

48. Chu, W.P., and Robinson, D.M., "Scattering from a Moving Spherical Particle by Two Crossed Coherent Plane Waves," Applied Optics, Vol. 16, 1977.

49. Wang, J.C.F., and Tichenor, D.A., "Particle Size Measurements Using an Optical Variable-Frequency-Grid Technique," Applied Optics, Vol. 20, 1981.

50. Hirleman, E.D. Jr., "Optical Technique for Particulate Characterization in Combustion Environments: The Multiple Ratio Single Particle Counter," Ph.D. Dissertation, Purdue University, 1977.

51. Hodkinson, J.R., "Particle Sizing by Means of the Forward Scattering Lobe," Applied Optics, Vol. 5, 1966.

52. Holve, D., and Self, S.A., "Optical Particle Sizing for In Situ Measurements," Applied Optics, Vol. 18, 1979.

53. For Instance, Climet Model CI-208 Airborne Particle Counter, Climet Instrument Company, Redlands, California.

54. Faxvog, F.R., "Detection of Airborne Particles Using Optical Extinction Measurements," Applied Optics, Vol. 13, 1974.

55. Bowman, Craig, T., "Probe Measurements in Flames," in B.T. Zinn (Ed)., Experimental Diagnostics in Gas-Phase Combustion Systems, Progress in Astronautics and Aeronautics, Vol. 53, pp. 3-24, 1977.

56. Cooper, H.B.H., and Rossano, A.T., Source Testing for Air Pollution, McGraw-Hill, 1974.

57. Kramlich, J.C., Samuelsen, G.S., and Seeker, W.R., "Carbonaceous Particulate Formation From Synthetic Fuel Droplets," Western States Paper No. WSCI 81-52, 1981.

58. Environmental Protection Agency, Source Assessment Sampling System; Design and Development, Document No. EPA-600/7-78-018, 1979.

59. Fenton, D.L., Luebcke, E.H., and Norstrom, E., "Physical Characterization of Particulate Material From a Turbine Engine," ASME Paper 79-GT-179, Presented at the ASME Gas Turbine Conference, San Diego, March 1979.

60. Dodds, W.J., Colket, M.B., and Mellor, A.M., "Radiation and Smoke from Gas Turbine Flames Part I. Carbon Particulate Measurements within a Model Turbine Combustion. Final Technical Report Part I," Technical Report No. 12163, Purdue Report No. Purdu-CL-76-06, Contract No. DAAE07-76-C-0063, July, 1976.

61. Prado, G.P., Lee, M.L., Hites, R.A., Hoult, D.P., and Howard, J.B., "Soot and Hydrocarbon Formation in a Turbulent Diffusion Flame," Sixteenth International Symposium on Combustion, pp. 649-661, The Combustion Institute, 1977.

62. Pierce, R.C. and Katz, M., "Dependency of Polynuclear Aromatic Hydrocarbon Content on Size Distribution of Atmospheric Aerosols," Environ Sci Technol, Vol. 9, No. 4, 1975.

63. Bjorseth, A., "Determination of Polynuclear Aromatic Hydrocarbons in the Working Environment," Polynuclear Aromatic Hydrocarbons, edited by P.W. Jones and P. Leber, Ann Arbor Science Publishing, 1979.

64. Chen, C.Y., "Filtration of Aerosols by Fibrous Media," Chem. Review, Vol. 55, 1955.

65. Lundgren, D.A. and Gunderson, T.C., "Efficiency and Loading Characteristics of EPA's High Temperature Quartz Fiber Filter Media," Am Ind Hyg Assoc J, 1975.

66. Lee, F.S.C., Prater, T.J. and Ferris, F. "PAH Emissions from a Stratified-Charge Vehicle with and without Qxidation Catalyst: Sampling and Analysis Evaluation," Polynuclear Aromatic Hydrocarbons, edited by P.W. Jones and P. Leber, Ann Arbor Science Publishing, 1979.

67. Natusch, D.F.S. and Tomkins, B.A., "Theoretical Consideration of the Adsorption of Polynuclear Aromatic Hydrocarbon Vapor onto Fly Ash in a Coal-Fired Power Plant," Carcinogenisis Vol. 3: Polynuclear Aromatic Hydrocarbons, edited by P.W. Jones and R.I. Freudenthal, Raven Press, 1978.

68. Strup, P.E., Wilkinson, J.E. and Jones, P.E., "Trace Analysis of Polycyclic Aromatic Hydrocarbons in Aqueous Systems Using XAD-2 Resin and Capillary Column Gas Chromatography-Mass Spectrometry Analysis," Carcinogenisis: Vol. 3: Polynuclear Aromatic Hydrocarbons, edited by P.W. Jones and R.I. Freudenthal, Raven Press, 1978.

69. Adams, J. Menzies, K. and Levins, P., NTIS Rep. No. PB-268559, 1977.

70. Hanson, R.L., Clark, C.R., Carpenter, R.L. and Hobbs, C.H., "Evaluation of Tenax-GC and XAD-2 as Polymer Adsorbents for Sampling Fossil Fuel Combustion Products containing Nitrogen Osides," Environ Sci Technol, Vol. 15, No. 6, 1981.

71. Lentzen, D.E. Wagoner, D.E., Estes, E.D. and Gutknecht, W.F., "IERL-RTP Procedures Manual: Level 1 Environmental Assessment (Second Edition)," EPA-600/7-78-201, 1978.

72. Griest, W.H., Yeates Jr., L.B. and Caton, J.E., "Recovery of Polycyclic Aromatic Hydrocarbons Sorbed on Fly Ash for Quantitative Determination," Anal Chem, Vol. 52, 1980.

73. Falk, H.L. and Steiner, P.E., "The Identification of Aromatic Polycyclic Hydrocarbons in Carbon Blacks," Cancer Res, Vol. 12, 1952.

74. del Vecchio, V., Valuri, P., Melchiori, C. and Grella, A., "Polycyclic Aromatic Hydrocarbons from Gasoline Engine and Liquified Petroleum Gas Engine Exhausts," Pure Applied Chem, Vol. 24, 1970.

75. Golden, C. and Sawicki, E., "Ultrasonic Extraction of Total Particulate Aromatic Hydrocarbons (TpAH) from Airbone Particles at Room Temperature," Int J Environ Anal Chem, Vol. 4, 1975.

76. Lee, M.L., Novotny, M.V. and Bartle, K.D., Analytical Chemistry of Polycyclic Aromatic Compounds, Academic Press, 1981.

77. Natusch, D.F.S. and Tomkins, B.A., "Isolation of Polycyclic Organic Compounds by Solvent Extraction with DMSO," Anal Chem, Vol. 50, 1978.

78. Thomas, R. and Zander, M., "On the High Pressure Liquid Chromatography of Polycyclic Aromatic Hydrocarbons," Anal Chem, Vol. 48, 1976.

79. Lee, M.L. and Wright, B.W., "Capillary Column Gas Chromatography of Polycyclic Aromatic Compounds: A Review," J of Chrom Sci, Vol. 18, 1980.

80. Lee, M.L., Vassilaros, D.L., White, C.M. and Novotny, M., "Retention Indices for Programmed-Temperature Capillary Column Gas Chromatography of Polycyclic Aromatic Hydrocarbons," Anal Chem, Vol. 51, 1979.

81. Brum, R.D., Samuelsen, G.S., and Ikioka, L.M., "Assessment of a Candidate Combustor Configurations as Test Beds for Modeling Complex Flows," ASME Paper 82-HT-36, 1982.

82. Brum, R.D., Samuelsen, G.S., "Assessment of a Dilute Swirl Combustor as a Bench Scale, Complex Flow Test Bed for Modeling, Diagnostics, and Fuels Effects Studies," AIAA Paper 82-1263, 1982.

83. Roquemore, W.M., Bradley, R.P., Stutrud, J.S., Reeves, C.M., and Krishnamurthy, L., "Preliminary Evaluation of a Combustor for Use in Modeling and Diagnostics Development," ASME-80-GT-93, Twenty-fifth Annual International Gas Turbine Conference, The American Society of Mechanical Engineers, New Orleans, Louisiana, 1980.

84. Samuelsen, G.S., Hack, R.L., Poon, C.C., and Bachalo, W.D., "Study of Soot Formation in Premixed and Nonpremixed Flows with Complex Aerodynamics," Presented at the Combustion Institute, Western States Section, 1980 Spring Meeting, WSCI 80-10, 1980.

85. Hack, R.L., Samuelsen, G.S., Poon, C.C., and Bachalo, W.D., "An Exploratory Study of Soot Sample Integrity and Probe Perturbation in a Swirl-Stabilized Combustor," ASME Paper 81-GT-27, 1981.

86. Hack, R.L., Samuelsen, G.S., Poon C.C., and Bachalo, W.D., "An Exploratory Study of Soot Sample Integrity and Probe Perturbation in a Swirl-Stabilized Combustor," J of Eng Power, Vol. 103, No. 10, 1981.

87. Samuelsen, G.S., Hack, R.L., Poon, C.C., Bachalo, W.D., and Clewell, H., "A Comparison of Soot Size and Number Density Measured Simultaneously in A Swirl-Stabilized Combustor by Extractive and Non-Intrusive Optical Probe," Third EPA Symposium on Advances in Particle Sampling Measurement, 1981.

88. Himes, R.M., Samuelsen, G.S., and Hack, R.L., "Chemical and Physical Properties of Soot as a Function of Fuel Molecular Structure in a Swirl Stabilized Combustor," ASME Paper 82-GT-109, 1982.

89. Holdeman, J.D., and Walker, R.E., "Mixing of a Row of Jets with a Confined Crossflow," AIAA Journal, Vol. 15, No. 2, February 1977.

90. Waldman, L., and Schmitt, K.H., "Thermophoresis and Diffusiophoresis of Aerosols," Aerosol Science, Edited by C.N. Davies, Academic Press, New York, 1966.

91. Peterson, P.R. and Himes, R.M., "Opposed Jet Combustor Experimental Facility," UCI Combustion Laboratory Report UCI-ARTR-78-8, 1978.

92. Beer, J.M. and Chigier, N.A., Combustion Aerodynamics, Applied Science Publisher, Ltd., 1972.

93. Wilmhurst, J.R., "Gas Chromatographic Analysis of Polynuclear Arenes," J Chromatogr, Vol. 17, 1965.

94. Graham, S.C., Homer, J.B. and J.L.J. Rosenfeld, "The Formation and Coagulation of Soot Aerosols," International Shock Tube Symposium, 10th Proceedings, p. 621, 1975.

95. Gelman, C. and Marshall, J.C., "High Purity Fibrous Air Sampling Media," Am Ind Hyg Assoc J, Vol. 36, 1975.

96. Benjamin, B.M., Hagaman, E.W., Raaen, V.F. and Collins, C.J., "Pyrolysis of Tetralin," Fuel, Vol. 58, 1979.

(The reverse of this page is blank)